NASA TECHNICAL NOTE

NASA TN D-4237

NASA TN D-4237

EFFECT OF GROUND PROXIMITY ON THE LONGITUDINAL, LATERAL, AND CONTROL AERODYNAMIC CHARACTERISTICS OF A TILT-WING FOUR-PROPELLER V/STOL MODEL

by Kenneth W. Goodson

Langley Research Center
Langley Station, Hampton, Va.

NATIONAL AERONAUTICS AND SPACE ADMINISTRATION • WASHINGTON, D. C. • DECEMBER 1967

EFFECT OF GROUND PROXIMITY ON THE LONGITUDINAL, LATERAL, AND CONTROL AERODYNAMIC CHARACTERISTICS OF A TILT-WING FOUR-PROPELLER V/STOL MODEL

By Kenneth W. Goodson

Langley Research Center
Langley Station, Hampton, Va.

NATIONAL AERONAUTICS AND SPACE ADMINISTRATION

For sale by the Clearinghouse for Federal Scientific and Technical Information
Springfield, Virginia 22151 – CFSTI price $3.00

EFFECT OF GROUND PROXIMITY ON THE LONGITUDINAL, LATERAL, AND CONTROL AERODYNAMIC CHARACTERISTICS OF A TILT-WING FOUR-PROPELLER V/STOL MODEL

By Kenneth W. Goodson
Langley Research Center

SUMMARY

A wind-tunnel investigation of a four-propeller tilt-wing V/STOL configuration was conducted to determine the longitudinal, lateral, and control aerodynamic characteristics in ground proximity. The tests were made utilizing the moving-belt ground plane.

The investigation showed that reductions in lift and drag occurred on the tilt-wing configuration when in ground proximity. Smoke-flow observations showed that ground proximity caused the slipstream to be deflected forward of the model. At certain ground heights and wing-tilt—flap-deflection angles, these self-generated disturbances became quite erratic. For some wing-flap angle combinations, the unsteady flow caused erratic yawing moments at 0° sideslip. Smoke-flow observations also showed that the ground-height-to-chord ratio at which the onset of flow recirculation occurred was proportional to the ratio of disk loading to free-stream dynamic pressure. The extent of the recirculation in front of the wing was dependent upon the wing-tilt angle at a given flap deflection and ground height.

Ground proximity reduced the aileron yaw control by about 50 percent for the design condition $\left(\delta_{a_L} = -50^{\circ};\ \delta_{a_L}\right.$ is the left-wing aileron deflection$\left.\right)$ at the lowest ground height of the tests. Increasing the aileron deflection to $\delta_{a_L} = -70^{\circ}$ and deflecting a 0.10-chord upper-surface spoiler increased the control yawing moment to about 70 percent of original out-of-ground-effect value obtained with $\delta_{a_L} = -50^{\circ}$. Ground proximity also considerably reduced the adverse rolling moment due to aileron deflection for yaw control.

INTRODUCTION

One of the problems encountered by tilt-wing V/STOL aircraft (both the XC-142, ref. 1, and the VZ-2, ref. 2) is that of self-generated disturbances experienced in ground proximity. These self-generated disturbances are encountered when the downward-deflected slipstreams impinge on the ground and are deflected forward of the aircraft

producing a disturbed region within which the aircraft must fly. The present investigation was undertaken to investigate these problems as well as to extend the work of references 3 and 4 and to explore the effects of various controls such as ailerons, spoilers, and differential propeller thrust.

The investigation was conducted on a 1/11-scale model in the 17-foot (5.18-meter) test section of the Langley 300-MPH 7- by 10-foot tunnel. Other related work on the same configuration is presented in references 5 and 6.

SYMBOLS AND COEFFICIENTS

This investigation covered simulated flight conditions in the transition speed range both in and out of ground proximity. In order to avoid the problems of conventional coefficients approaching infinity as the low-speed conditions are approached, the data are presented as coefficients based on the dynamic pressure in the slipstream. The coefficients based on slipstream dynamic pressure are indicated by the subscript s.

The positive directions of forces, moments, and angles are indicated in figure 1. Data for the complete model are presented about the stability axes with moments presented about the center of gravity, as shown in figures 1 and 2.

Measurements for this investigation were taken in the U.S. Customary Units. Equivalent values in the International System of Units (SI) are indicated herein in parentheses in the interest of promoting the use of this system in future NASA reports. Details concerning the use of SI, together with physical constants and conversion factors, are given in reference 7. (Also, see the appendix.)

A	propeller disk area, ft^2 $(meters^2)$
b	wing span, ft (meters)
c	wing chord, ft (meters)
$\bar{c}$	wing mean geometric chord, ft (meters)
$C_{D,s}$	drag coefficient based on slipstream, $\frac{Drag}{q_s S}$
$\Delta C_{D,s}$	incremental change in drag coefficient
$C_{L,s}$	lift coefficient based on slipstream, $\frac{Lift}{q_s S}$

$\Delta C_{L,s}$ incremental change in lift coefficient

$C_{l,s}$ rolling-moment coefficient based on slipstream, $\frac{\text{Rolling moment}}{q_s S b}$

$\Delta C_{l,s}$ incremental change in rolling-moment coefficient

$C_{m,s}$ pitching-moment coefficient based on slipstream, $\frac{\text{Pitching moment}}{q_s S \bar{c}}$

$\Delta C_{m,s}$ incremental change in pitching-moment coefficient

$C_{n,s}$ yawing-moment coefficient based on slipstream, $\frac{\text{Yawing moment}}{q_s S b}$

$\Delta C_{n,s}$ incremental change in yawing-moment coefficient

$C_{T,s}$ average slipstream thrust coefficient based on slipstream and total thrust of all propellers, $\frac{\text{Thrust}}{q_s N \frac{\pi D^2}{4}}$

$C_{Y,s}$ side-force coefficient based on slipstream, $\frac{\text{Side force}}{q_s S}$

D propeller diameter, ft (meters)

h height of fuselage bottom above ground, ft (meters)

h_r height for onset of flow recirculation, ft (meters)

$h/\bar{c}$ ground-height ratio (ratio of fuselage height above ground to wing mean geometric chord)

i_t horizontal-tail incidence angle with respect to fuselage reference line, deg

i_w wing-tilt angle with respect to fuselage reference line, deg

N number of propellers

q free-stream dynamic pressure, $\frac{1}{2}\rho V^2$, lbf/ft^2 $(newtons/meter^2)$

q_s slipstream dynamic pressure, $q + \frac{T}{N\frac{\pi D^2}{4}}$, lbf/ft^2 (newtons/meter^2)

R maximum radius of propellers, ft (meters)

r propeller radius to any section, ft (meters)

S wing area, ft^2 (meters^2)

T total thrust of all propellers, lbf (newtons)

V free-stream velocity, ft/sec (meters/sec)

V_{belt} belt linear speed, ft/sec (meters/sec)

x forward extent of recirculation from wing pivot, ft (meters)

α angle of attack of fuselage reference line, deg

β angle of sideslip, deg

$\gamma_{h/\bar{c}}$ flight-path angle, $\tan^{-1}\frac{C_{D,s}}{C_{L,s}}$, deg

δ_a aileron deflection (positive when trailing edge is down), deg

δ_f flap deflection, deg

δ_v flap vane deflection, deg

ρ mass density of air, slugs/ft^3 (kilograms/meter^3)

Subscripts:

corr corrected

meas measured

inboard portion of flap inboard of inboard nacelles

outboard	portion of flap outboard of inboard nacelles
L	left wing
R	right wing
∞	out of ground proximity

MODEL AND APPARATUS

A drawing of the 1/11-scale complete model showing the important dimensions, airfoil sections, and other physical characteristics is presented in figure 2. The drawing shows the wing at 0° and 90° incidence (tilt angle). The wing construction consisted of an aluminum box spar covered with mahogany to give the airfoil contours. The wing was fitted with a double-slotted flap. (See fig. 3.) The double-slotted-flap deflection could be varied in 10° increments from 0° to 90° depending upon the wing-tilt—flap-deflection program for the model. For flap deflections of 0° to 30°, the vane of the double-slotted flaps was removed because the space was needed for motor-power and strain-gage leads; however, for flap deflections of 40°, 50°, 60°, and 80°, the vane was deflected 10°, 20°, 30°, and 50°, respectively. The wing-tilt angle could be changed remotely through an angle range from 0° to 90° with an electric motor operated mechanism; the angle was determined with a calibrated template. Figure 4(a) shows details of the leading-edge slat configuration used on the wing in conjunction with the flaps. Wing upper-surface spoilers and fuselage nose strakes are shown in figures 4(b) and 4(c), respectively.

The fuselage construction consisted of an aluminum frame covered with mahogany panels. A sketch showing fuselage cross sections is presented in figure 5. Wing-fuselage ramps used to improve the airflow in the center section are shown in figure 6. The all-movable horizontal tail could be set at various incidence angles.

The geometric characteristics of the propellers are shown in figure 7. The propellers were mounted 5.6 percent propeller diameter below the section wing chord line. The four-blade propellers were constructed of resin-bonded glass fibers over a balsa-wood core. The propellers were driven by four variable-frequency $7\frac{1}{2}$-horsepower (5600-watt) electric motors. The directions of rotation of the propellers are shown in figure 2. Each electric motor was instrumented to record the propeller thrust.

Photographs of the sting-supported model mounted on an electrical strain-gage balance in the 17-foot (5.18-meter) test section over the moving-belt ground plane are shown in figure 8. The tufts seen in these photographs were used to study the airflow stall behavior. A sketch showing some detail of the moving ground belt is shown in

figure 9. For some tests, a smoke generator was used to visualize the flow field around the model. The smoke generator consisted of a 1-inch-diameter (2.54-centimeter) copper pipe secured to a 7500-Btu/hr (2200-watt) electric heater. Kerosene was injected under low pressure into the hot copper pipe to generate the smoke.

TESTS

The investigation was conducted in the 17-foot (5.18-meter) test section of the Langley 300-MPH 7- by 10-foot tunnel, which is described in reference 8.

Test conditions were established out of ground proximity for the model at $\alpha = 0^{\circ}$ for the various wing-tilt—flap-deflection angles with the propellers operating at 7000 rpm by increasing the wind-tunnel airspeed until thrust-drag equilibrium (at $\alpha = 0^{\circ}$) was obtained. The tunnel dynamic pressures thus determined were used for other ground heights of this investigation at a given wing-tilt angle. This technique gives nominal out-of-ground-effect-level flight characteristics directly as well as showing what happens to the configuration as it moves closer to the ground plane. The thrust coefficients presented in this report are based on the total propeller thrust measured for each test point.

The thrust coefficient established at zero angle of attack did not remain constant because of changes in propeller characteristics with change in angle of attack as can be seen on the various data figures. The power-on tests were made at a slipstream dynamic pressure of approximately 10 lbf/ft^2 (478.8 newtons/meter^2). It should be noted that at the beginning of the test program an attempt was made to match the thrust of all propellers through the speed range. Some tests were made to determine the effect of asymmetric thrust on the aerodynamic characteristics by increasing the rpm (rotational speed) of the propellers on one wing panel while decreasing, by a like increment, the rpm of the propellers on the opposite wing panel. The effects of differential flaps were investigated by deflecting the flap sections between the two inboard nacelles at different angles from those of the flap sections outboard of the inboard nacelles. For most tests, the propellers on each wing panel rotated in the same direction (see fig. 2). However, for some tests, the outboard propeller rotation was reversed so that the upgoing blades were between the nacelles for a given wing semispan.

Ground-effect tests were made at several ground-height ratios with $h/\bar{c} = 4.20$ being the upper limit of the sting vertical travel. This upper limit, based on past experience, was considered to be essentially out of ground proximity for the present model. The model heights were measured relative to the bottom of the fuselage at $\alpha = 0^{\circ}$ with propeller power off. Small changes in the measured ground heights occur because of sting deflections due to lift and propeller thrust and because of translation of the fuselage reference point due to rotation of the angle-of-attack mechanism at various heights. For

the purpose of the present paper, these height changes do not affect the relative comparison of the data and consequently the heights have not been corrected. If height corrections are desired they can be obtained by use of the following equation:

$$h_{corr} = 38.4(1 - \cos \alpha) + (h_{meas})_{\alpha=0^o} \cos \alpha + 0.004(C_{L,s} \cos \alpha + C_{D,s} \sin \alpha) q_s S \cos \alpha$$

where $q_s \approx 10$ lbf/ft^2 (478.8 newtons/meter^2) for the model tests. All ground-proximity tests were made utilizing the moving-belt ground plane to eliminate the ground-plane boundary layer. The boundary layer was eliminated by bringing the belt linear speed up to that of the tunnel airstream. A few tests were made simulating a 16.9-ft/sec (5.15-meter/sec) head wind (over ground) by reducing the belt speed to the appropriate value.

The Reynolds number of these tests, based on the mean aerodynamic chord of 8.8 inches (23.35 centimeters) and the slipstream dynamic pressure of 10 lbf/ft^2 (478.8 newtons/meter^2), was about 0.51×10^6.

A study (ref. 9) of the effects of tunnel walls on the aerodynamic characteristics of V/STOL configurations, which uses the method of reference 10, shows that for small model-to-tunnel-size ratios, the corrections to lift and drag are small. In view of these findings and the relatively small size of the present model, wall corrections have not been applied to the present results.

Flow visualization tests were made by ejecting a 1-inch-diameter (2.54-centimeter) stream of smoke beneath the wing and between the nacelles of the right wing panel. Tests were made to determine the ground height at which flow recirculation was first encountered by setting up the equilibrium condition out of ground effect for a given wing-flap configuration (at $\alpha = 0^o$) and then lowering the model until recirculation of flow beneath the model was observed. Additional tests were made at a sensitive ground height ($h/\bar{c} = 1.08$) to determine the forward extent of the recirculation. Visual recordation of the smoke-flow recirculation was necessary because the smoke supply available became so diluted as not to respond to photography.

PRESENTATION OF RESULTS

Results of the present investigation are presented in the following figures:

	Figure
Longitudinal aerodynamic characteristics:	
Effect of ground belt moving and stopped	10
Ground-height effect for various wing-flap configurations ($i_t = 20^o$)	11

Figure

Comparison for several wing-tilt angles at $h/\bar{c} = 4.20$, 1.08, and 0.40 12
Effect of differential flap deflection 13
Effect of horizontal-tail incidence $(i_w = 30^o, \delta_f = 60^o)$ 14

Lateral aerodynamic characteristics in sideslip:
Repeatability of sideslip data 15
Ground-height effects for various wing-flap configurations $(i_t = 20^o)$ at –
$\alpha = 0^o$ 16
$\alpha = 10^o$ 17
Comparison of several wing-flap configurations at $h/\bar{c} = 4.20$, 1.08, and 0.40 . . . . . 18 to 20
Effect of differential flap deflection 21
Effect of simulated head wind 22
Effect of fuselage nose strakes 23
Effect of direction of propeller rotation 24

Control aerodynamic characteristics:
Effect of aileron deflection over a ground-height range ($\alpha = 0^o$, $\beta = 0^o$) 25
Effect of aileron-spoiler deflection over a ground-height range ($\alpha = 0^o$, $\beta = 0^o$) 26
Effect of aileron deflection in sideslip 27
Effect of spoiler deflection in sideslip 28
Effect of asymmetric rpm in sideslip 29
Variation of aerodynamic coefficients with asymmetric rpm ($\alpha = 0^o$, $\beta = 0^o$) for –
Various ground-height ratios $(\delta_a = 0^o)$ 30
Various aileron deflections 31
Spoiler off and on; aileron on 32

Flow visualization:
Variation of flow recirculation height-chord ratio with ratio of propeller disk loading to dynamic pressure for various wing-tilt angles 33
Forward extent of disturbed flow as a function of wing-tilt angles at $h/\bar{c} = 1.08$ 34

Summary:
Effect of ground proximity on lift and drag coefficients 35
Lateral characteristics in sideslip . . . . . 36 and 37
Variation of roll and yaw sideslip derivatives with ground-height ratio . . . 38 and 39
Effect of lateral controls through the ground-height range 40

DISCUSSION

The present investigation was undertaken primarily to investigate problem areas indicated by flight tests of the airplane. The problems occurred during landing transitions and were believed to be associated with self-generated disturbances which affected the longitudinal, lateral, and control aerodynamic characteristics of the airplane. In order to investigate the problem area, it was deemed necessary to obtain additional longitudinal data for the configuration for wing-flap combinations not previously obtained. (See refs. 3 and 4.) These additional longitudinal data are presented in figures 10 to 14. Since the problem areas also seemed to be connected with lateral aerodynamic characteristics of the airplane, a considerable amount of data was obtained with the model sideslipped for various wing-flap configurations, ground heights, directions of propeller rotation, and so forth. (See figs. 15 to 24.) Also, because of the control problems associated with the landing transitions, the various controls (ailerons, spoiler, and differential thrust) were investigated in sideslip at several ground heights as shown in figures 25 to 32. Results of smoke-flow observations are presented in figures 33 and 34. The data are summarized in figures 35 to 40.

Because the results of reference 2 showed that ground-plane boundary layer could appreciably affect the aerodynamic characteristics of tilt-wing configurations, the present data were obtained with the ground-plane boundary layer removed. Figure 10 illustrates the effect of removing the boundary layer $\left(V_{belt} = V\right)$ for a typical wing-flap combination $\left(i_w = 30^o, \ \delta_f = 60^o\right)$. For more information on effect of ground-plane boundary layer, see reference 2. Details on the installation and operation of the moving-belt ground plane are presented in reference 11. It is interesting to note the good repeatability of data as shown in figure 15. Discussion of the present results will be concerned with the stated problems. The bulk of data is presented for further analysis by the reader if desired.

Longitudinal and Lateral Aerodynamic Characteristics

The present longitudinal results, in general, substantiate the ground-effect losses in lift and drag reported in reference 2. (See figs. 11, 12, and 35.) These losses in ground effect are associated with flow recirculation effects as illustrated in figures 33 and 34. Figure 33 shows (from smoke-flow visualization studies) that the height-to-chord ratio at which the onset of flow recirculation occurs is essentially proportional to the ratio of disk loading to dynamic pressure, as indicated by the straight line fairing through the experimental data. The equation of the faired line is $\frac{h_r}{\bar{c}} = 0.16\left(\frac{T/A}{q}\right)^{1.13}$. In addition, the forward extent of the recirculation at a given height, as expected, is dependent upon the wing-tilt angle for a given flap deflection. (See fig. 34.)

The smoke-flow studies showed that very erratic flows were generated at certain ground heights. For example, for $i_w = 45^o$ and $\delta_f = 60^o$, the smoke stream ejected under the wing between the inboard and outboard nacelles at a ground-height ratio of $h/\bar{c} = 1.08$ (measured from fuselage bottom) showed that the recirculation vortex flow was moving inboard underneath the wing, generally toward the fuselage nose, and then was swept upward and back over the fuselage. For this wing-flap combination, the fact that the fluctuating flows seemed to attach and detach from the fuselage nose at $h/\bar{c} = 1.08$ indicated that perhaps this was the cause of the problems encountered on the airplane. The fluctuating flow caused erratic changes in yawing moments at 0^o sideslip; however, as the sideslip angle was increased slightly (within $\beta = \pm 5^o$), the flows became established and the yaw (as well as roll) was repeatable. (See figs. 16, 17, 36, and 37.) When the model height was increased, the recirculation intensity became less and the flow tended to move outboard before being swept downstream. When moved to a lower ground height ($h/\bar{c} = 0.40$), the erratic flows subsided considerably and the yawing and rolling moments became reasonably steady at $\beta = 0^o$. In order to determine whether the fluctuating flow on the nose was the contributing factor in the erratic yawing moments, strakes were attached to the sides of the fuselage nose. The fuselage nose strakes had no appreciable effect on the measured results in sideslip – probably because of the low dynamic pressure at the nose. (See fig. 23.) Some tests were then made to determine the effect of changing the wing spanwise loading by deflecting the flaps differentially. (See figs. 13 and 21.) These results show that the discontinuity in yawing-moment coefficient with sideslip between $\beta = \pm 5^o$ was improved somewhat, indicating that the erratic yawing moments were produced by the wing and propellers. To pursue this further, the direction of rotation of the outboard propellers was reversed. The change in the direction of propeller rotation (fig. 24) improved the erratic yawing-moment characteristics but also reduced somewhat the directional stability. (Although data are not available for the model of the present investigation, it should be noted that changing the direction of propeller rotation could affect wing stall and the descent capability of the configuration.)

It is apparent that the tilt-wing configuration must, by nature, traverse the self-induced disturbances at some point in its transition from forward speed to hover. Several wing-flap combinations were investigated to see whether a wing-flap program could be achieved which would avoid the erratic, self-induced flows at low speeds in ground proximity. The smoke-flow studies and force data show that the disturbances cannot be avoided, although the effects may be minimized somewhat by proper programing of the wing and flap or possibly by change of propeller rotation. As indicated by reference 12, properly located wing fences and vertical location of the thrust line might also improve the flow characteristics.

The directional stability of the four-propeller tilt wing is generally low (figs. 16 to 20, 38, and 39) and varies considerably, depending upon the wing-flap combination and the ground height. The effective dihedral is also low, but it is less affected by configuration and ground height than the directional stability.

Since wind-tunnel tests show that the ground-plane boundary layer can alter the aerodynamic characteristics (ref. 4), the present configuration was tested (in sideslip) with the ground-plane belt speed reduced to simulate the effect of a 16.9-ft/sec (5.15-meter/sec) head wind such as might be encountered in take-off or landing under wind conditions. The effect of this head wind was found to be small or negligible. (See fig. 22.)

Control Characteristics

Because of the erratic nature of the yawing moment of some wing-flap combinations caused by self-induced disturbances and because of the low directional stability of the tilt wing, adequate lateral control capability is of primary importance. To determine the control capability, the present model was tested extensively with various control inputs (that is, ailerons, spoilers, and asymmetric rpm).

As shown in figure 25 for $i_w = 30^\circ$ and 45° $\left(\delta_f = 60^\circ\right)$, the aileron yaw control capability is considerably reduced as the ground is approached. For the design condition $\left(\delta_{a_L} = -50^\circ\right)$, the aileron yaw control was reduced by about 50 percent at the lowest ground height ($h/\bar{c} = 0.40$). These reduced yaw control characteristics can be overcome somewhat by increasing the aileron deflection beyond the design value of $\delta_{a_L} = -50^\circ$ to $\delta_{a_L} = -70^\circ$ and by addition of an upper-surface spoiler to the up-aileron wing. (See figs. 25, 26, and 40.) The spoiler increases the yaw control substantially throughout the ground-height range. The combination of $\delta_{a_L} = -70^\circ$ and a 0.10-chord spoiler on the left wing gave a yaw-control increment $\Delta C_{n,s} \approx 0.035$ at the lowest ground height of the tests ($h/\bar{c} = 0.40$), which is about 70 percent of the out-of-ground-effect value obtained with the maximum design aileron deflection of $\delta_{a_L} = -50^\circ$. (See fig. 40.) An additional yaw increment was also obtained $\left(\text{for } i_w = 45^\circ \text{ to } 60^\circ\right)$ by deflecting the aileron downward on the right wing. (See the data of fig. 31 at the symmetrical 7000-rpm condition.) It should be noted that for some wing-tilt—flap-deflection combinations, yaw control (aileron and spoiler deflection) produces unfavorable rolling moments. At low transition speeds (near hover – large wing-tilt angles), it is desirable to keep the roll changes associated with yaw control as small as possible to avoid attitude changes when changing heading. The adverse roll due to yaw control is, as far as roll control is concerned, of small consequence since roll control at these tilt angles is provided by the use of differential thrust across the wing span. The rolling moment due to yaw control, like the

yawing moment, is also greatly reduced when in close ground proximity. (See figs. 25, 26, and 40.) It should be noted that application of differential thrust in a direction to correct for the adverse roll due to yaw control also adds a favorable increment of yawing moment. (See figs. 29 and 31 at 7000 rpm.)

The effect of the ailerons $\left(\delta_{a_L} = -50^{\circ}\right)$ and the spoiler on the lateral aerodynamic characteristics in sideslip is shown in figures 27 and 28, respectively, at $h/\bar{c} = 1.08$. The improvement in yawing moment remains fairly constant over the sideslip range of this investigation. Note, however, that at large positive sideslip angles (fig. 27(b)), the aileron yaw control does introduce some nonlinearities in the rolling-moment coefficient – probably due to flow separation effects. The application of differential thrust to produce a positive roll eliminates this nonlinearity in roll with sideslip (fig. 29).

The pitching-moment data are affected to various degrees by use of lateral controls, the degree varying with wing-tilt angle and the control used. The pitching moment poses no special control problem other than the change in trim and control programing through the speed range since the tail rotor (not used in these tests) is a powerful pitch control.

It should be remembered that the aforementioned observations are general and that at different wing-flap combinations the characteristics will vary somewhat.

CONCLUDING REMARKS

A wind-tunnel investigation of a four-propeller tilt-wing V/STOL configuration was conducted in ground proximity with various wing-tilt—flap-angle combinations in sideslip and pitch, and with various control inputs.

The results showed losses in lift and drag due to ground proximity associated with flow recirculation effects. Smoke-flow observations showed that ground proximity caused the slipstream to be deflected forward of the model, the forward extent of the recirculation being dependent upon the wing-tilt angle for a given flap deflection and ground height.

The smoke-flow observations also showed that very erratic flows occurred for certain wing-tilt—flap-deflection angles, especially for a wing-tilt angle of 45° and a flap deflection of 60° at a ground-height-to-chord ratio ($h/\bar{c}$) of 1.08. The unsteady flows experienced for this wing-flap combination produced very erratic yawing moments at 0° sideslip. The smoke-flow observations showed that the ground-height-to-chord ratio at which onset of flow recirculation occurred was essentially proportional to the ratio of disk loading to free-stream dynamic pressure.

Ground proximity reduced the aileron yaw control by about 50 percent for the design control condition $\left(\delta_{a_L} = -50^{\circ};\ \delta_{a_L}\right.$ is the left-wing aileron deflection$\left.\right)$ at the lowest ground height of the tests ($h/\bar{c} = 0.40$). Increasing the aileron deflection to $\delta_{a_L} = -70^{\circ}$ and adding an upper-surface spoiler to the wing increased the control yawing moment at $h/\bar{c} = 0.40$ to about 70 percent of the value obtained out of ground effect with $\delta_{a_L} = -50^{\circ}$.

Langley Research Center,
National Aeronautics and Space Administration,
Langley Station, Hampton, Va., March 9, 1967,
721-01-00-35-23.

APPENDIX

CONVERSION TO INTERNATIONAL SYSTEM OF UNITS (SI)

Factors required for converting the U.S. Customary Units used herein to the International System of Units (SI) are given in the following table:

Physical quantity	U.S. Customary Unit	Conversion factor (*)	SI Unit
Area	ft^2	0.0929	$meters^2$ (m^2)
Density	$slugs/ft^3$	515.379	$kilograms/meter^3$ (kg/m^3)
Force	lbf	4.4482	newtons (N)
Length	in.	2.54	centimeters (cm)
	ft	0.3048	meters (m)
Moment	ft-lbf	1.3558	meter-newtons (m-N)
Power	horsepower (hp)	746	watts (W)
	Btu/hr	0.2929	watts (W)
Pressure	lbf/ft^2	47.8803	$newtons/meter^2$ (N/m^2)
Velocity	ft/sec	0.3048	meters/second (m/sec)

*Multiply value given in U.S. Customary Unit by conversion factor to obtain equivalent value in SI Unit.

REFERENCES

1. Goodson, Kenneth W.: Comparison of Wind-Tunnel and Flight Results on a Four-Propeller Tilt-Wing Configuration. Conference on V/STOL and STOL Aircraft, NASA SP-116, 1966, pp. 51-62.

2. Kuhn, Richard E.: Ground Effects on V/STOL and STOL Aircraft. Conference on Aircraft Operating Problems, NASA SP-83, 1965, pp. 287-298.

3. Goodson, Kenneth W.: Longitudinal Aerodynamic Characteristics of a Flapped Tilt-Wing Four-Propeller V/STOL Transport Model. NASA TN D-3217, 1966.

4. Goodson, Kenneth W.: Ground Effects on a Four-Propeller Tilt-Wing Configuration Over a Fixed and a Moving Ground Plane. NASA TN D-3938, 1967.

5. Deckert, Wallace H.; Page, V. Robert; and Dickinson, Stanley O.: Large-Scale Wind-Tunnel Tests of Descent Performance of an Airplane Model With a Tilt Wing and Differential Propeller Thrust. NASA TN D-1857, 1964.

6. Newsom, William A., Jr.; and Kirby, Robert H.: Flight Investigation of Stability and Control Characteristics of a 1/9-Scale Model of a Four-Propeller Tilt-Wing V/STOL Transport. NASA TN D-2443, 1964.

7. Mechtly, E. A.: The International System of Units – Physical Constants and Conversion Factors. NASA SP-7012, 1964.

8. Kuhn, Richard E.; and Hayes, William C., Jr.: Wind-Tunnel Investigation of Longitudinal Aerodynamic Characteristics of Three Propeller-Driven VTOL Configurations in the Transition Speed Range, Including Effects of Ground Proximity. NASA TN D-55, 1960.

9. Staff of Powered-Lift Aerodynamics Section, NASA Langley Res. Center: Wall Effects and Scale Effects in V/STOL Model Testing. AIAA Aerodynamic Testing Conference, Mar. 1964, pp. 8-16.

10. Heyson, Harry H.: Linearized Theory of Wind-Tunnel Jet-Boundary Corrections and Ground Effect for VTOL-STOL Aircraft. NASA TR R-124, 1962.

11. Turner, Thomas R.: A Moving-Belt Ground Plane for Wind-Tunnel Ground Simulation and Results for Two Jet-Flap Configurations. NASA TN D-4228, 1967.

12. Hassell, James L., Jr.; and Kirby, Robert H.: Descent Capability of Two-Propeller Tilt-Wing Configurations. Conference on V/STOL and STOL Aircraft, NASA SP-116, 1966, pp. 41-50.

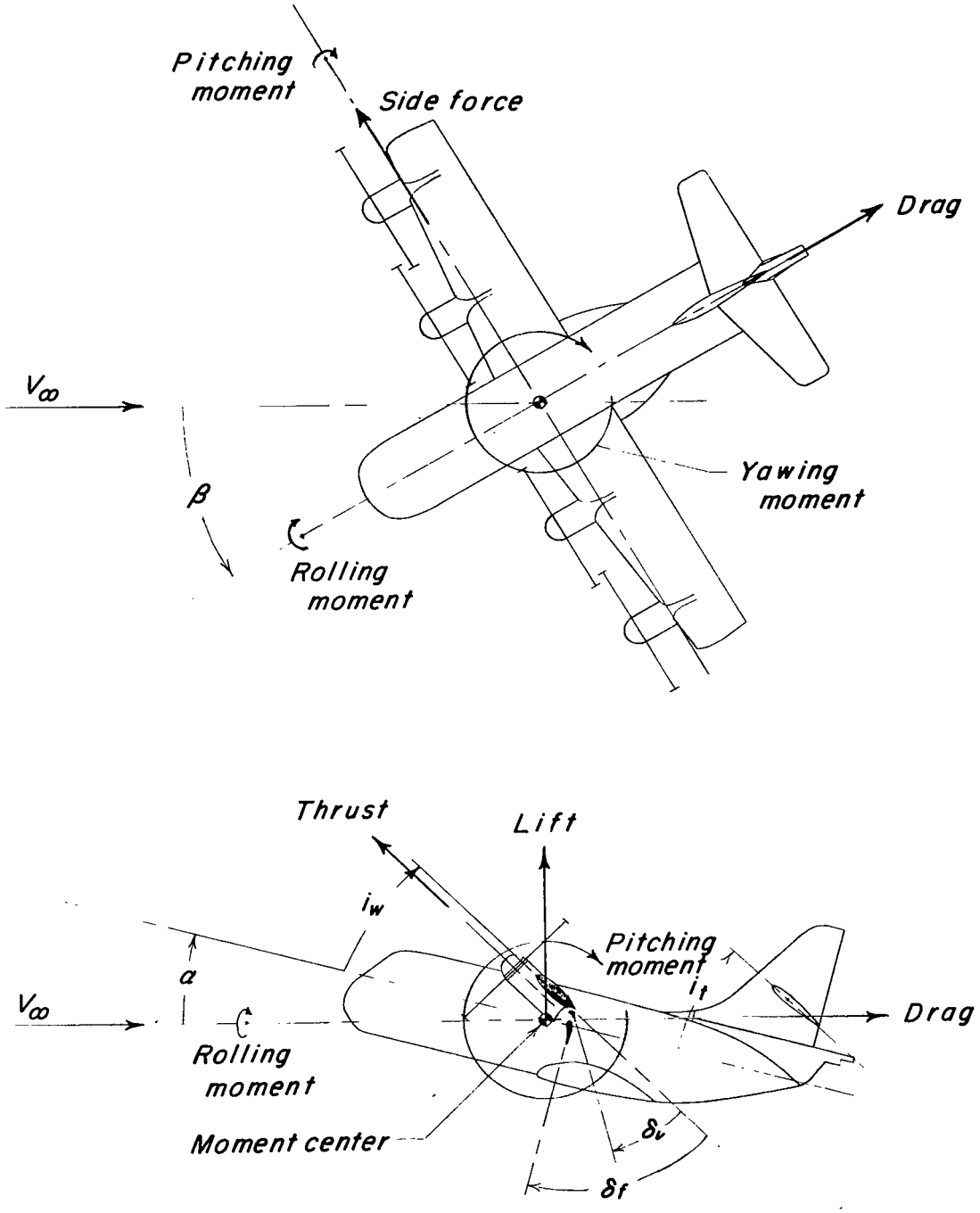

(a) Complete model.

Figure 1.- System of axes. Positive directions of forces, moments, and angles are indicated by arrows.

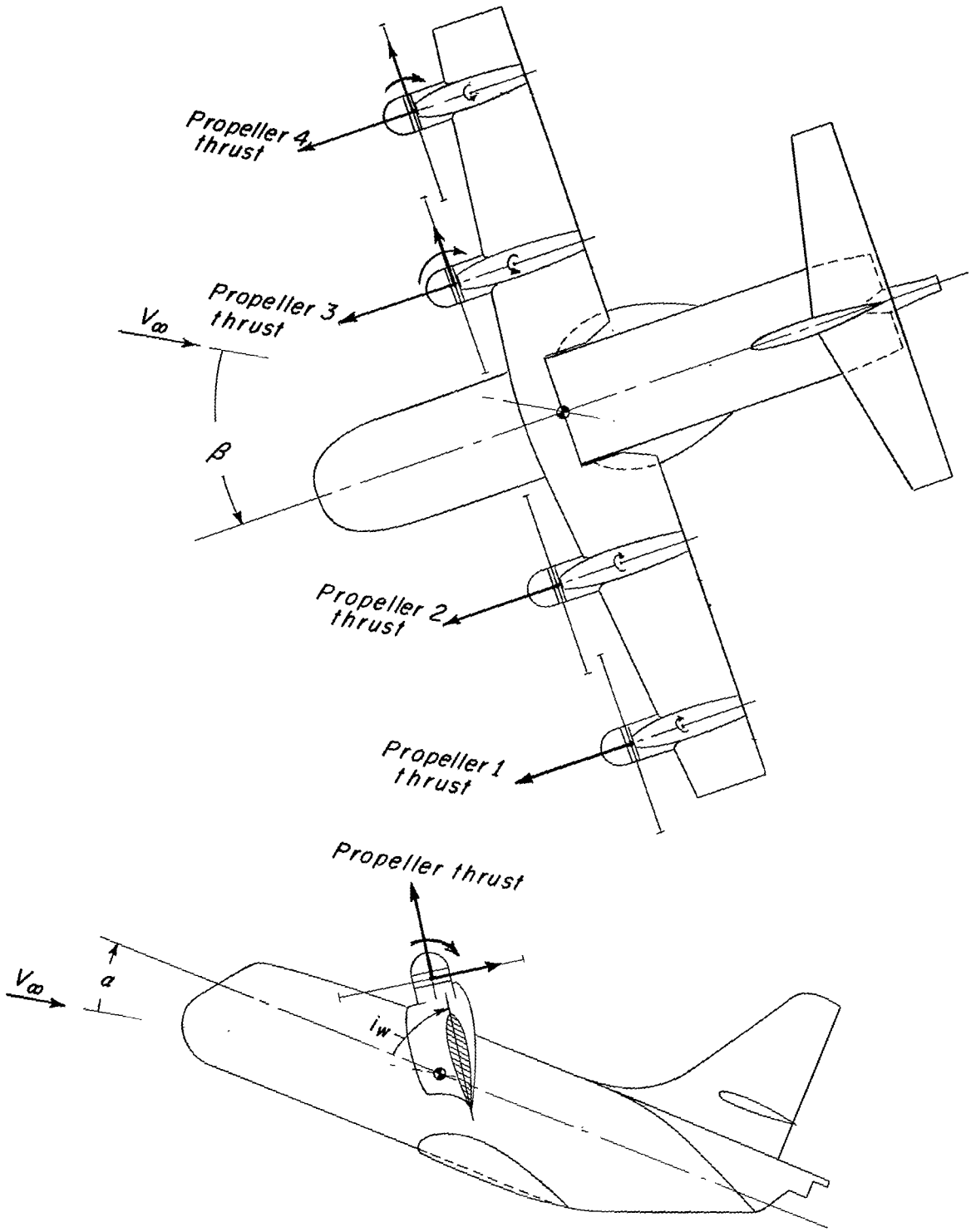

(b) Propellers.

Figure 1.- Concluded.

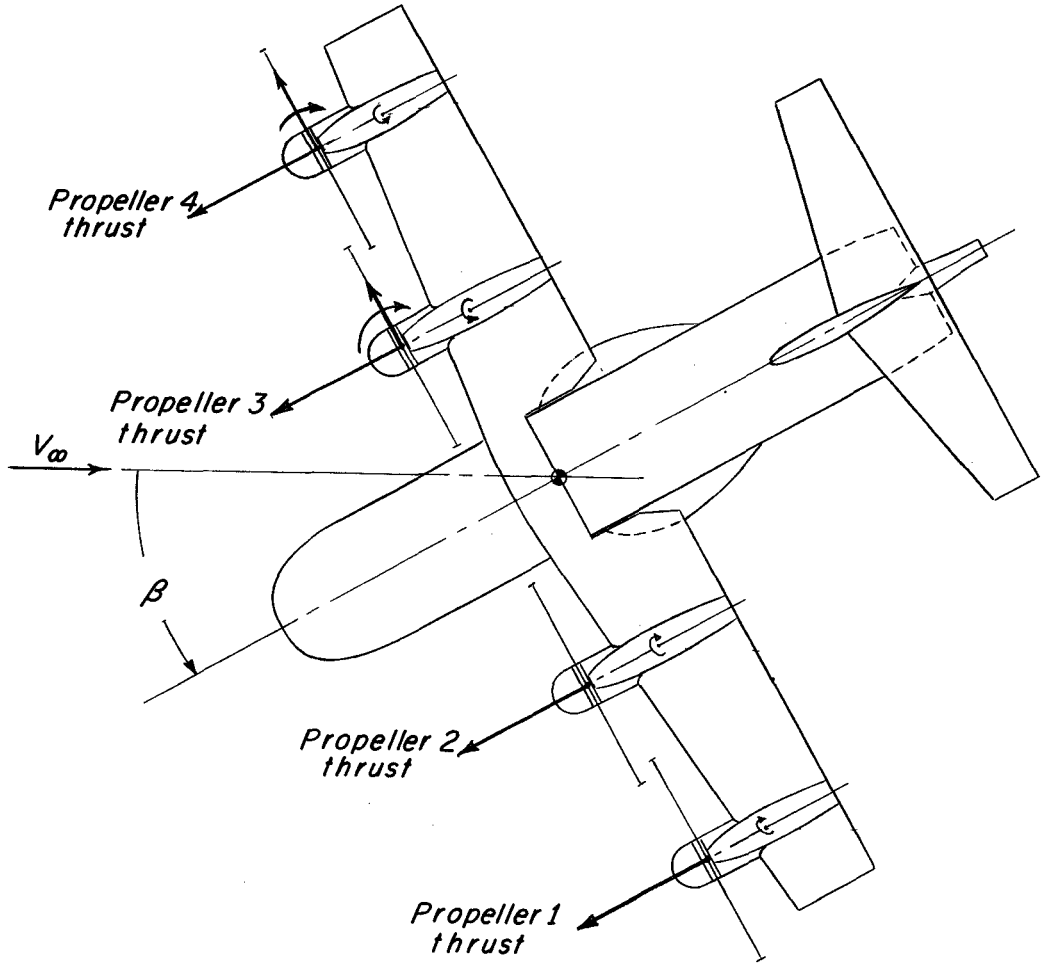

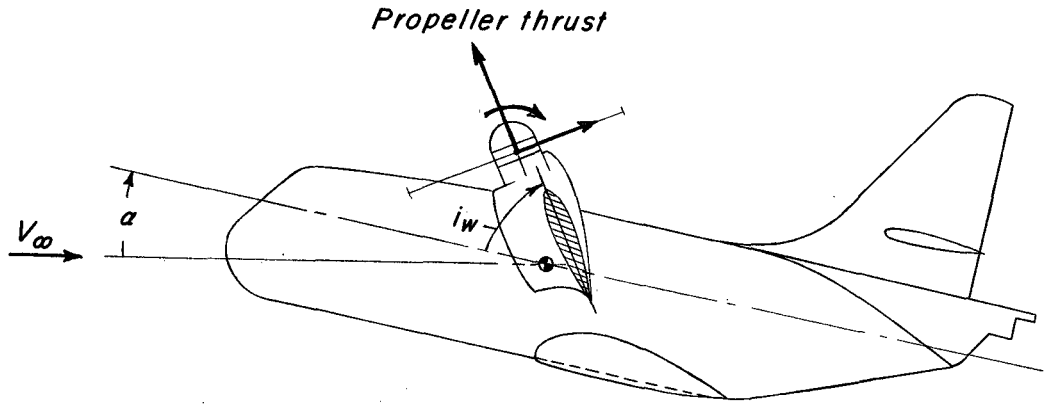

(b) Propellers.

Figure 1.- Concluded.

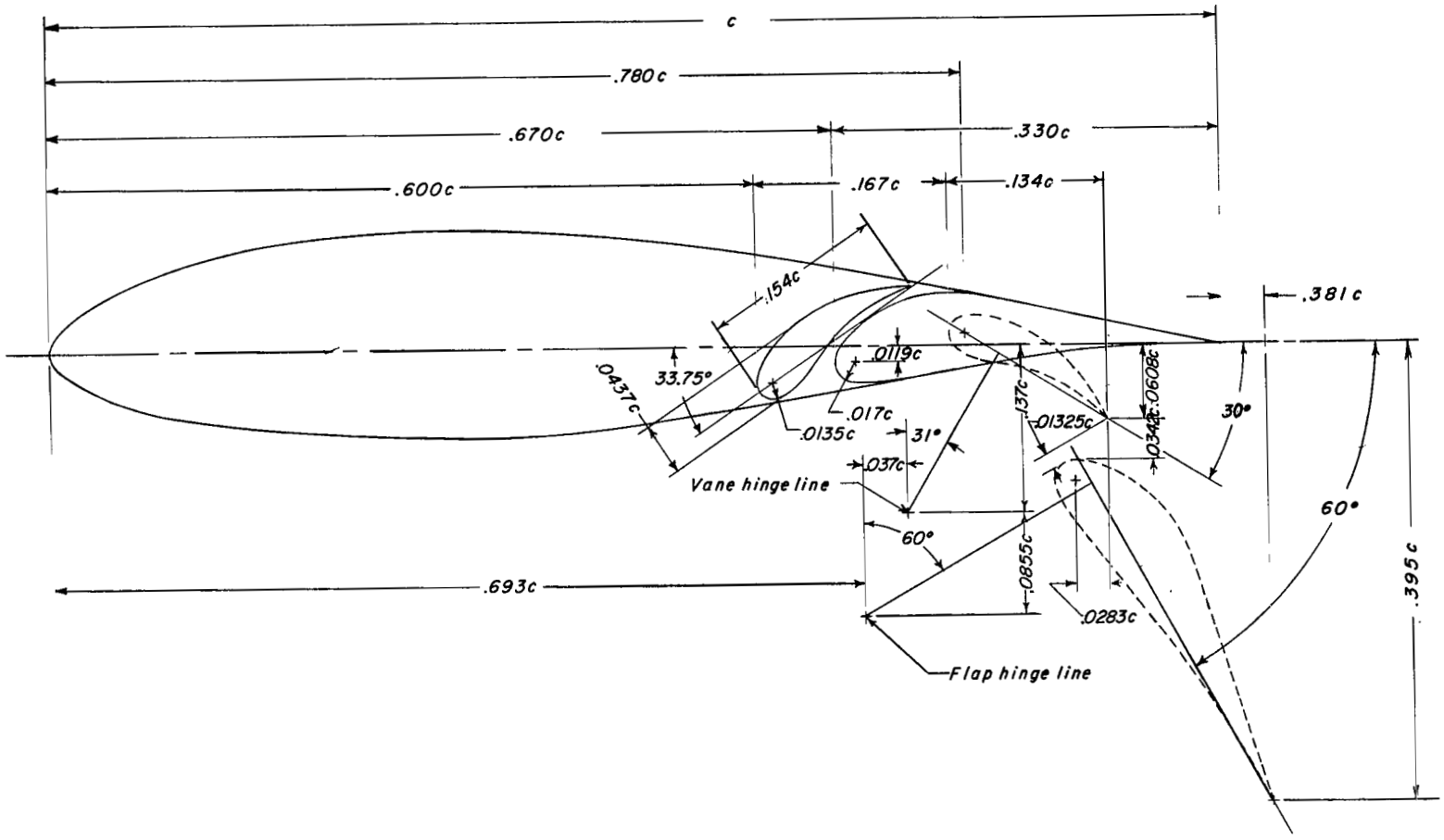

Figure 3.- Details of the flap system of the 1/11-scale tilt-wing VTOL model.

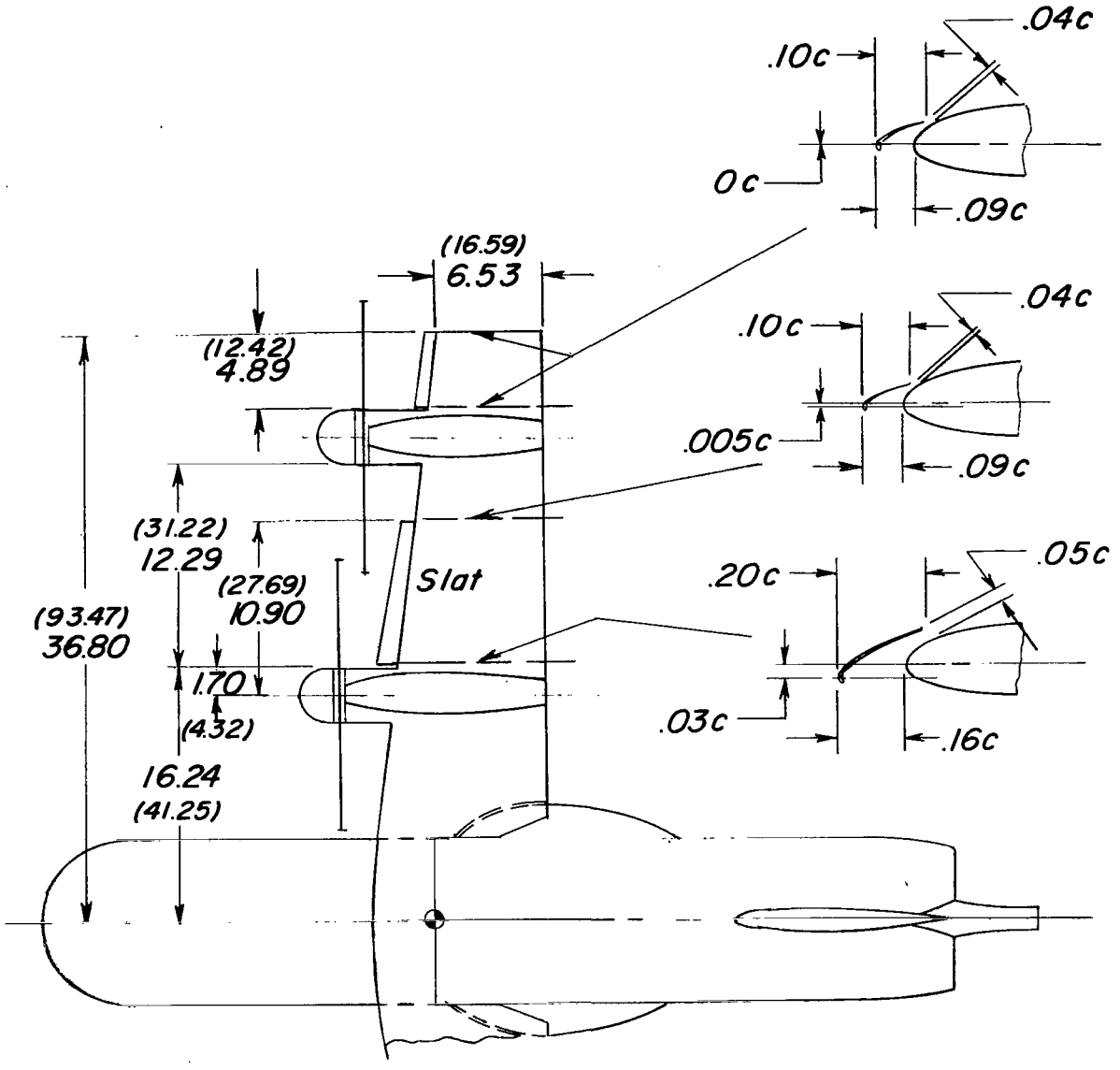

(a) Wing leading-edge slats.

Figure 4.- Details of the wing leading-edge slats, fuselage-nose strakes, and wing spoilers of the 1/11-scale tilt-wing VTOL model. All dimensions in inches; parenthetical values in centimeters.

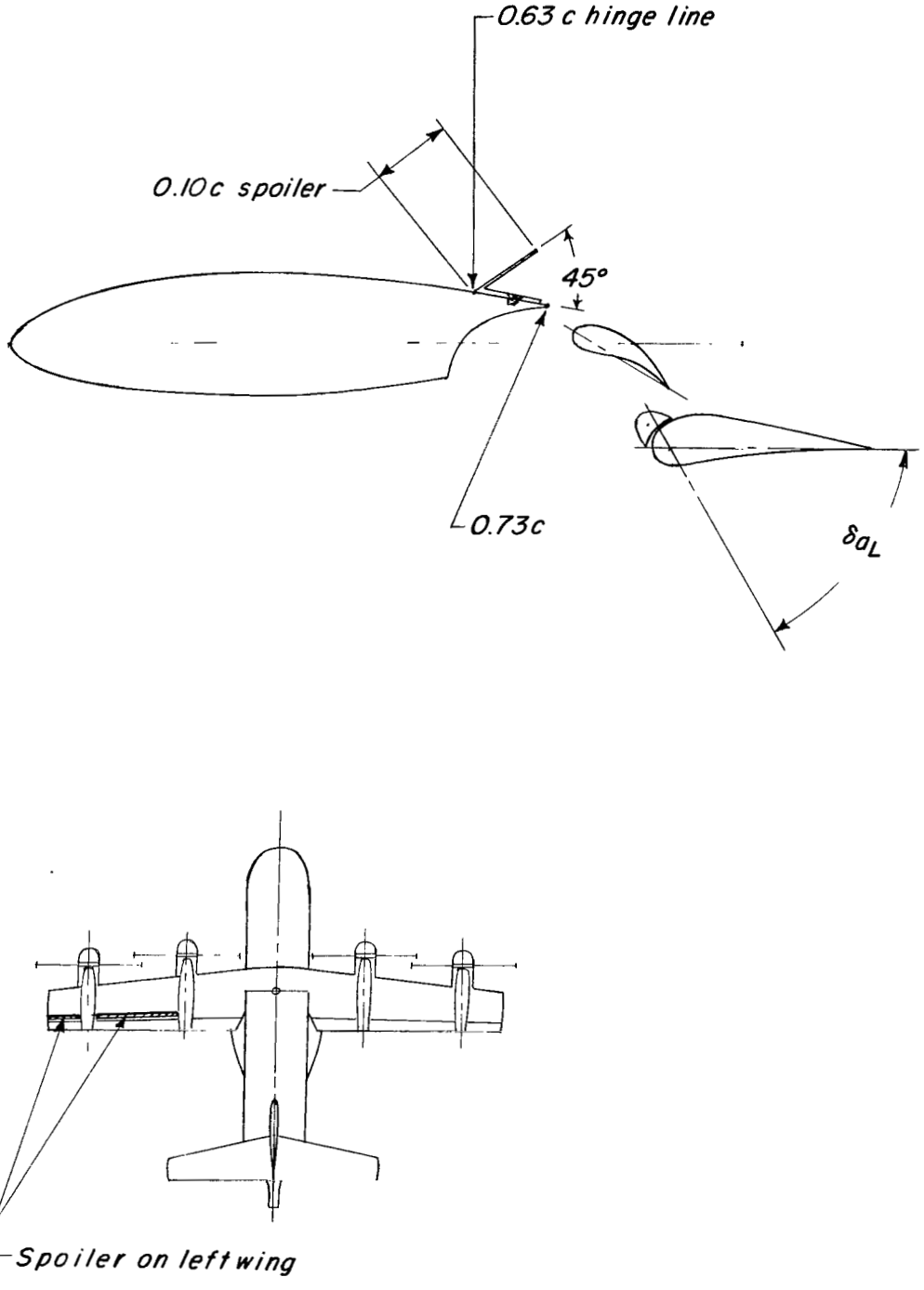

(b) Wing upper-surface spoiler.

Figure 4.- Continued.

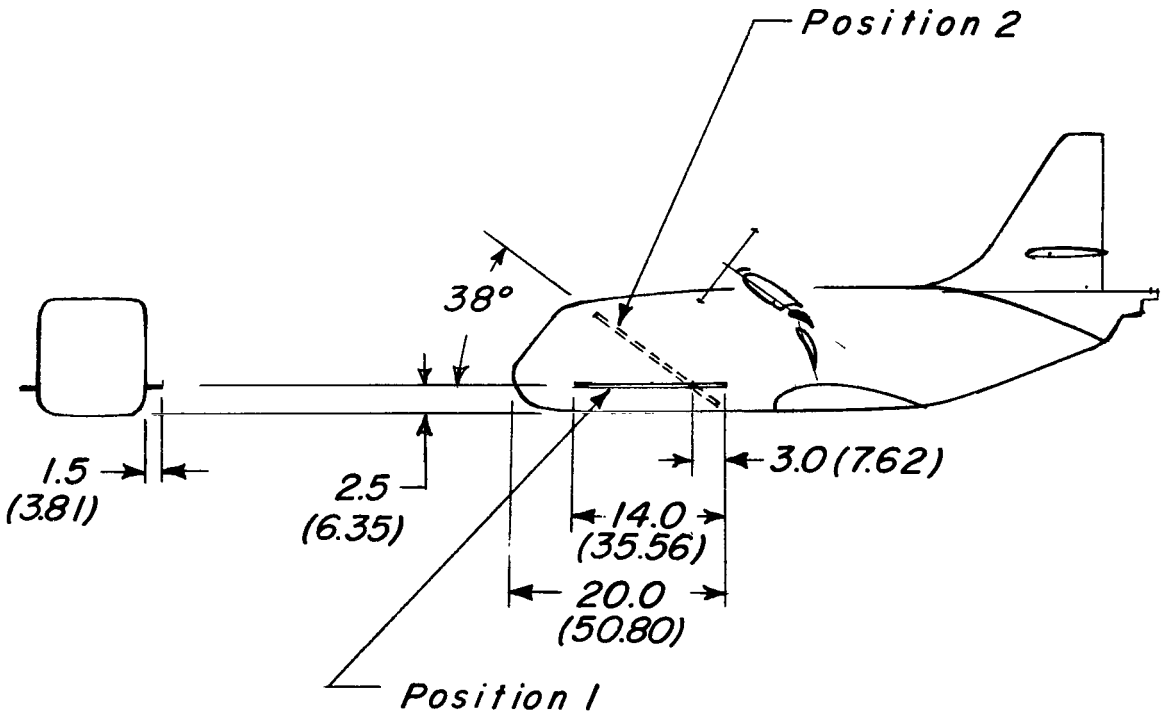

(c) Fuselage nose strakes.

Figure 4.- Concluded.

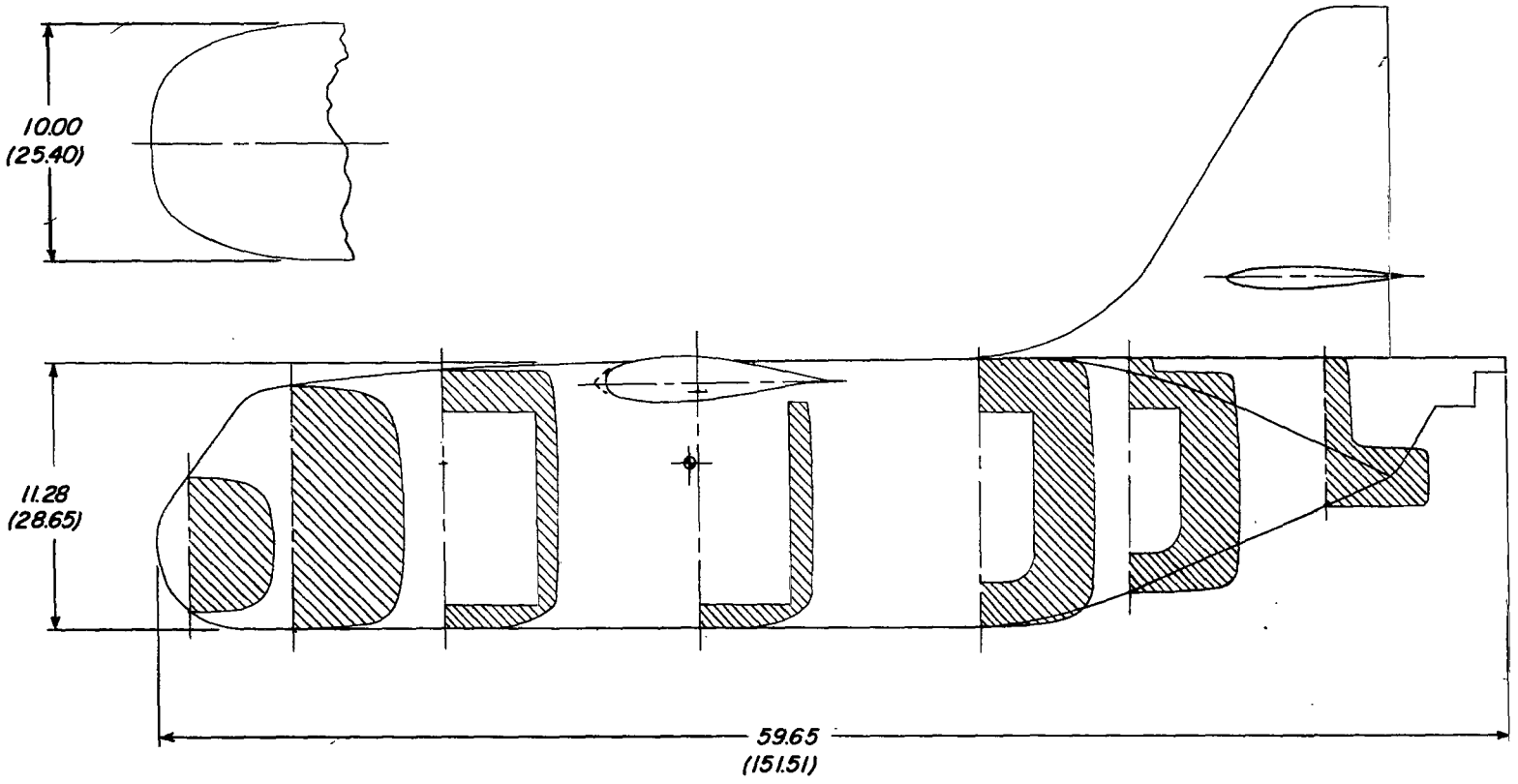

Figure 5.- Fuselage cross sections of a 1/11-scale tilt-wing VTOL model. All dimensions in inches; parenthetical values in centimeters.

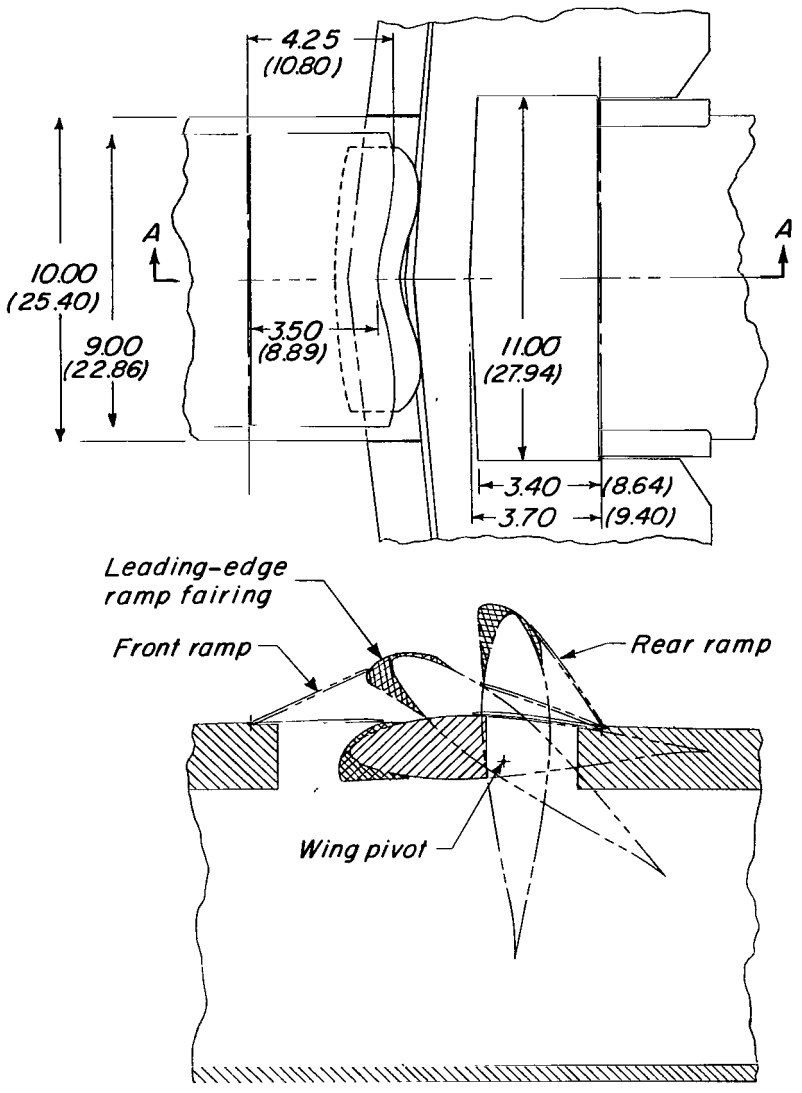

Figure 6.- Wing-fuselage ramps of the 1/11-scale tilt-wing VTOL model. All dimensions in inches; parenthetical values in centimeters.

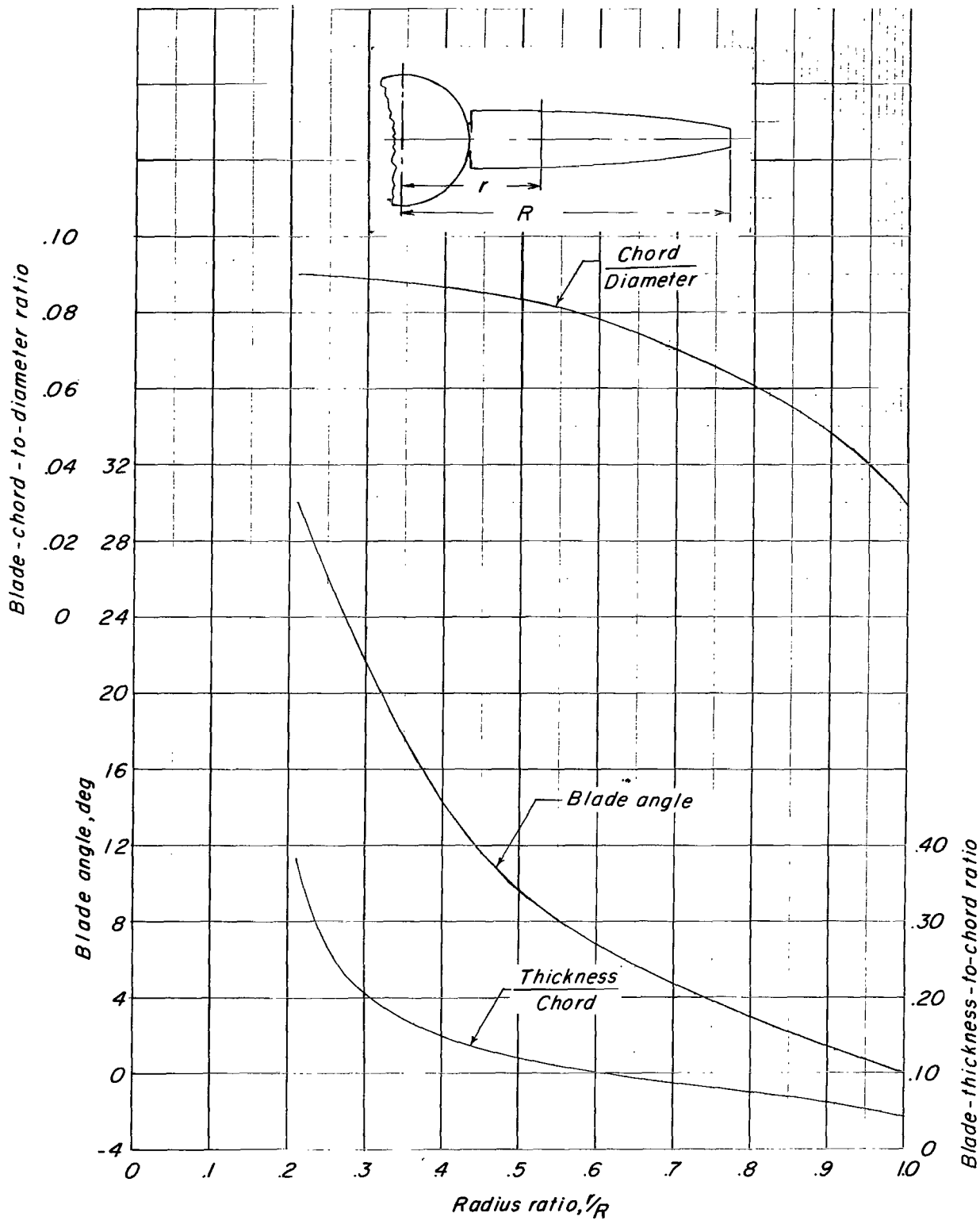

Figure 7.- Propeller blade geometric characteristics of a 1/11-scale tilt-wing VTOL model.

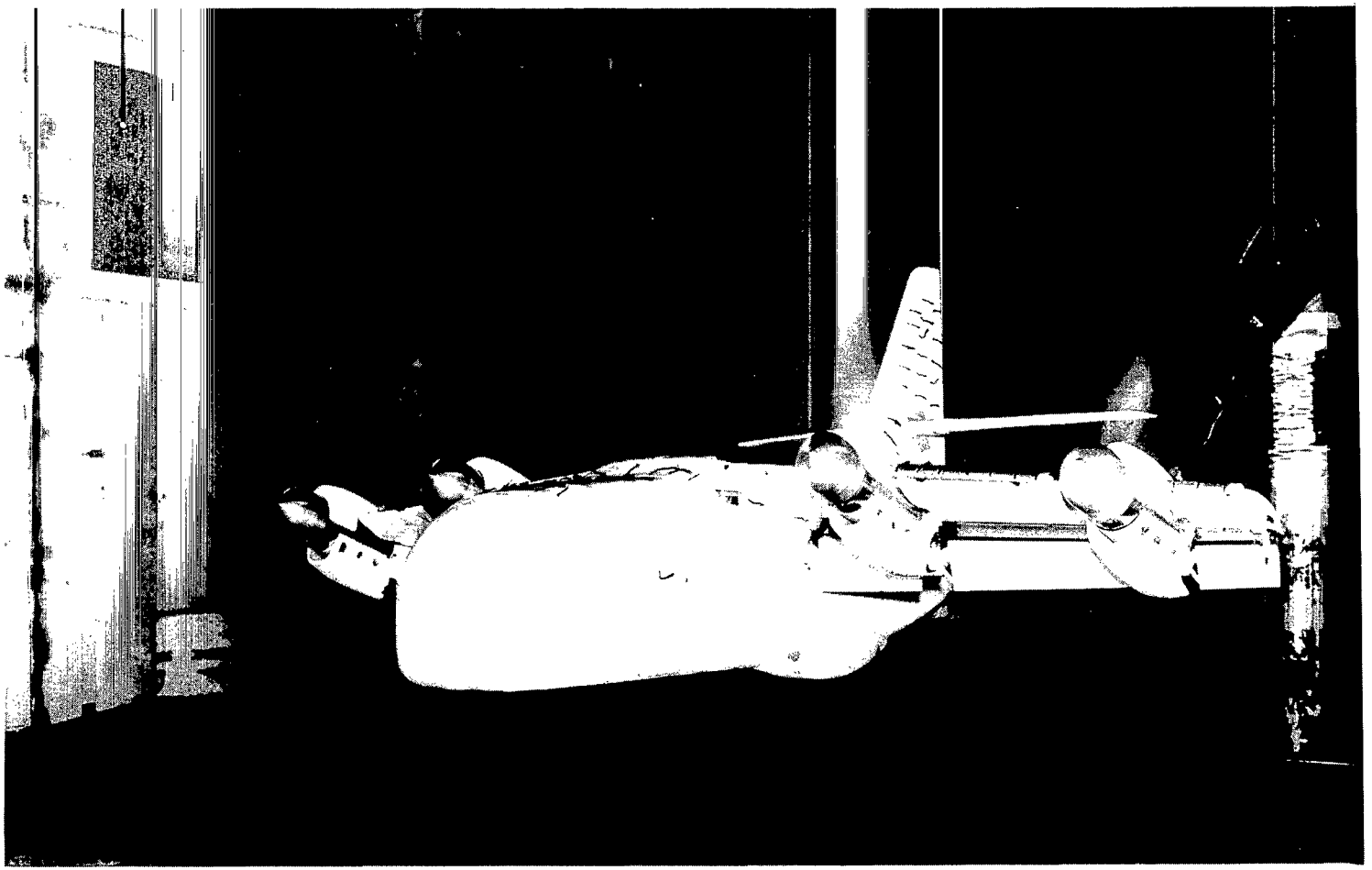

(a) Over the moving ground plane. Front view. L-64-10,166

Figure 8.- Photographs of the model in the 17-foot (5.18-meter) test section.

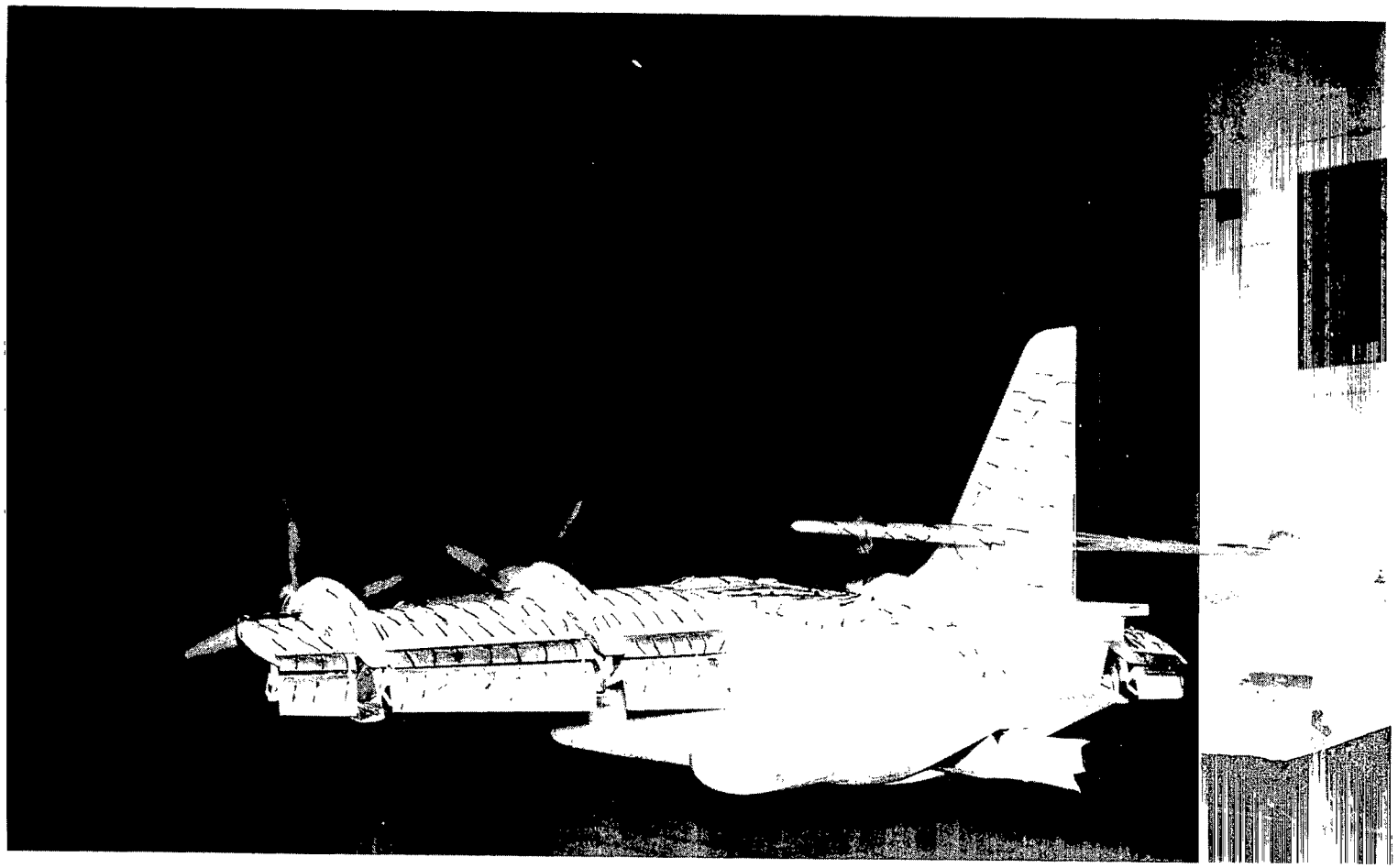

(b) Over the moving ground plane. Rear view. L-64-10,165

Figure 8.- Concluded.

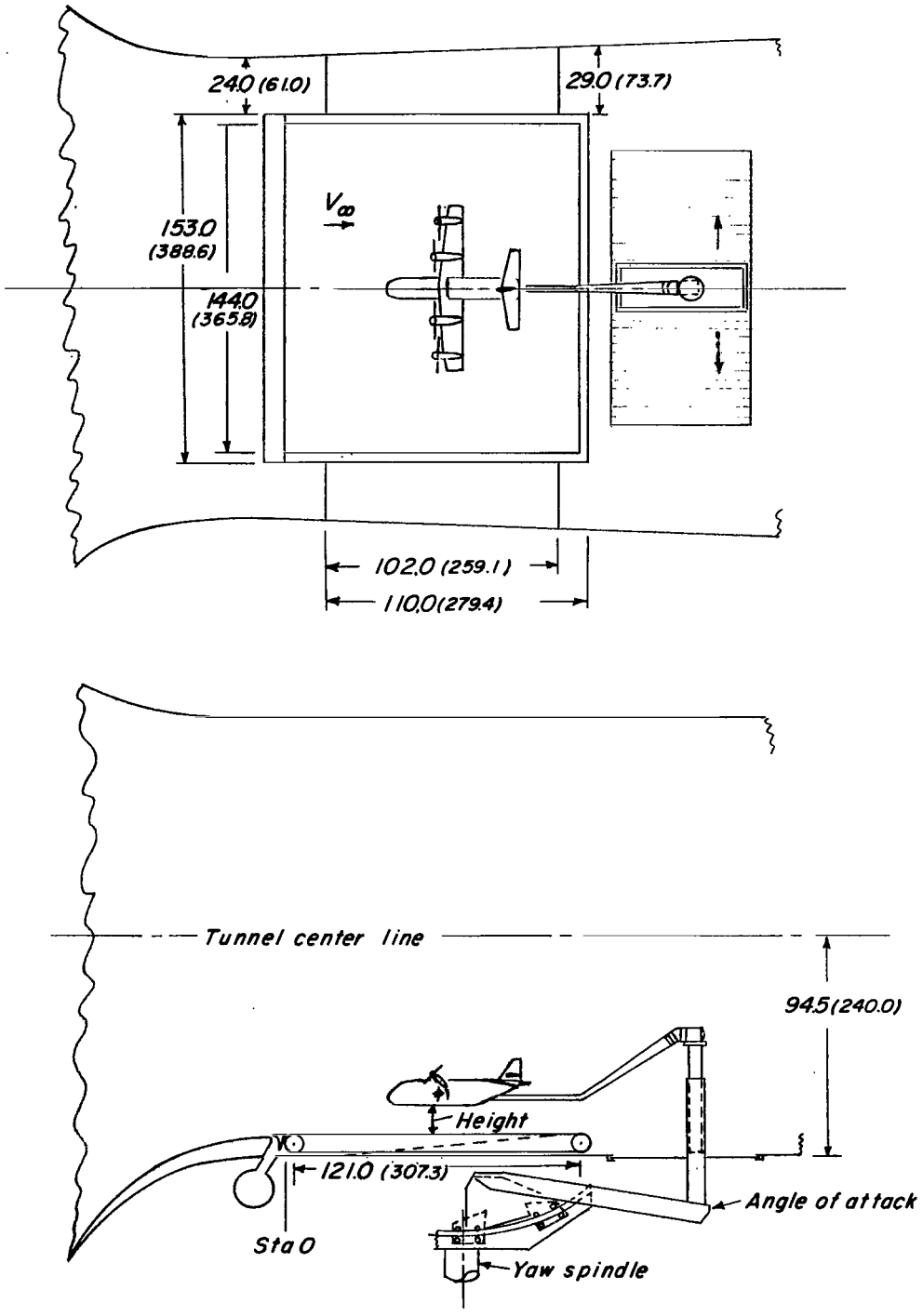

Figure 9.- Sketch of moving-belt ground-plane setup. All dimensions in inches; parenthetical values in centimeters.

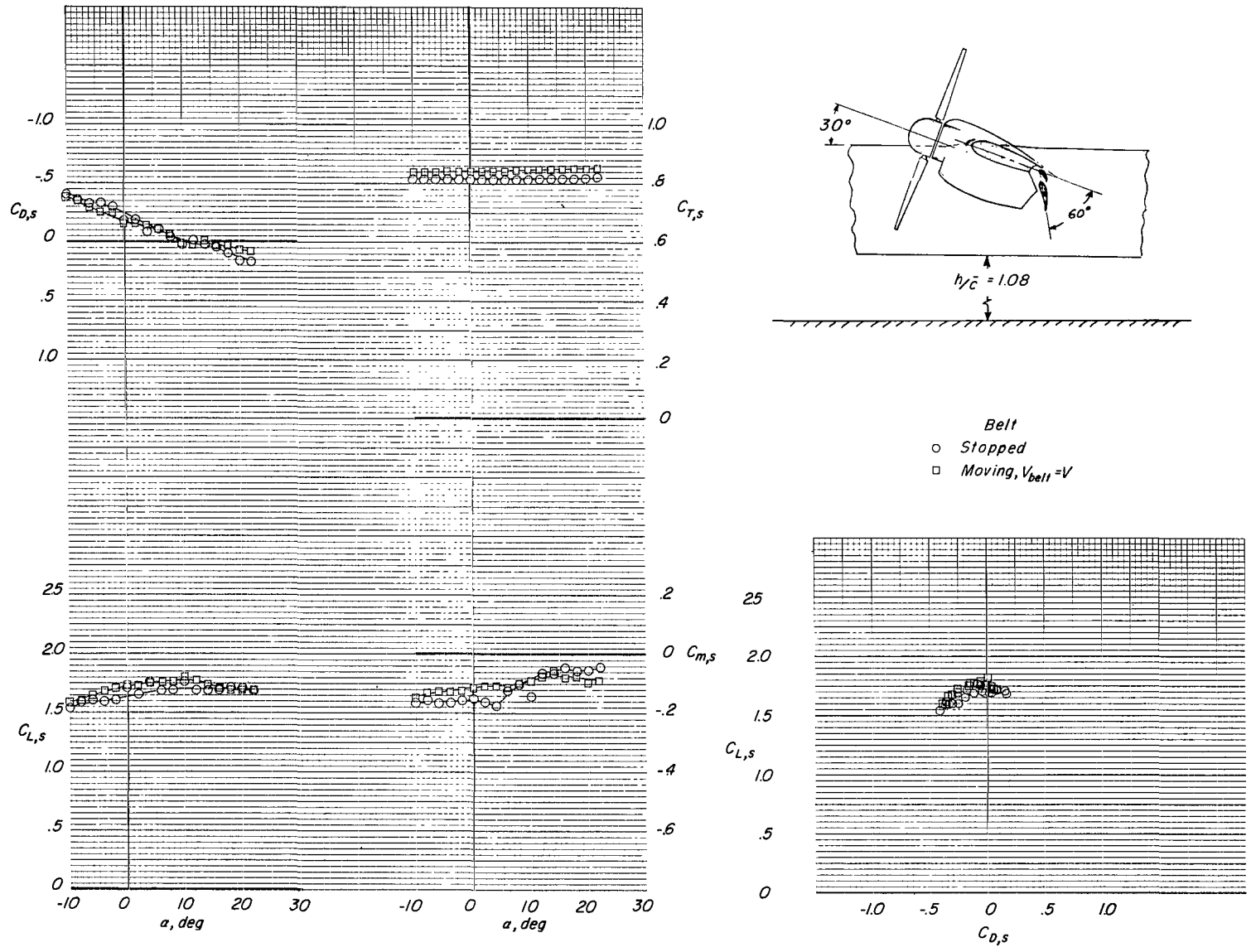

Figure 10.- Comparison of longitudinal aerodynamic characteristics with the ground belt stopped and moving. $i_w = 30^0$; $\delta_f = 60^0$; $h/\bar{c} = 1.08$; $q = 1.55$ lbf/ft^2 (74.21 N/m^2); 7000 rpm; $\beta = 0^0$; $\delta_a = 0^0$; slat on; $i_t = 20^0$.

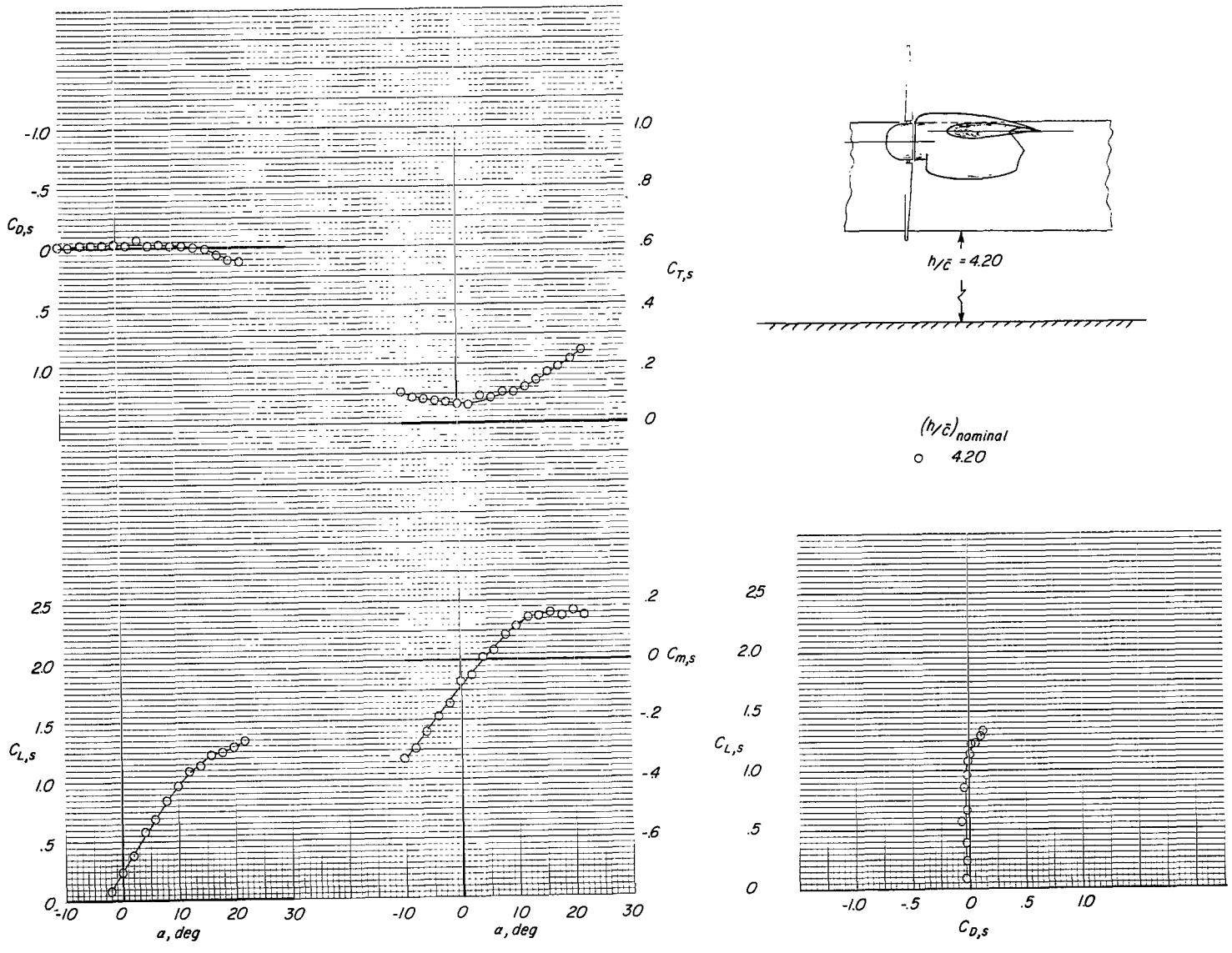

(a) $i_w = 0^0$; $\delta_f = 0^0$.

Figure 11.- Longitudinal aerodynamic characteristics at various ground-height ratios for various wing-incidence—flap-deflection combinations. Belt moving; 7000 rpm; $\beta = 0^0$; $\delta_a = 0^0$; slat on and $i_t = 20^0$ (except for $i_w = 0^0$ and $\delta_f = 0^0$, where horizontal tail and slat were off). (q was established at Drag ≈ 0 for $h/\bar{c} = 4.20$ and $\alpha = 0^0$.)

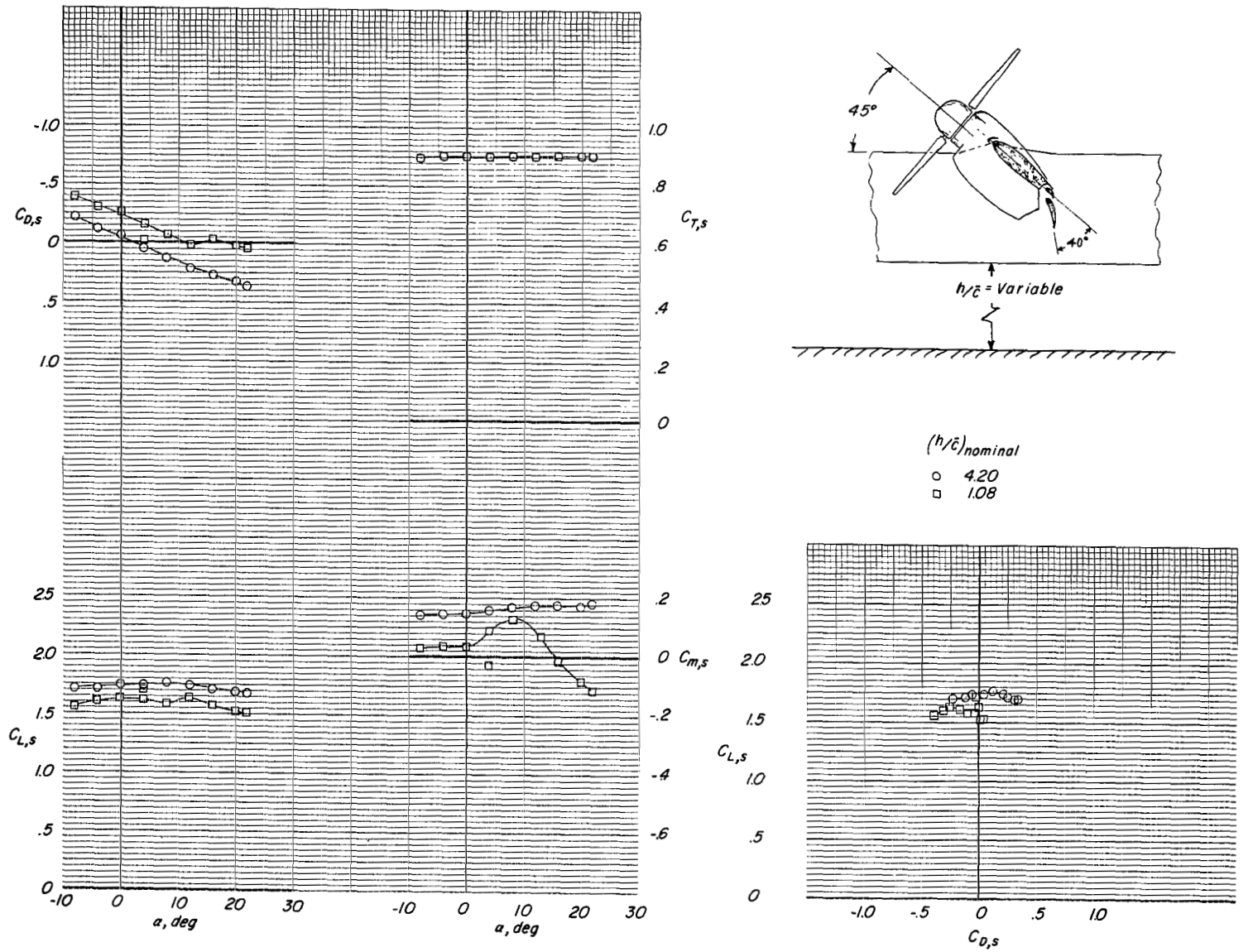

(b) $i_w = 45^0$; $\delta_f = 40^0$.

Figure 11.- Continued.

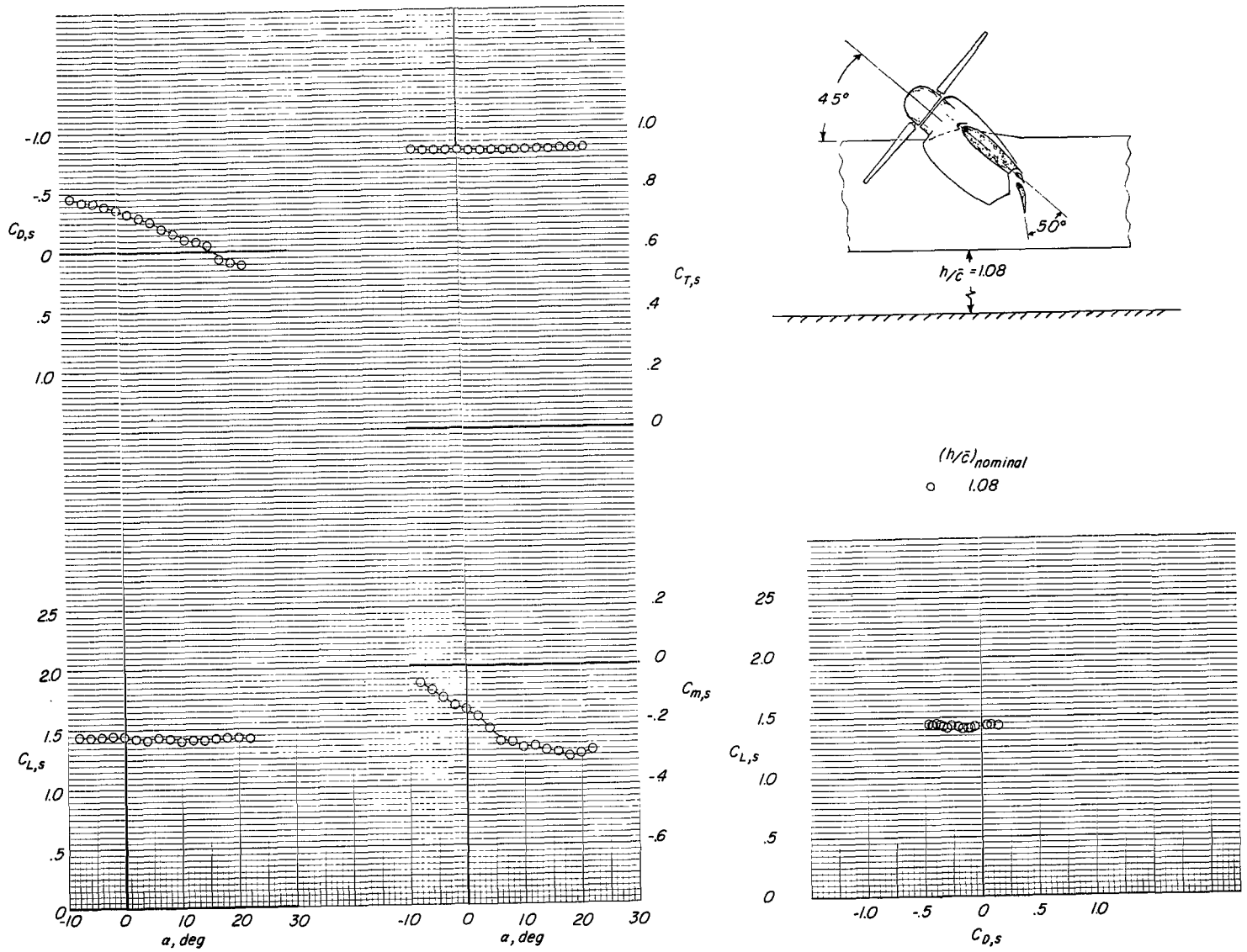

(c) $i_w = 45^0$; $\delta_f = 50^0$.

Figure 11.- Continued.

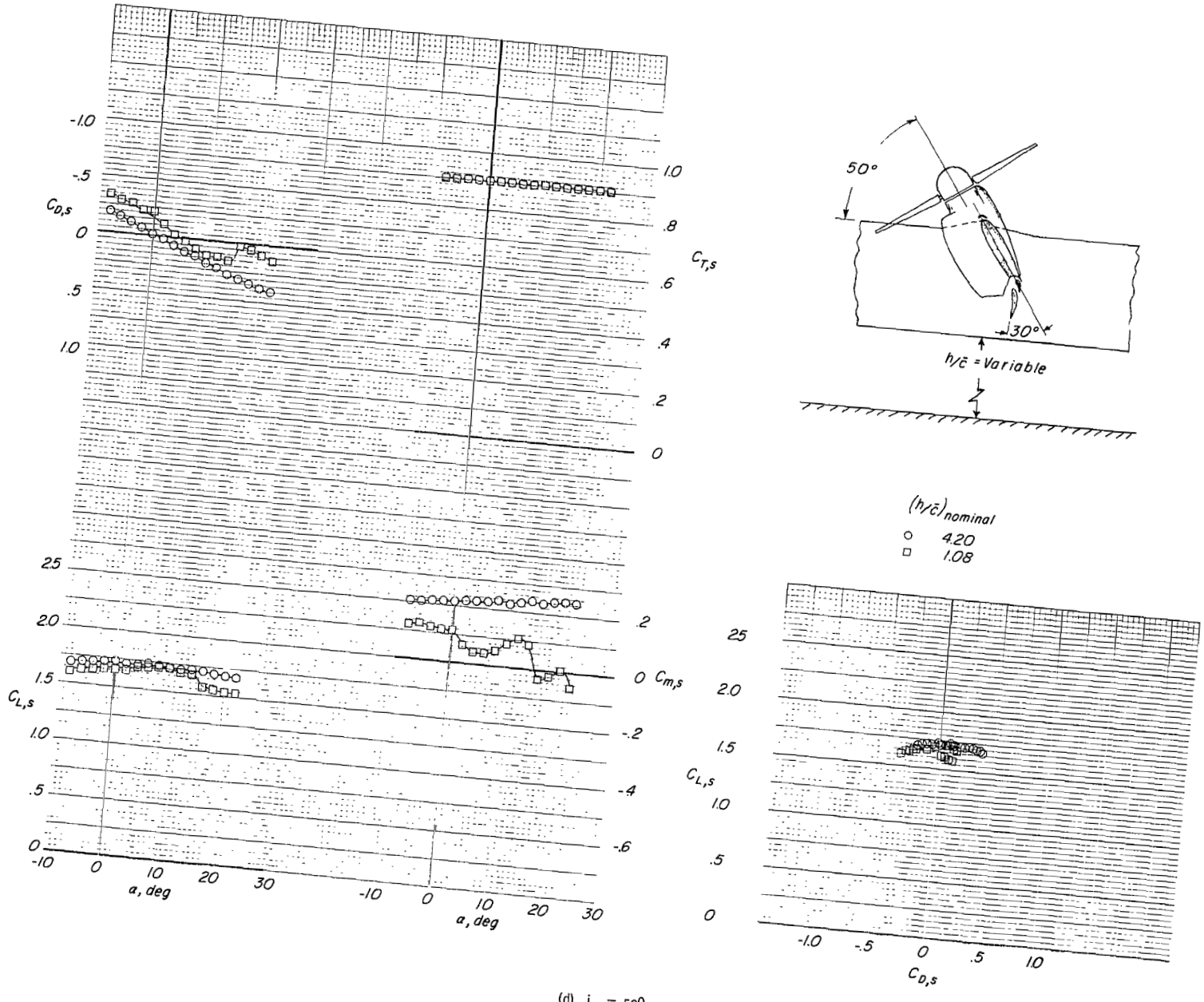

(d) $i_w = 50^0$; $\delta_f = 30^0$.

Figure 11.- Continued.

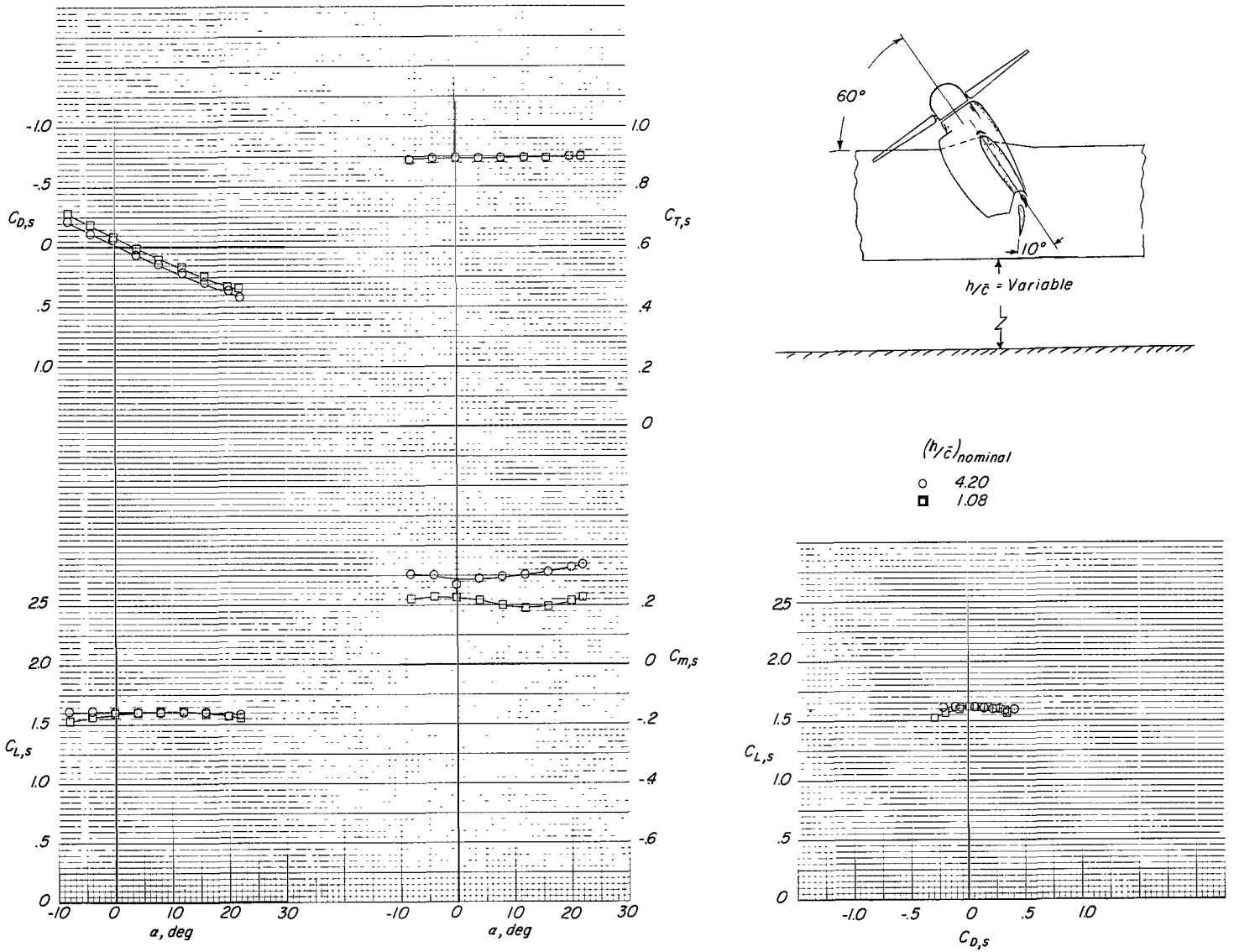

(e) $i_W = 60^0$; $\delta_f = 10^0$.

Figure 11.- Continued.

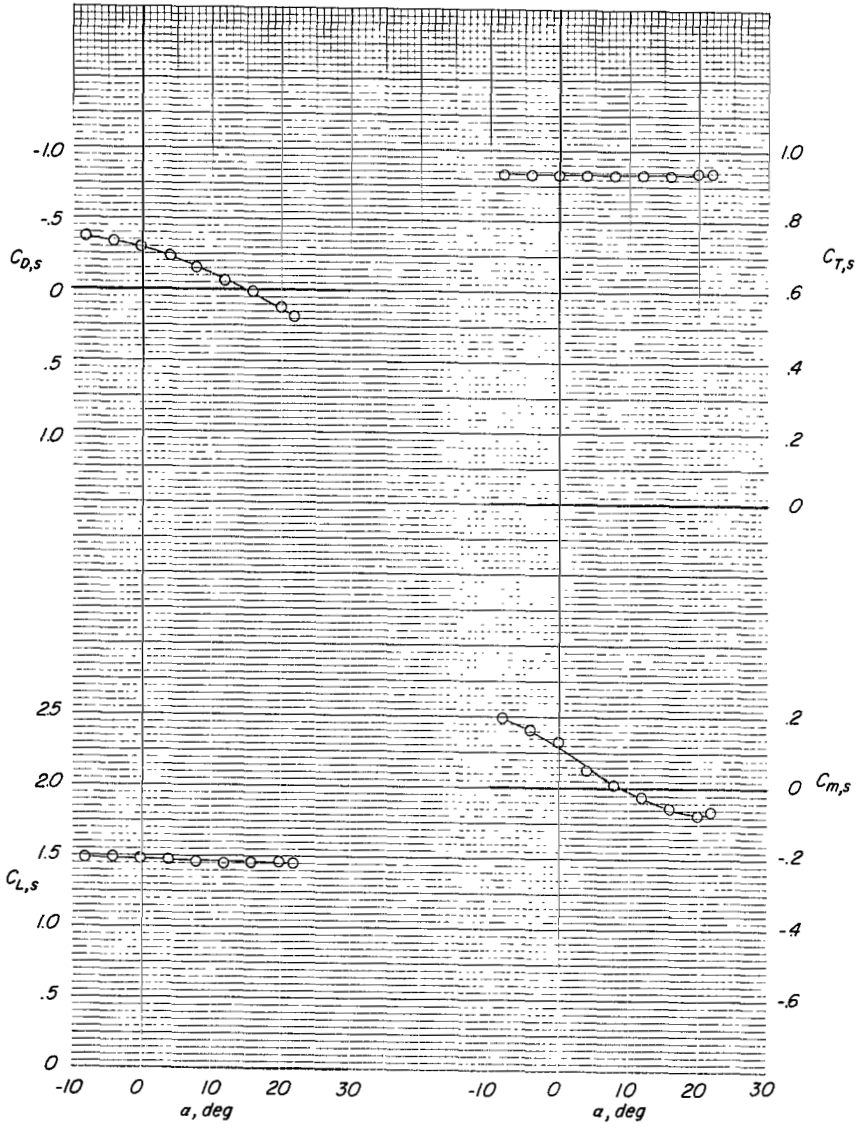

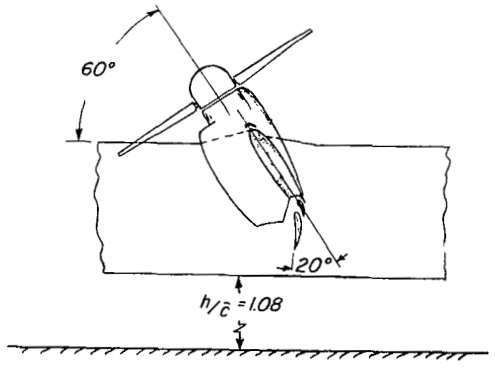

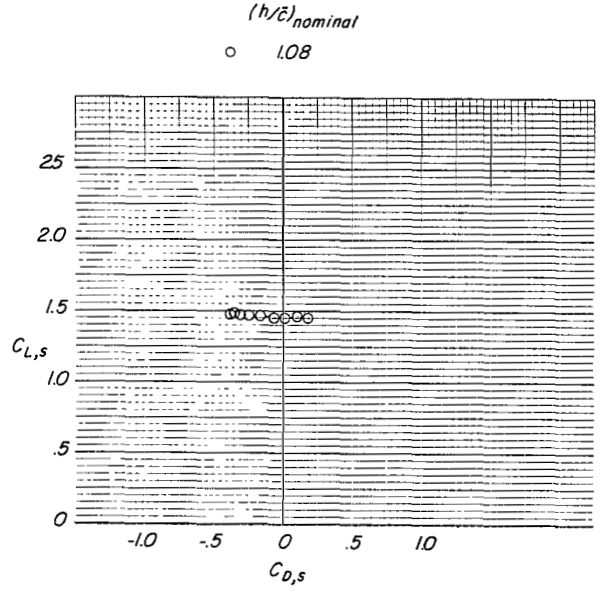

(f) $i_w = 60^0$; $\delta_f = 20^0$.

Figure 11.- Continued.

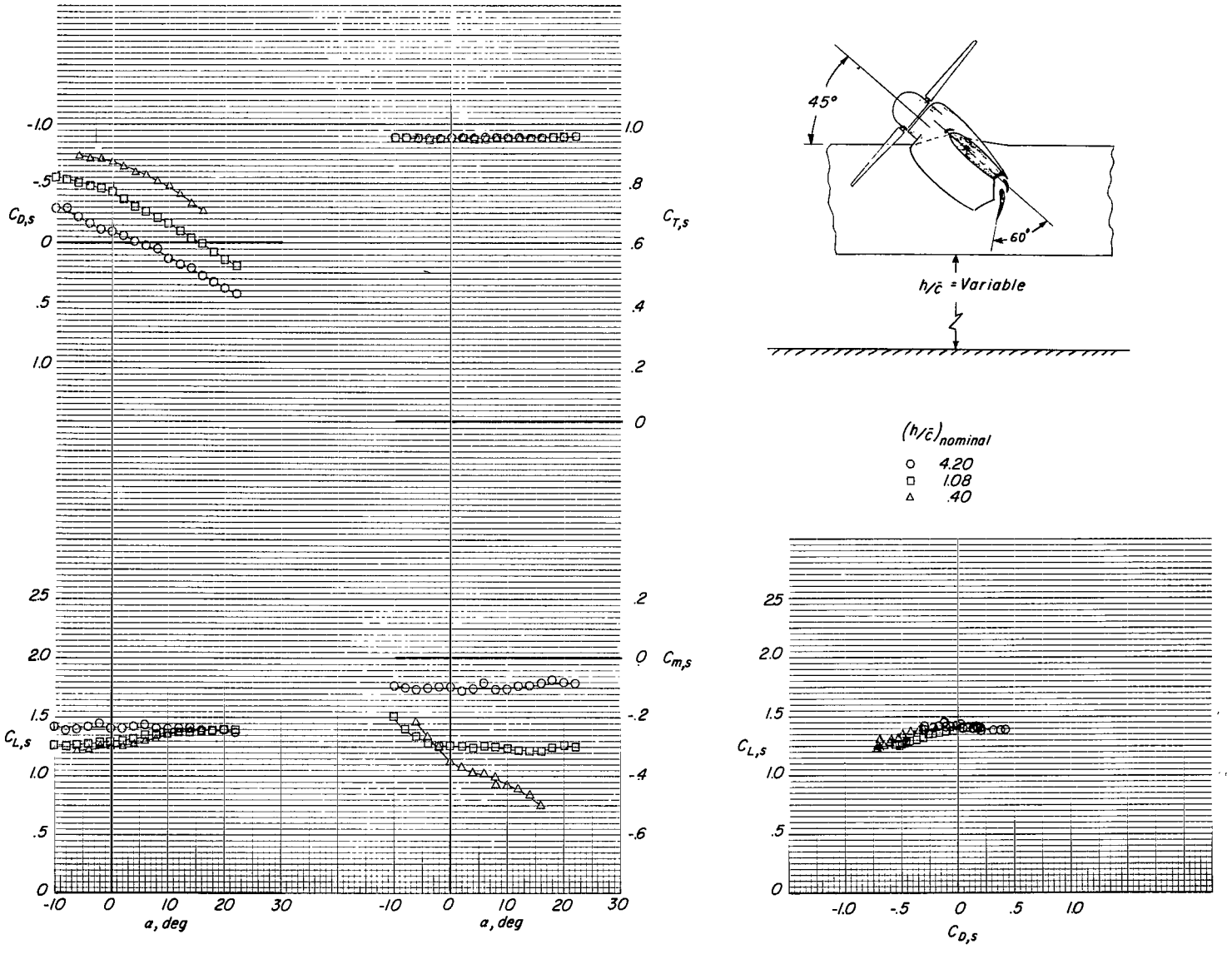

(g) $i_w = 45^0$; $\delta_f = 60^0$.

Figure 11.- Continued.

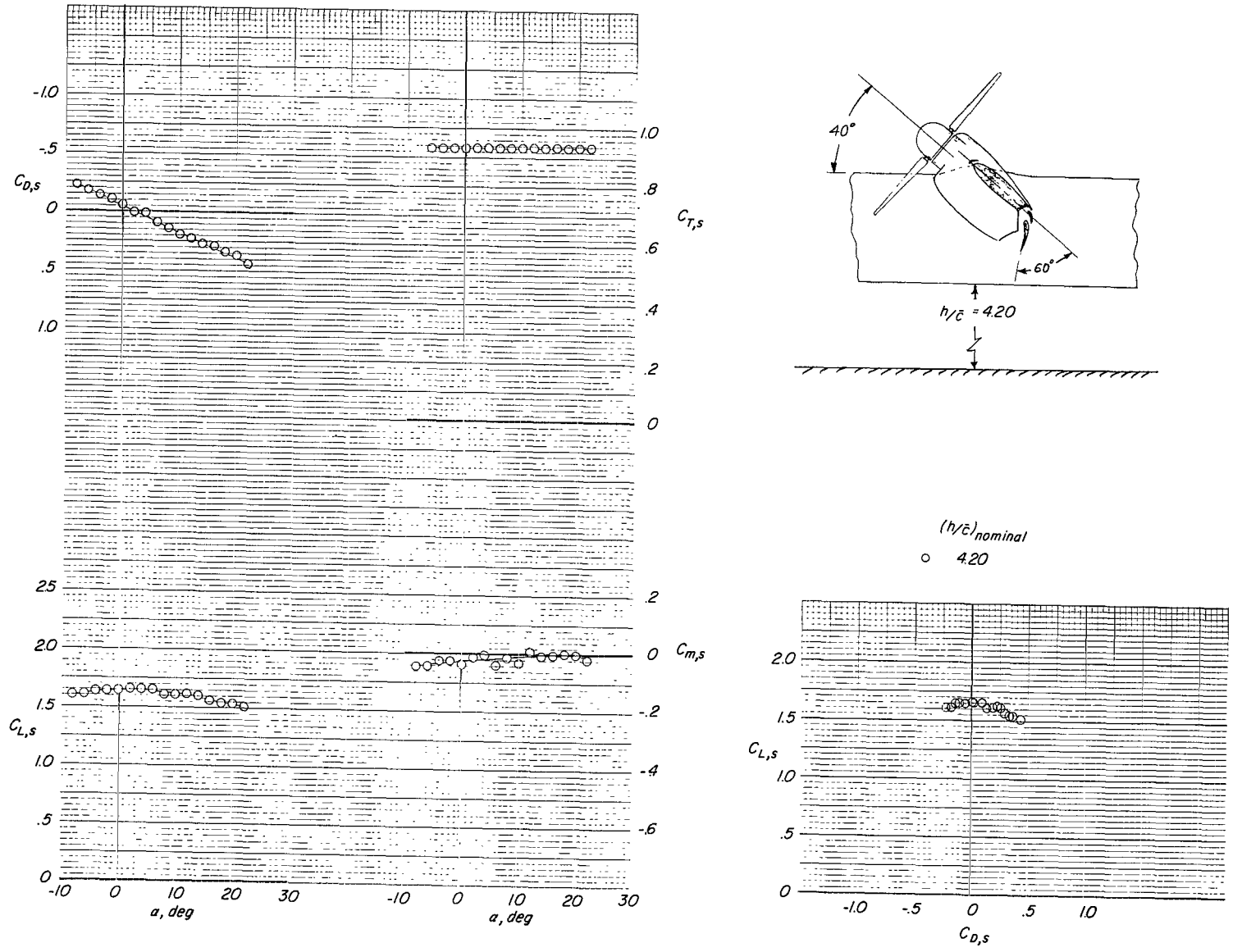

(h) $i_w = 40^0$; $\delta_f = 60^0$.

Figure 11.- Continued.

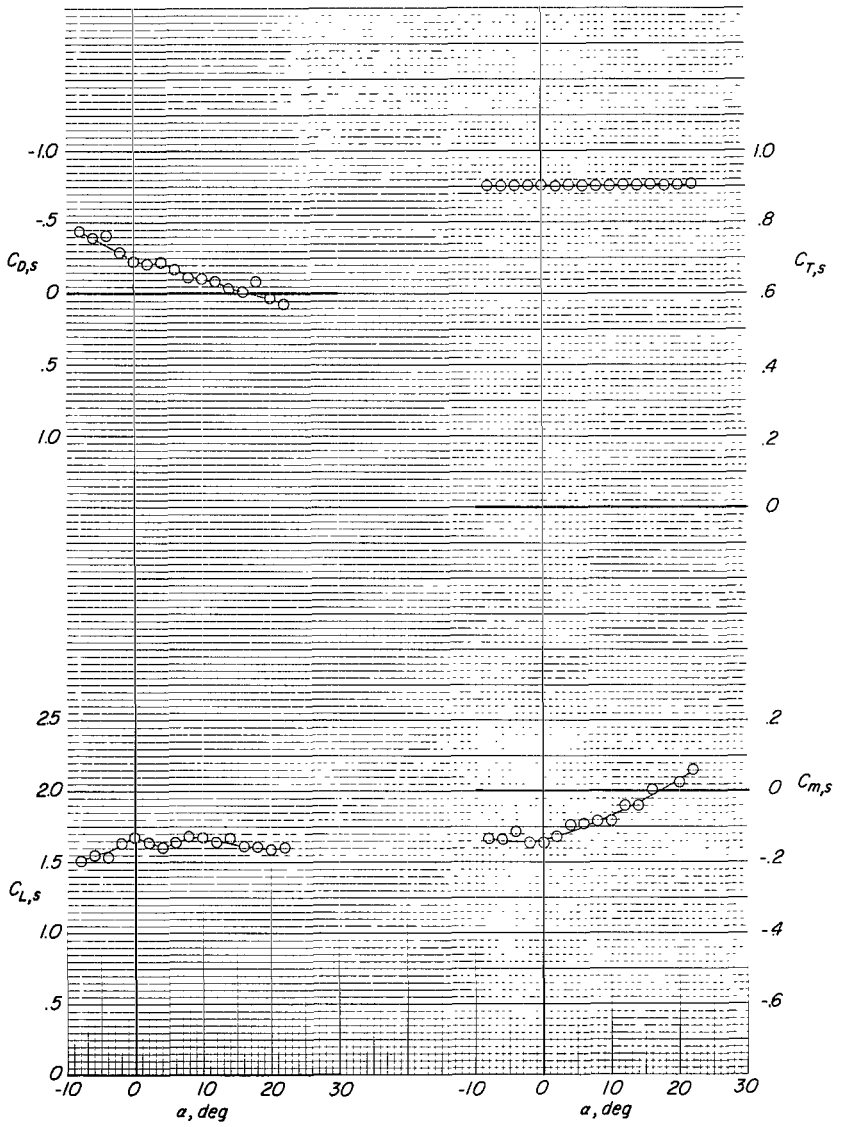

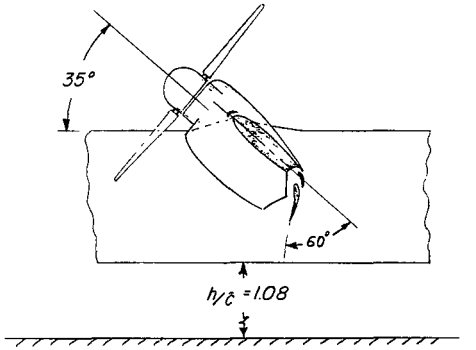

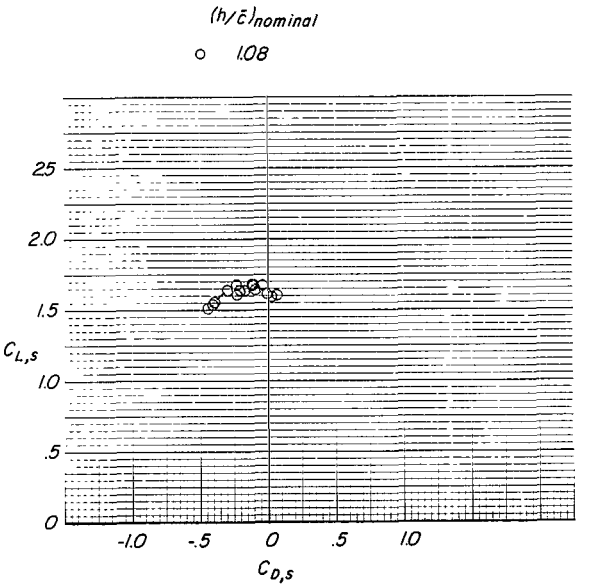

(i) $i_w = 35^0$; $\delta_f = 60^0$.

Figure 11.- Continued.

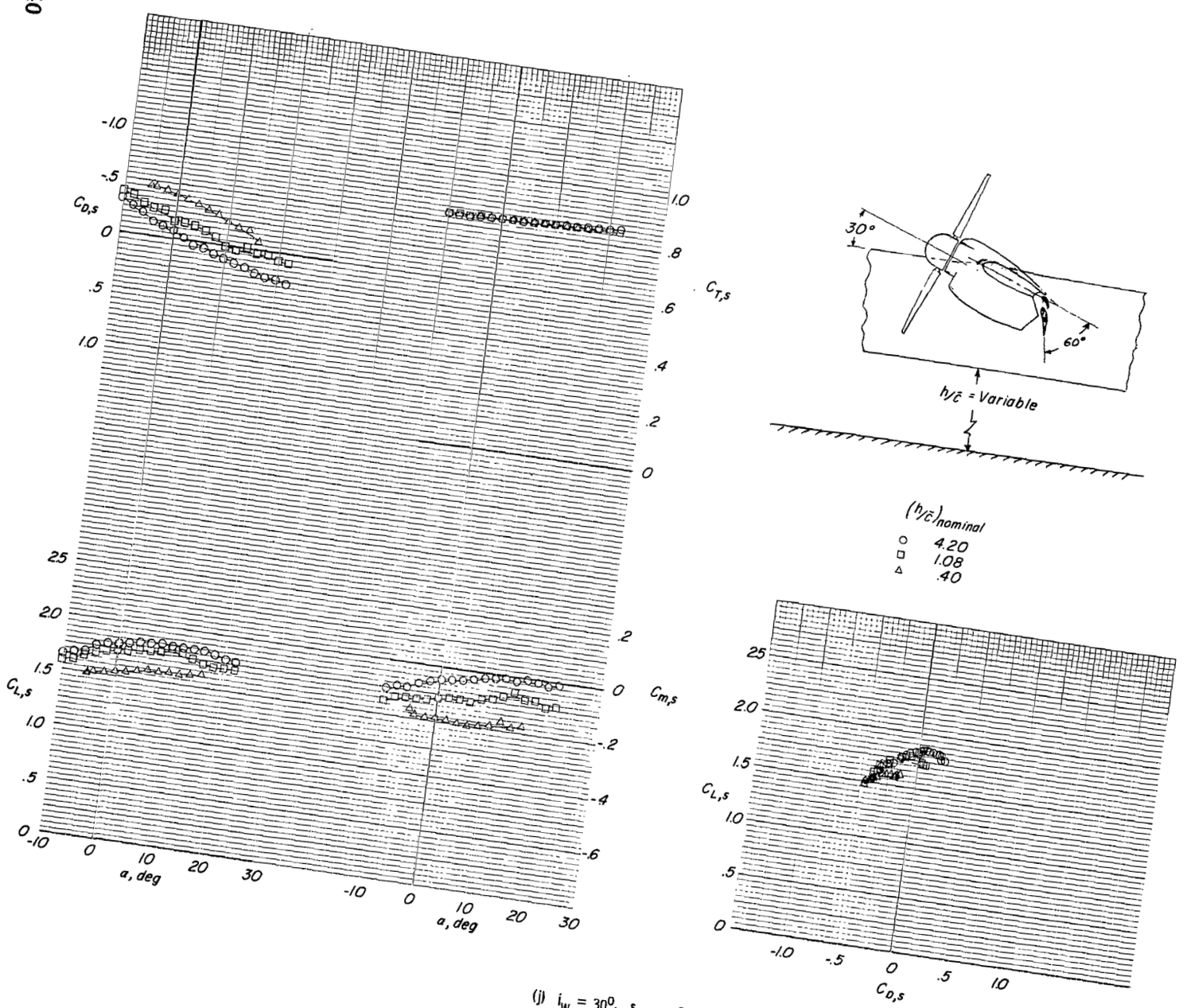

(j) $i_w = 30^0$; $\delta_f = 60^0$.

Figure 11.- Concluded.

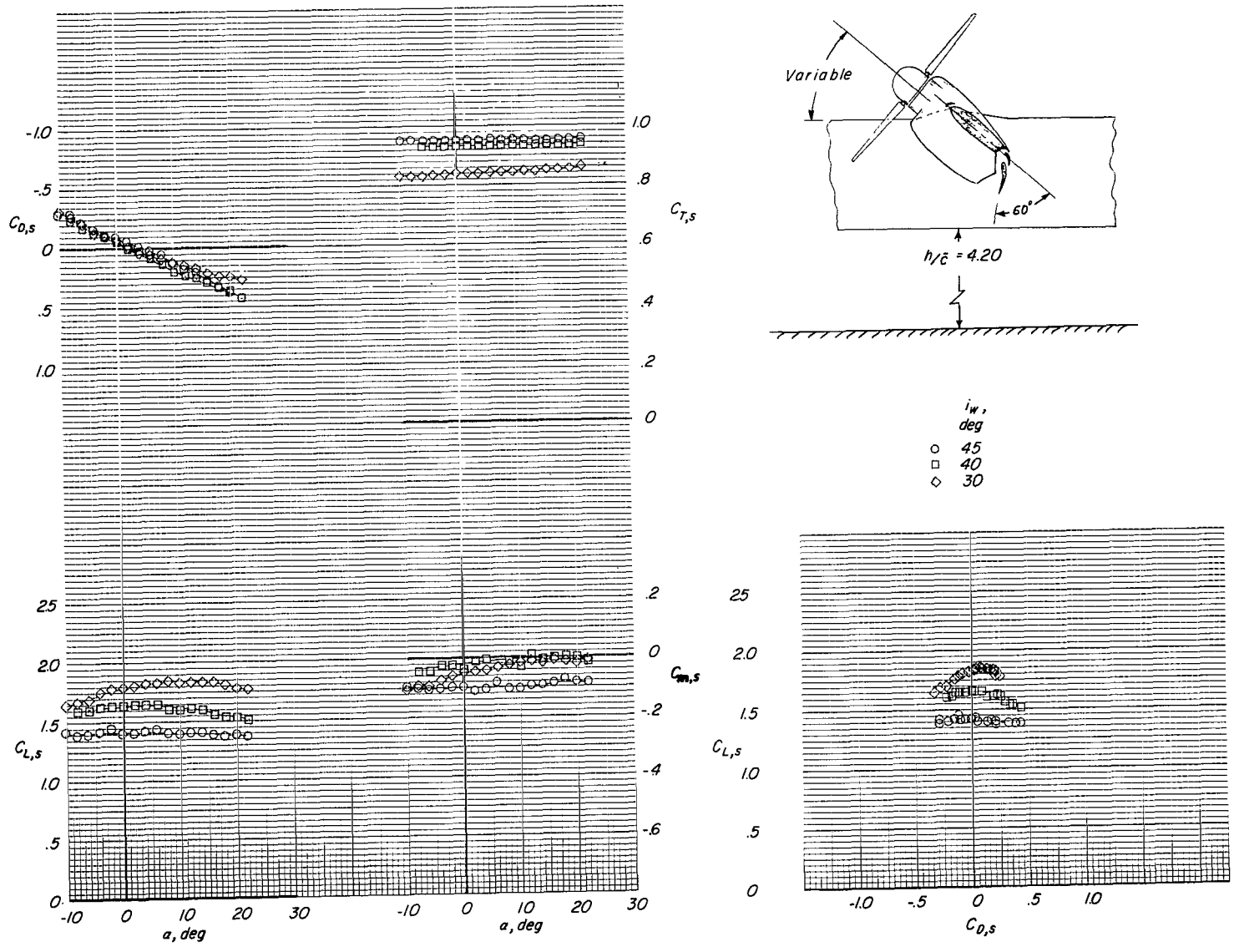

(a) $h/\bar{c} = 4.20$.

Figure 12.- Longitudinal aerodynamic characteristics at various wing-tilt angles for several ground-height ratios. $\delta_f = 60^0$; belt moving; 7000 rpm; $\beta = 0^0$; $\delta_a = 0^0$; slat on; $i_t = 20^0$. (q was established at Drag $\approx$ 0 for $h/\bar{c} = 4.20$ and $\alpha = 0^0$.)

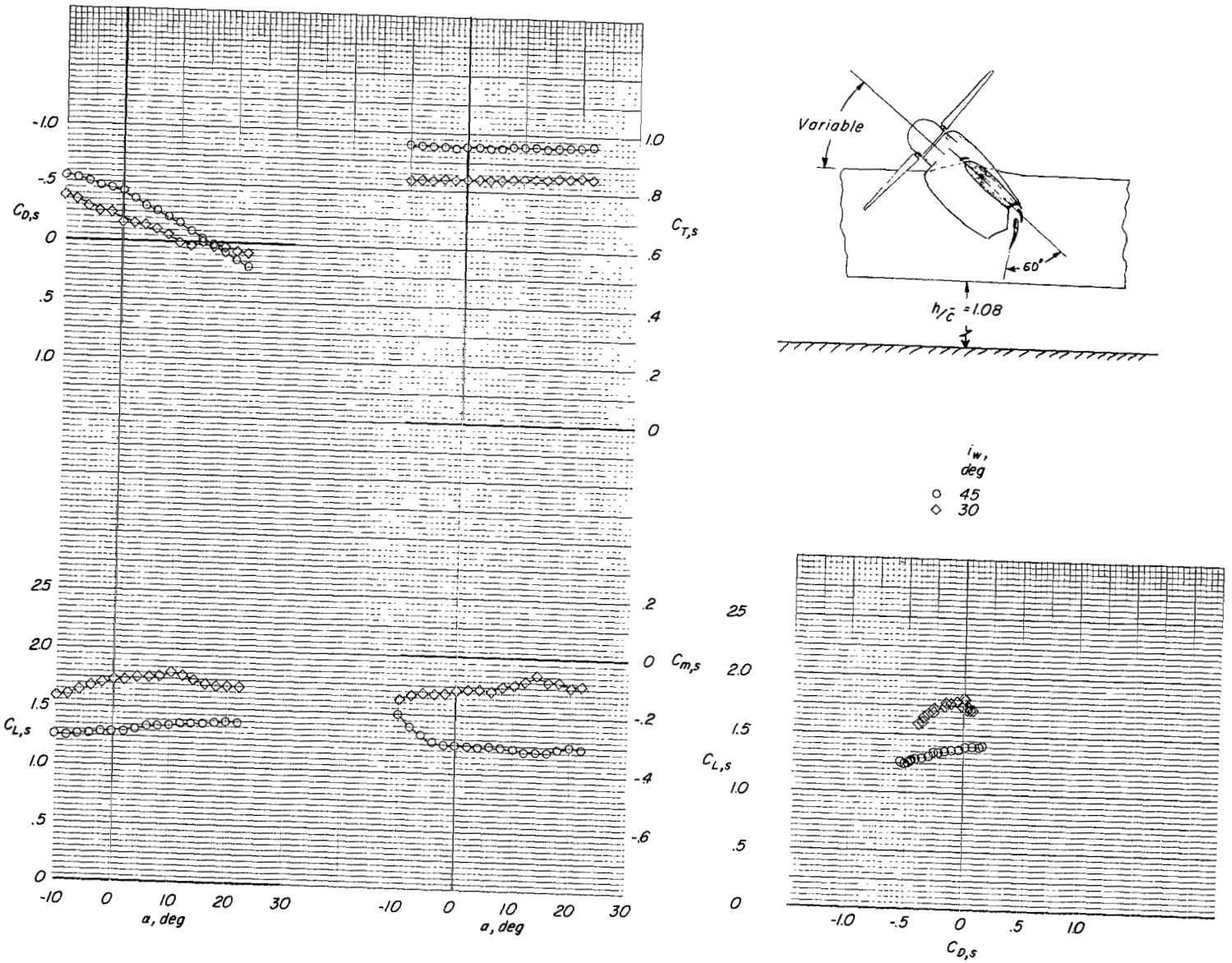

(b) $h/\bar{c} = 1.08$.

Figure 12.- Continued.

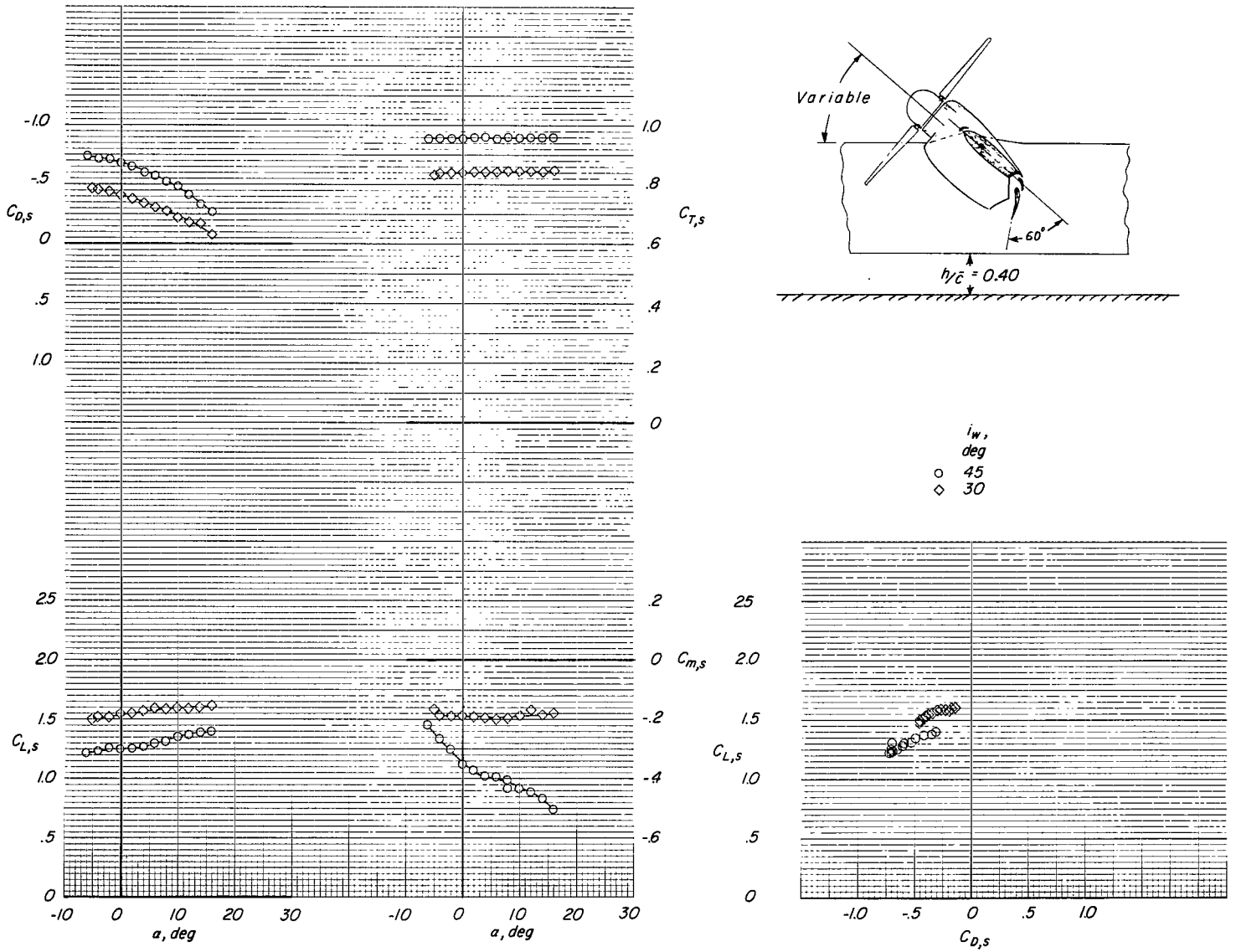

(c) $h/\bar{c}$ = 0.40.

Figure 12.- Concluded.

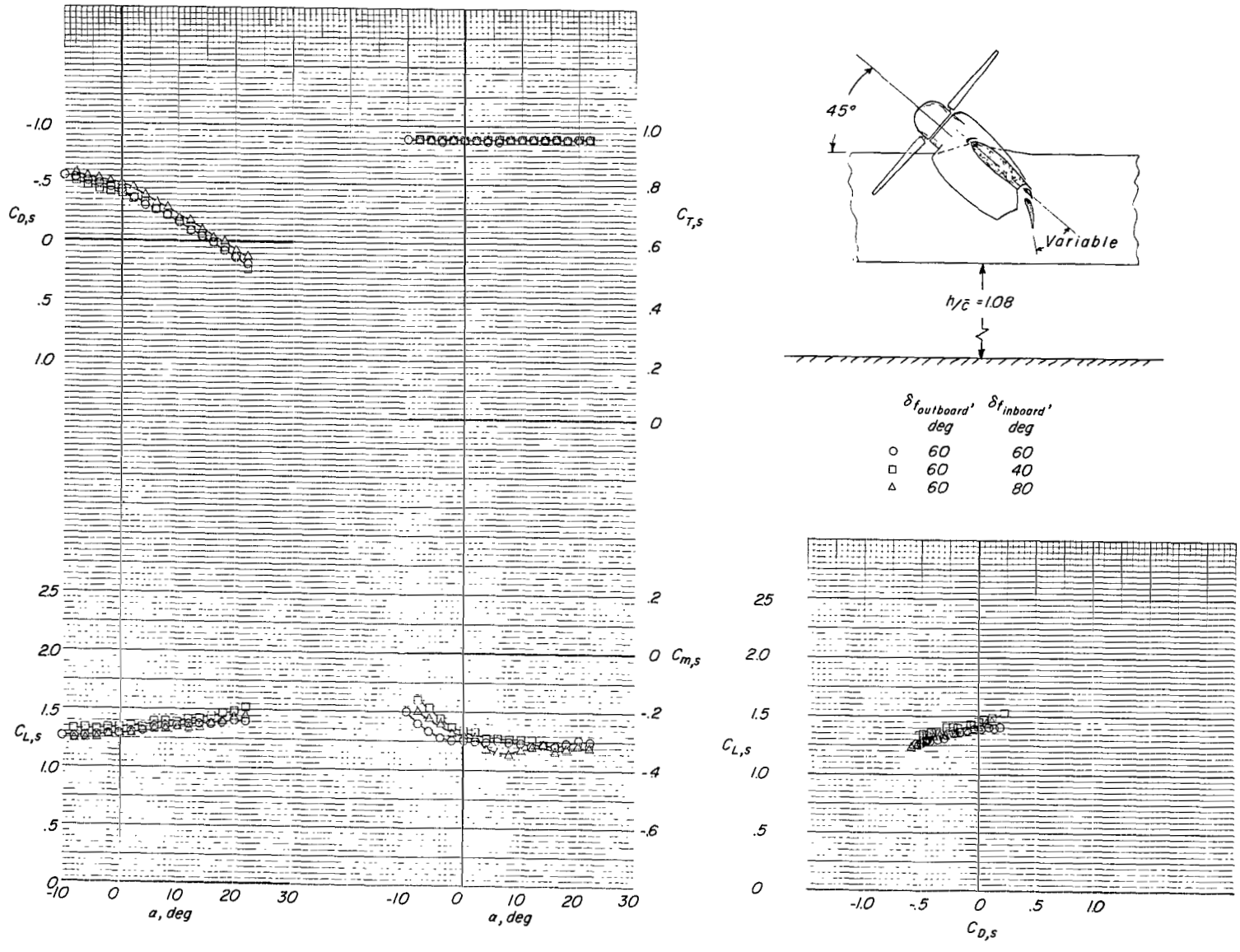

Figure 13.- Effect of differential flap deflection on the longitudinal aerodynamic characteristics with $i_w = 45^0$. Belt moving; $h/\bar{c} = 1.08$; 7000 rpm; $\beta = 0^0$; $\delta_a = 0^0$; slat on; $i_t = 20^0$. (q was established at Drag $\approx$ 0 for $h/\bar{c} = 4.20$ and $\alpha = 0^0$.)

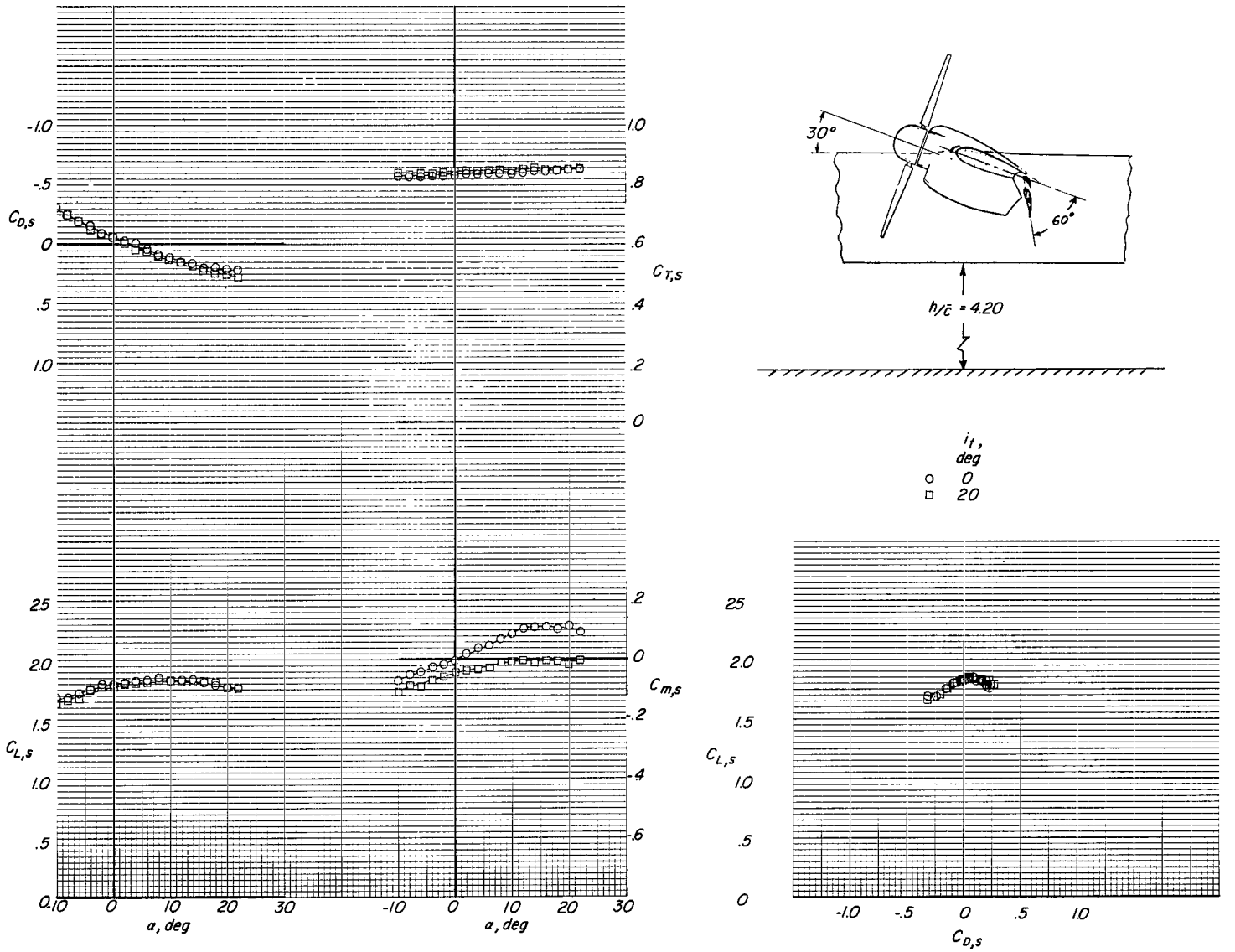

Figure 14.- Effect of horizontal-tail incidence on the longitudinal aerodynamic characteristics with $i_w = 30^0$. $\delta_f = 60^0$; belt moving; $h/\bar{c} = 4.20$; 7000 rpm; $\beta = 0^0$; $\delta_a = 0^0$; slat on. (q was established at Drag $\approx$ 0 for $h/\bar{c} = 4.20$ and $\alpha = 0^0$.)

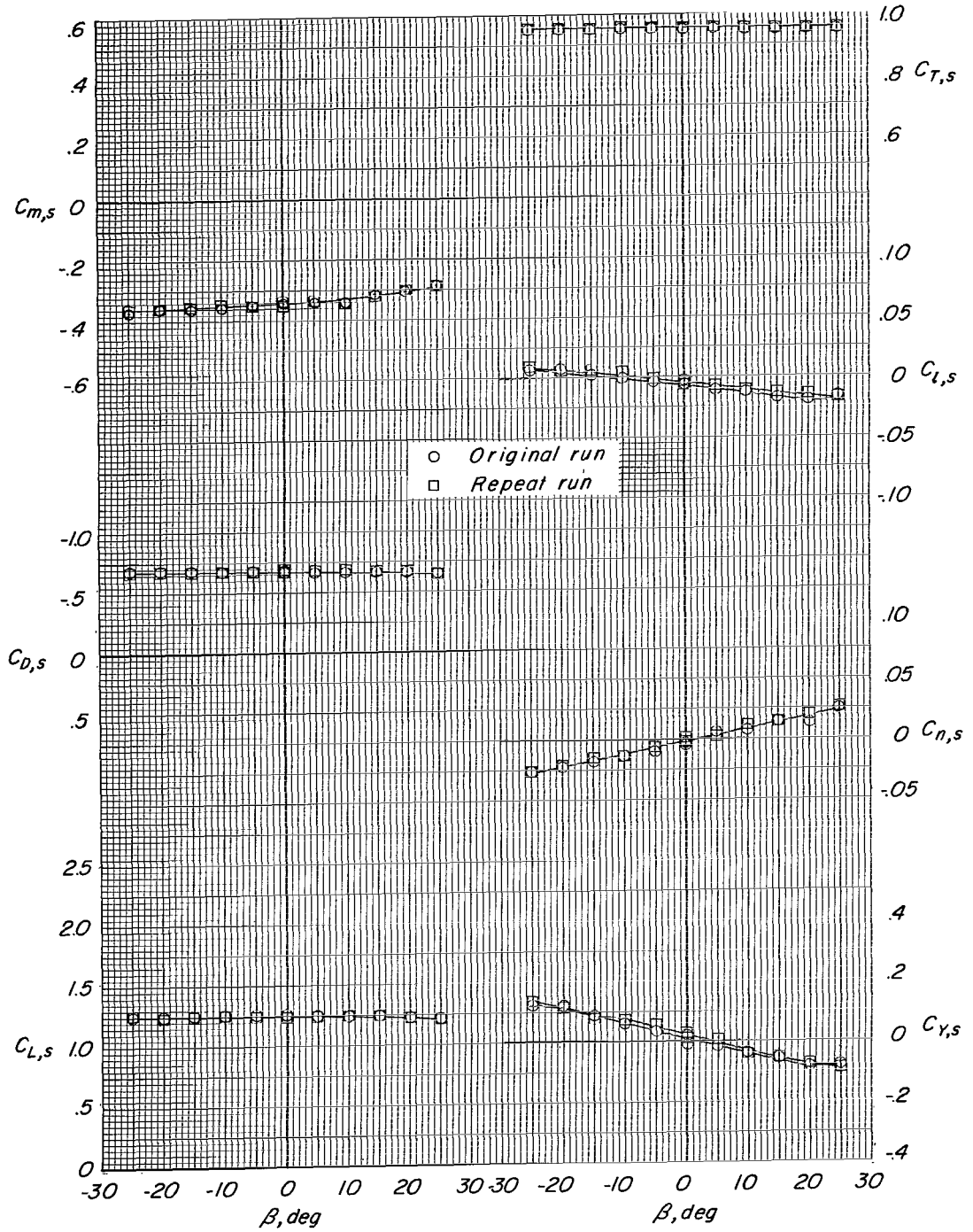

Figure 15.- Repeatability of lateral aerodynamic data with the model sideslipped. $i_w = 45^0$; $\delta_f = 60^0$; $h/\bar{c} = 0.40$; $\alpha = 0^0$; $i_t = 20^0$; $\delta_a = 0^0$; belt moving; slat on; 7000 rpm. (q was established at Drag $\approx$ 0 for $h/\bar{c} = 4.20$ and $\alpha = 0^0$.)

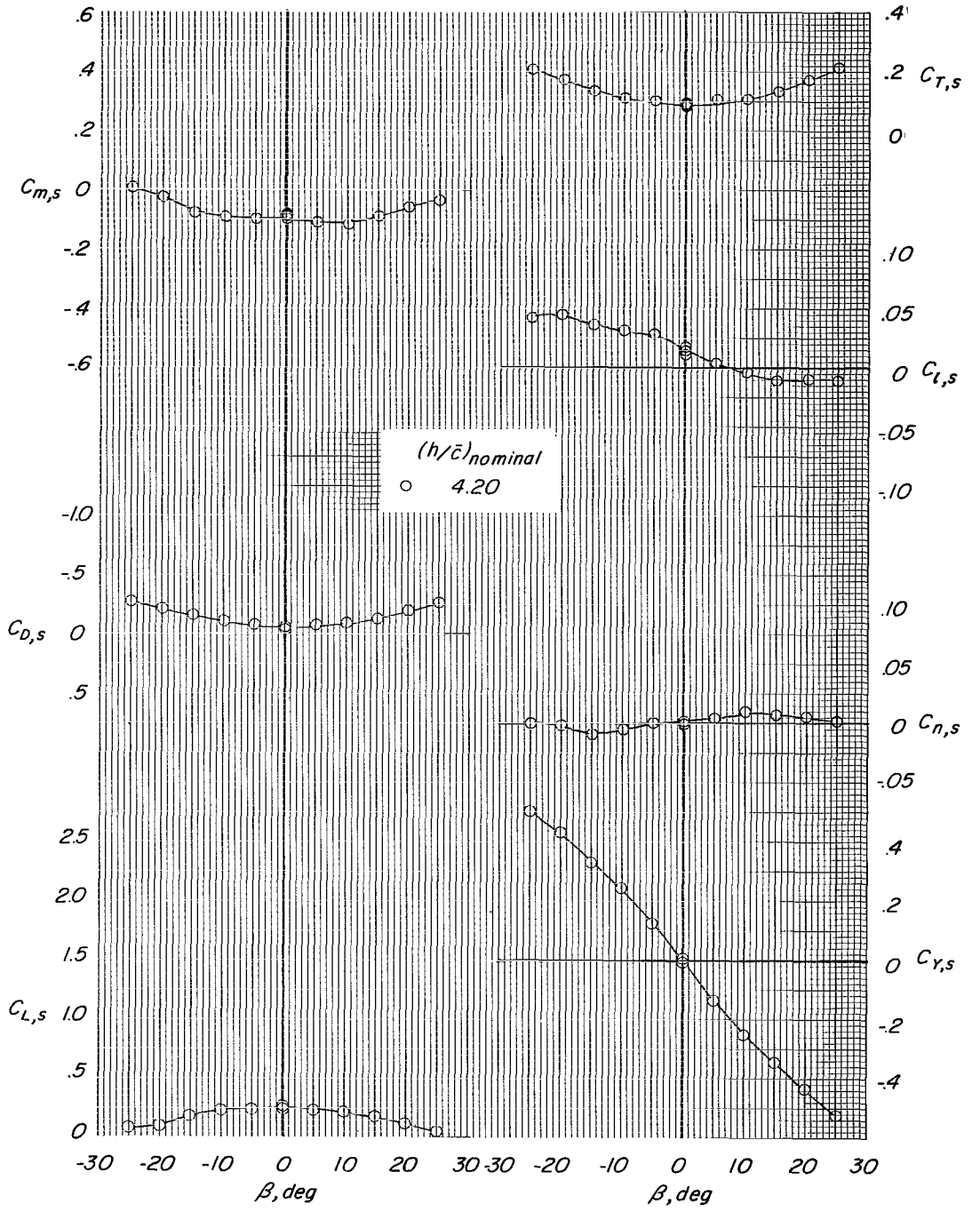

(a) $i_w = 0^0$; $\delta_f = 0^0$.

Figure 16.- Lateral aerodynamic characteristics at various ground-height ratios for various wing-incidence—flap-deflection combinations at $\alpha = 0^0$. Belt moving; 7000 rpm; $\delta_a = 0^0$; slat on and $i_t = 20^0$ (except for $i_w = 0^0$ and $\delta_f = 0^0$, where horizontal tail and slats were off). (q was established at Drag ≈ 0 for $h/\bar{c} = 4.20$ and $\alpha = 0^0$.)

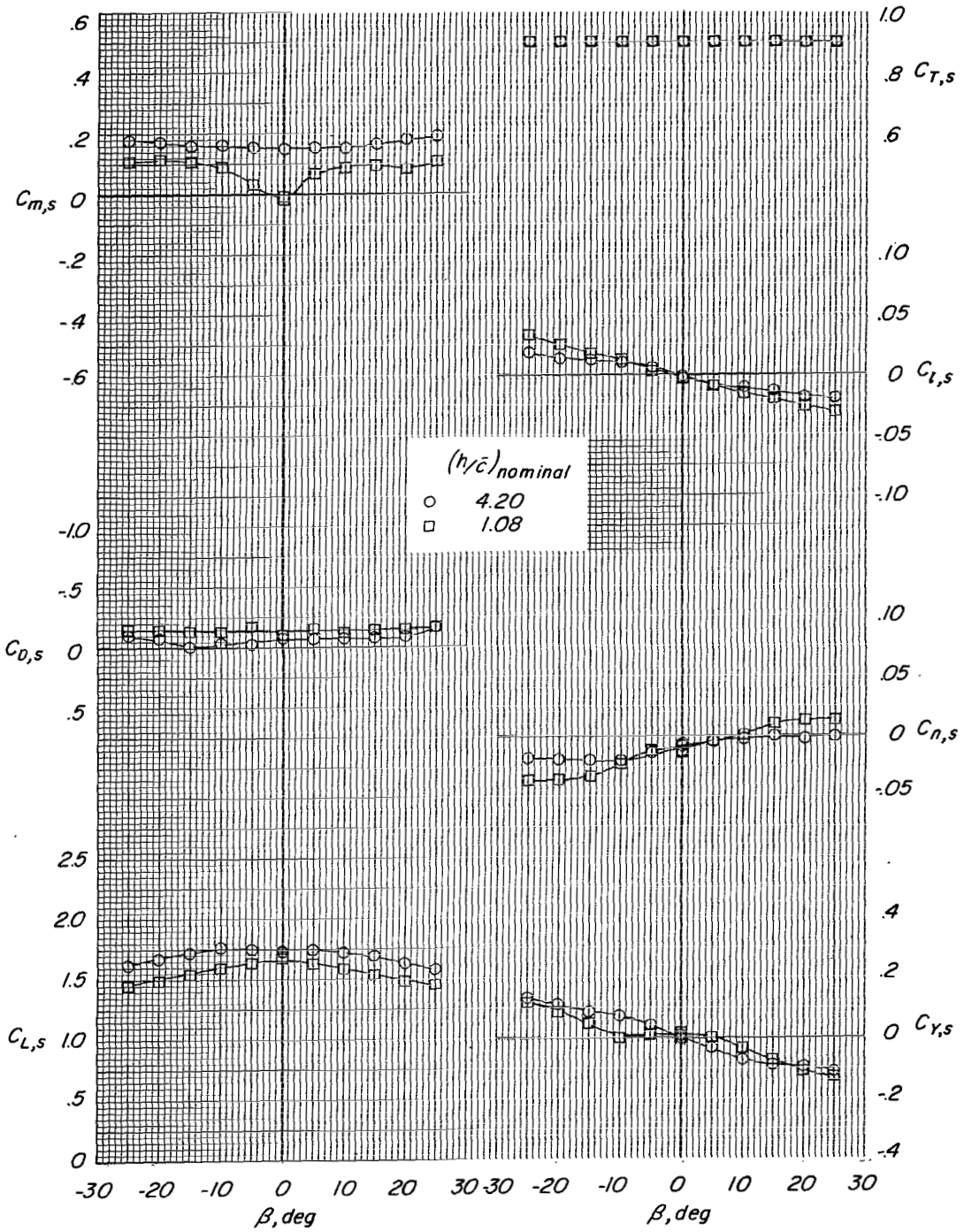

(b) $i_w = 45^0$; $\delta_f = 40^0$.

Figure 16.- Continued.

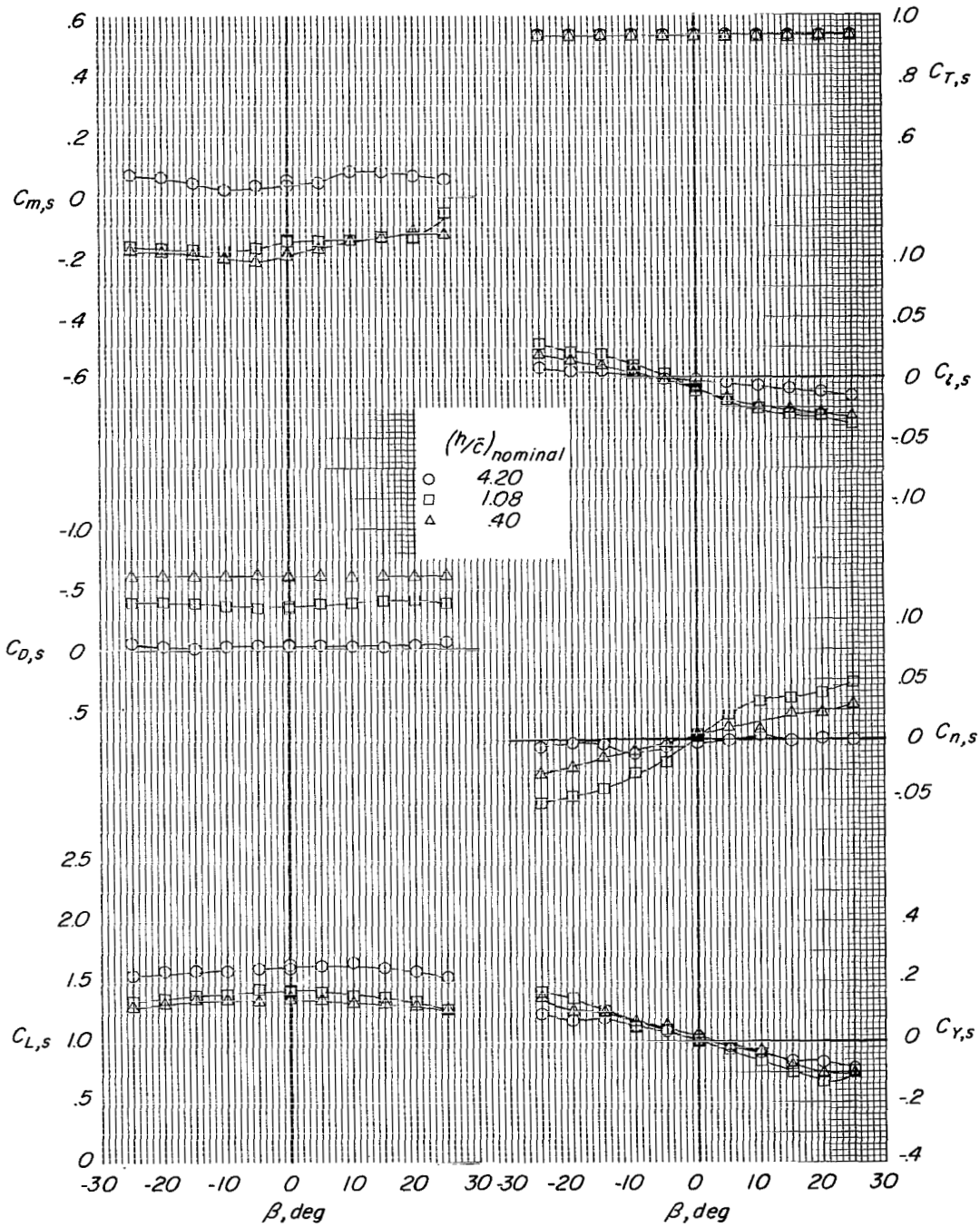

(c) $i_w = 45^0$; $\delta_f = 50^0$.

Figure 16.- Continued.

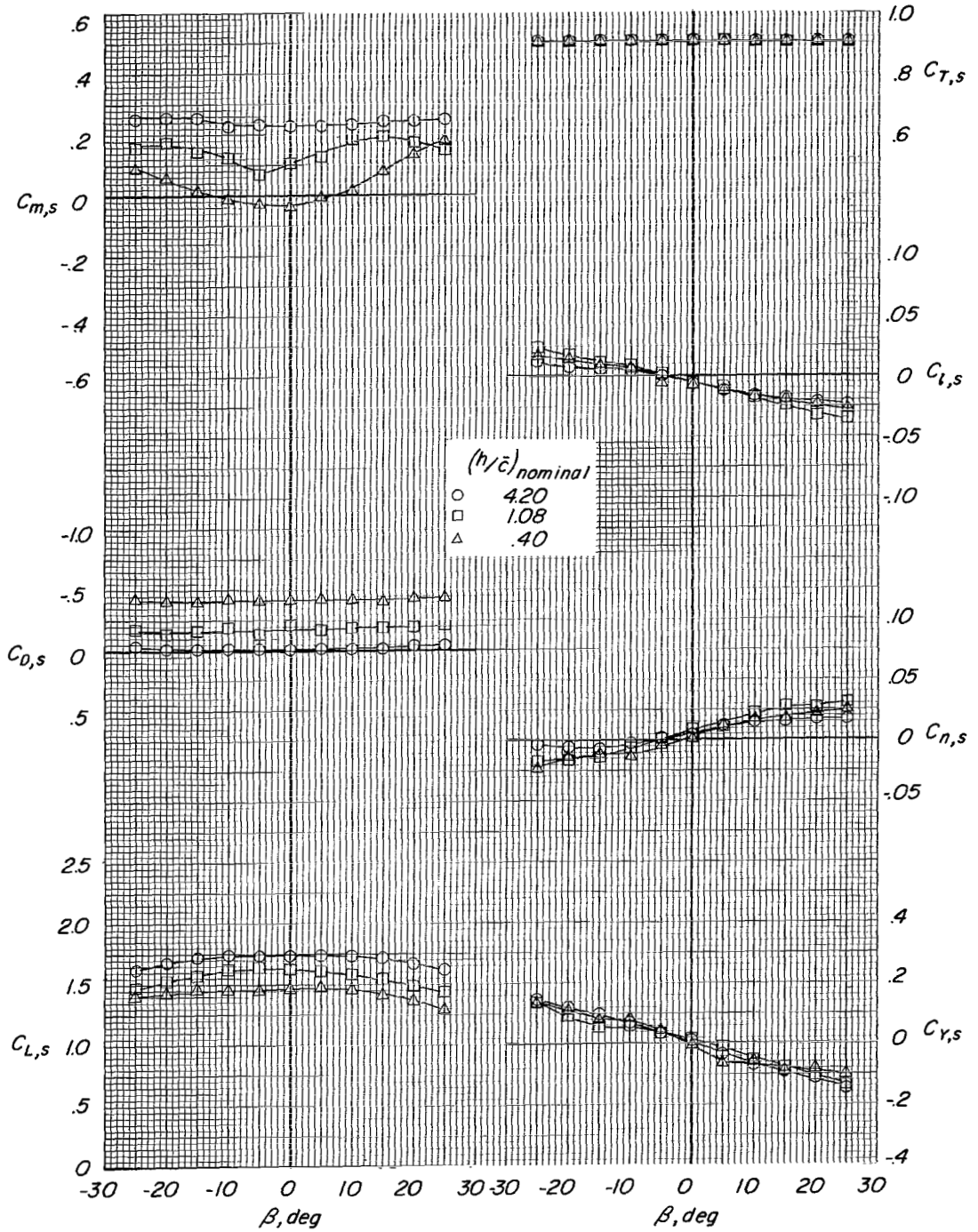

(d) $i_w = 50^0$; $\delta_f = 30^0$.

Figure 16.- Continued.

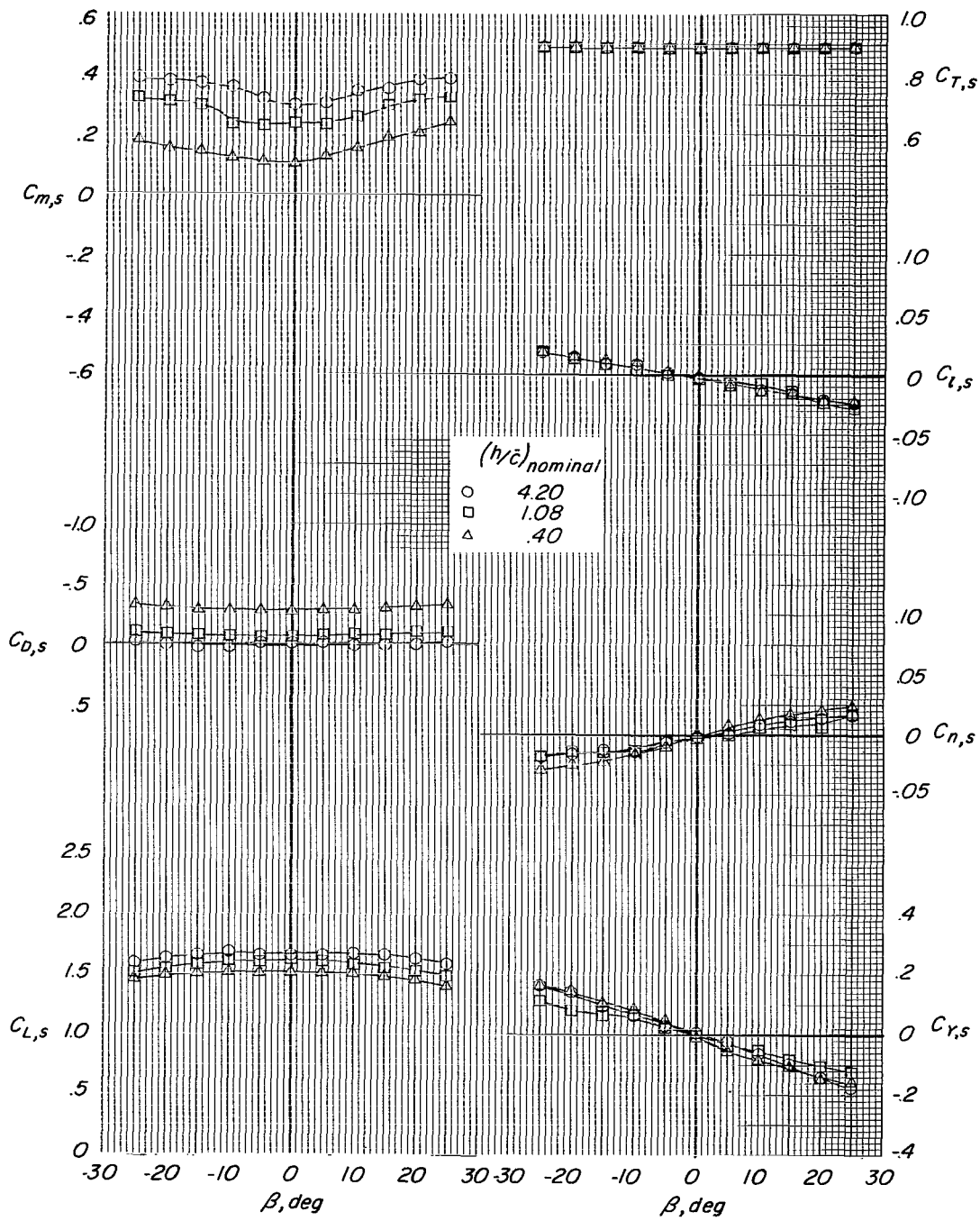

(e) $i_w = 60^0$; $\delta_f = 10^0$.

Figure 16.- Continued.

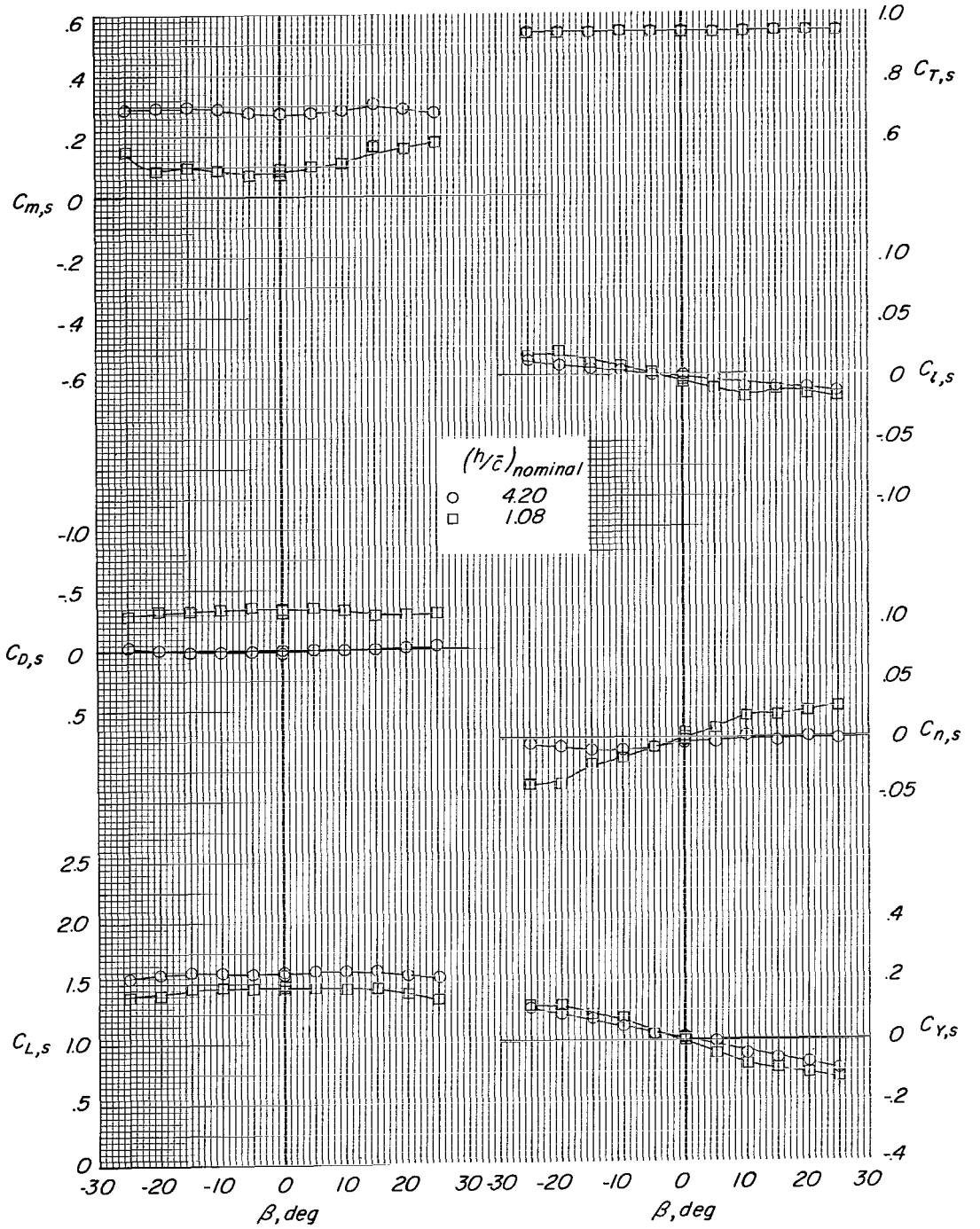

(f) $i_w = 60^0$; $\delta_f = 20^0$.

Figure 16.- Continued.

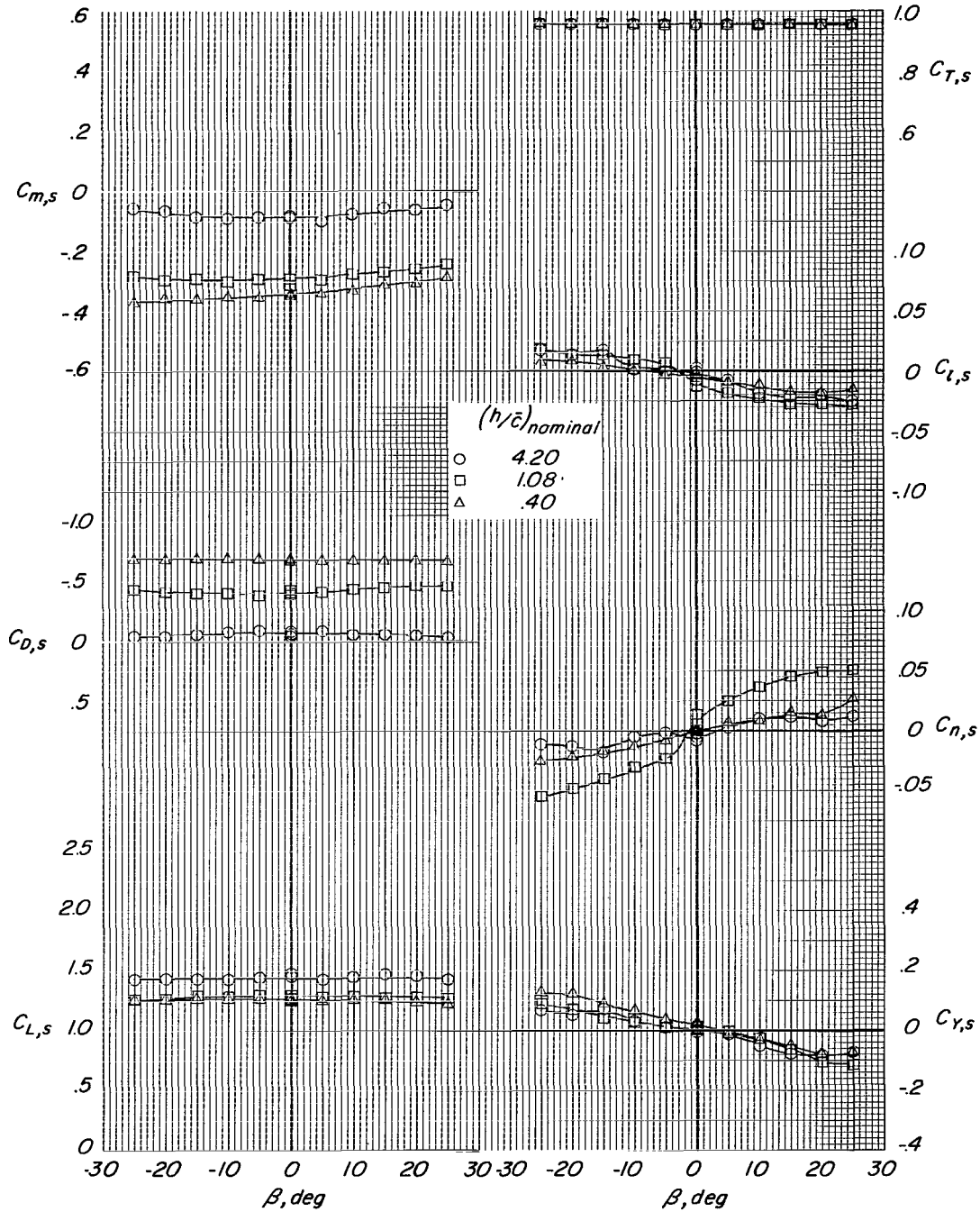

(g) $i_w = 45^0$; $\delta_f = 60^0$.

Figure 16.- Continued.

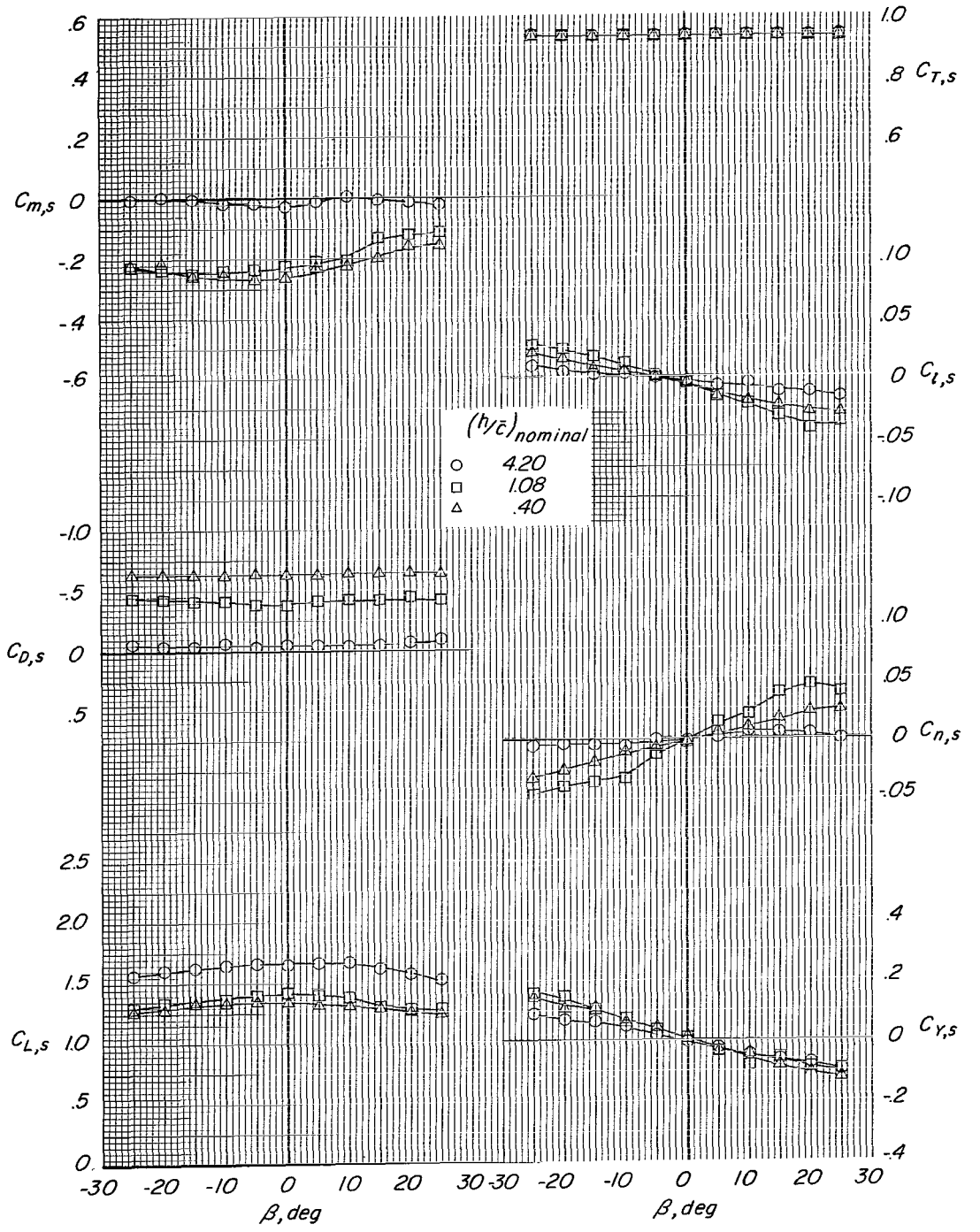

(h) $i_w = 40^0$; $\delta_f = 60^0$.

Figure 16.- Continued.

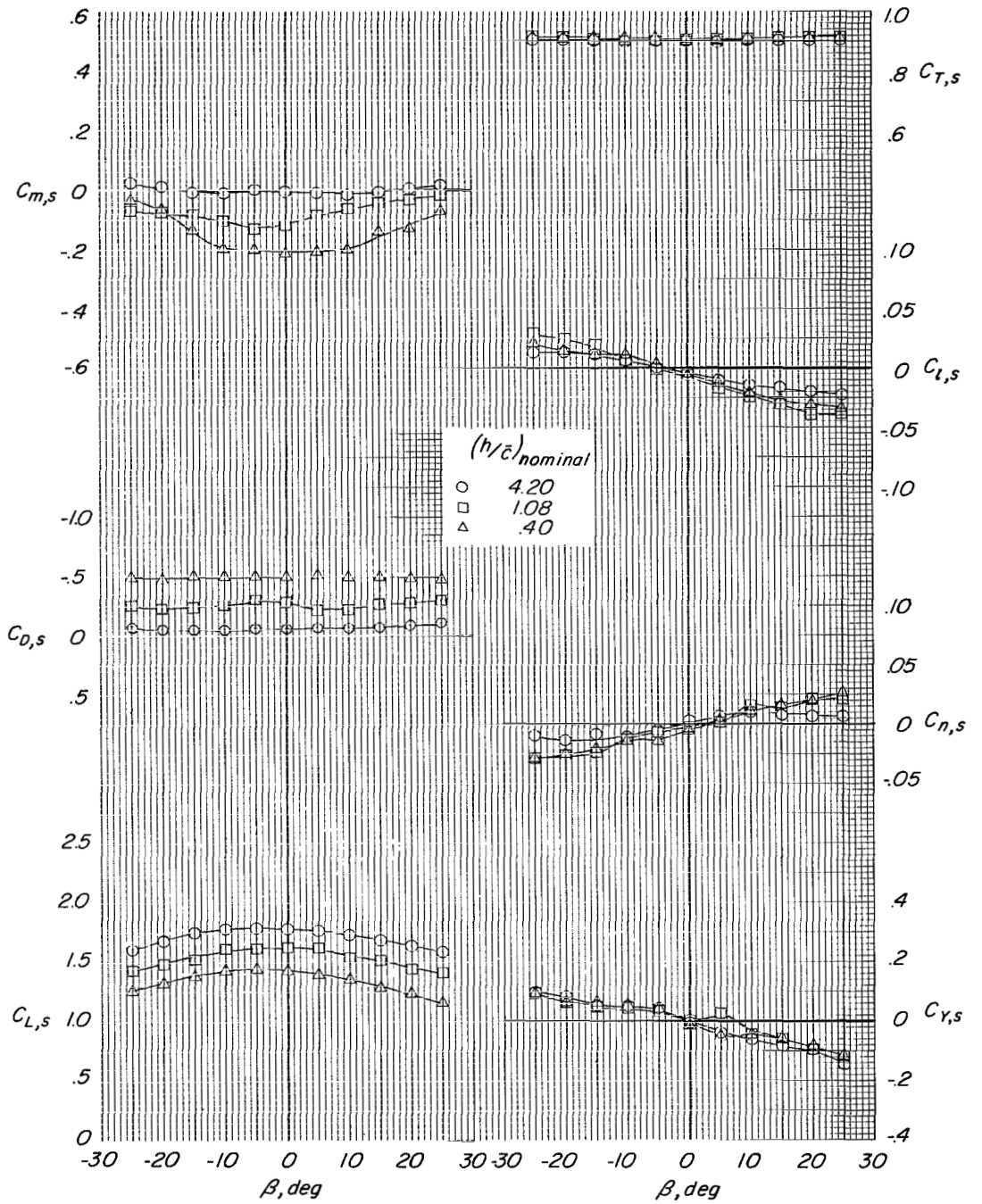

(i) $i_w = 35^0$; $\delta_f = 60^0$.

Figure 16.- Continued.

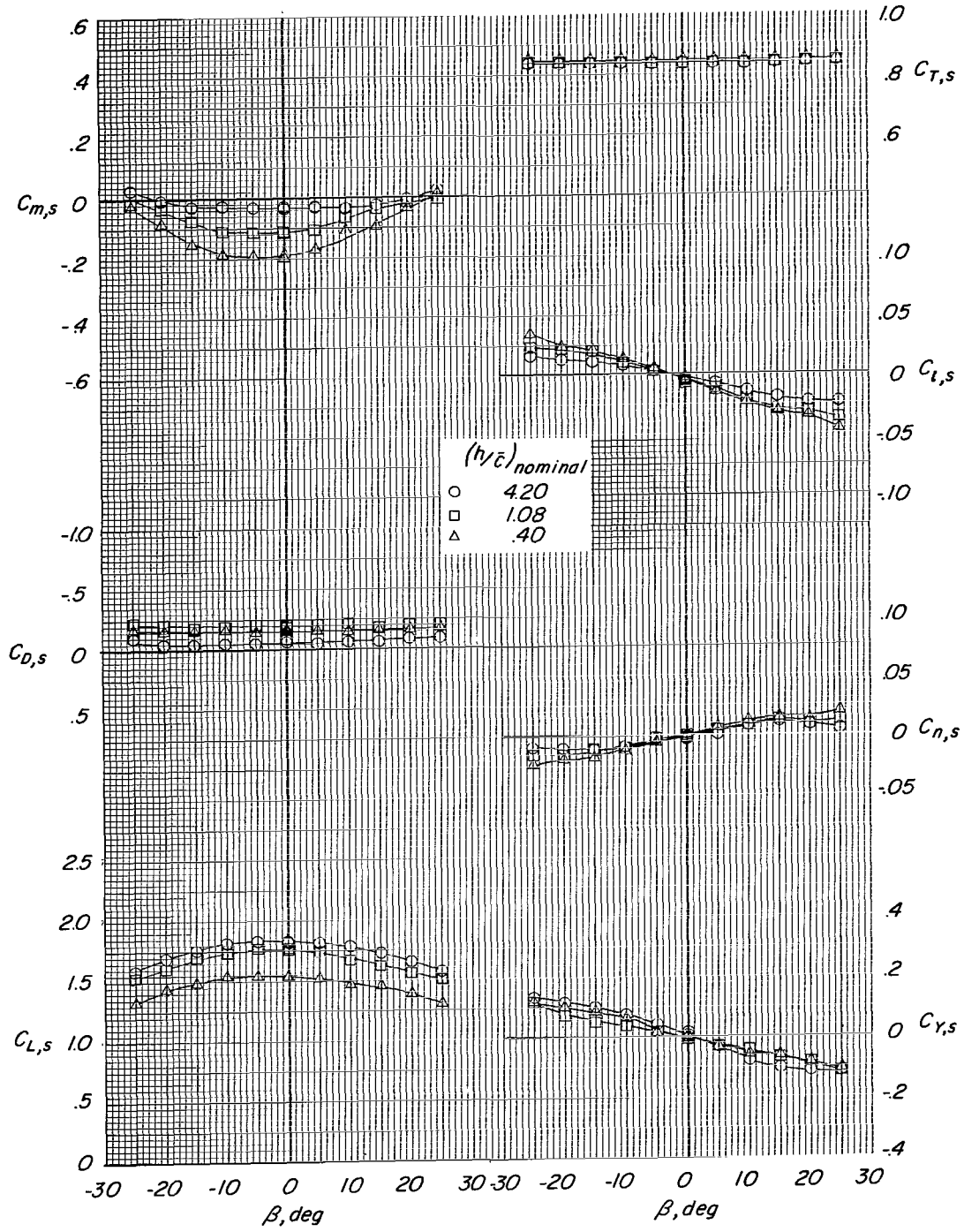

(j) $i_W = 30^0$; $\delta_f = 60^0$.

Figure 16.- Concluded.

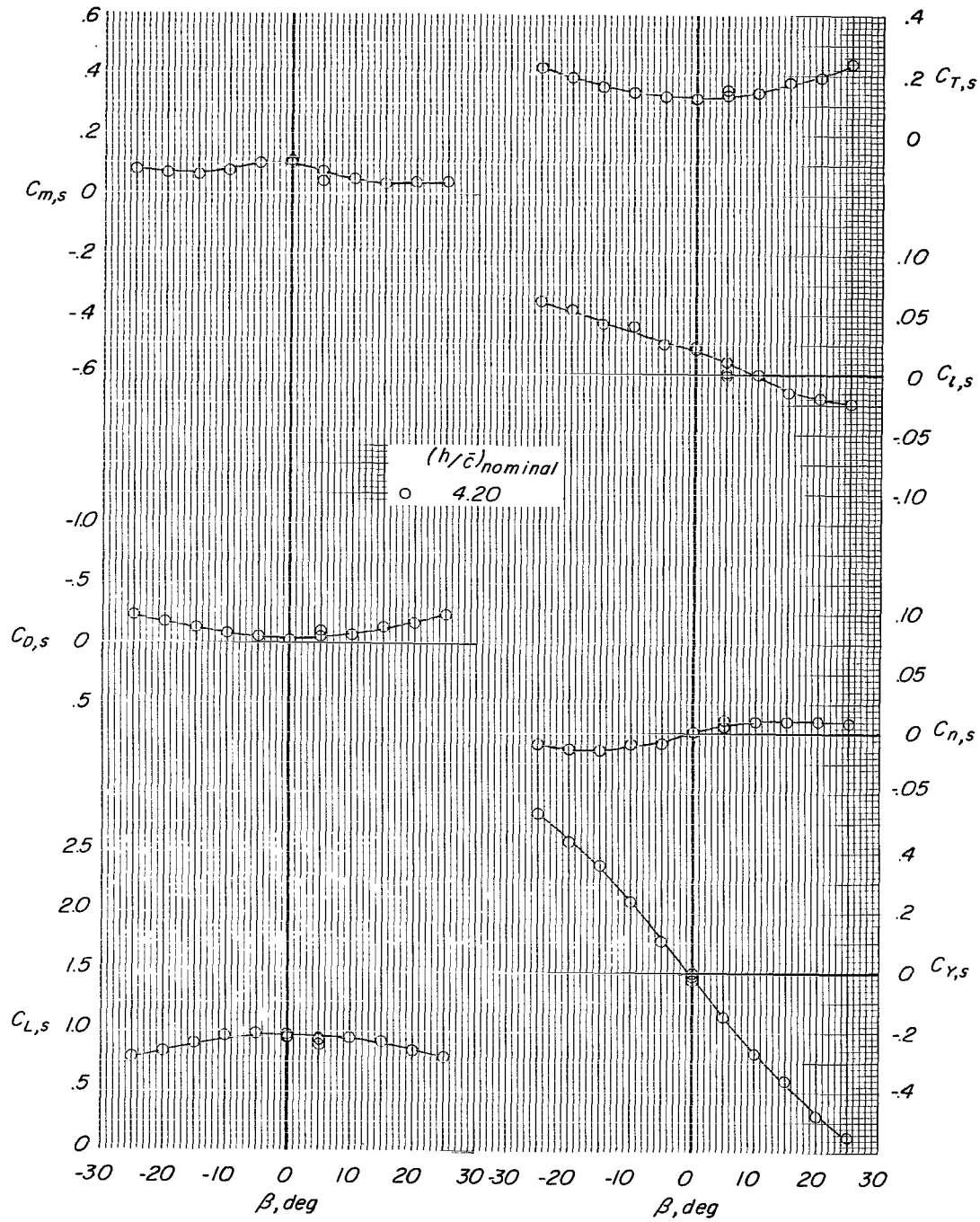

(a) $i_w = 0^0$; $\delta_f = 0^0$.

Figure 17.- Lateral aerodynamic characteristics at various ground-height ratios for various wing-incidence—flap-deflection combinations at $\alpha = 10^0$. Belt moving; 7000 rpm; $\delta_a = 0^0$; slat on and $i_t = 20^0$ (except for $i_w = 0^0$ and $\delta_f = 0^0$, where horizontal tail and slats were off). (q was established at Drag $\approx$ 0 for $h/\bar{c} = 4.20$ and $\alpha = 0^0$.)

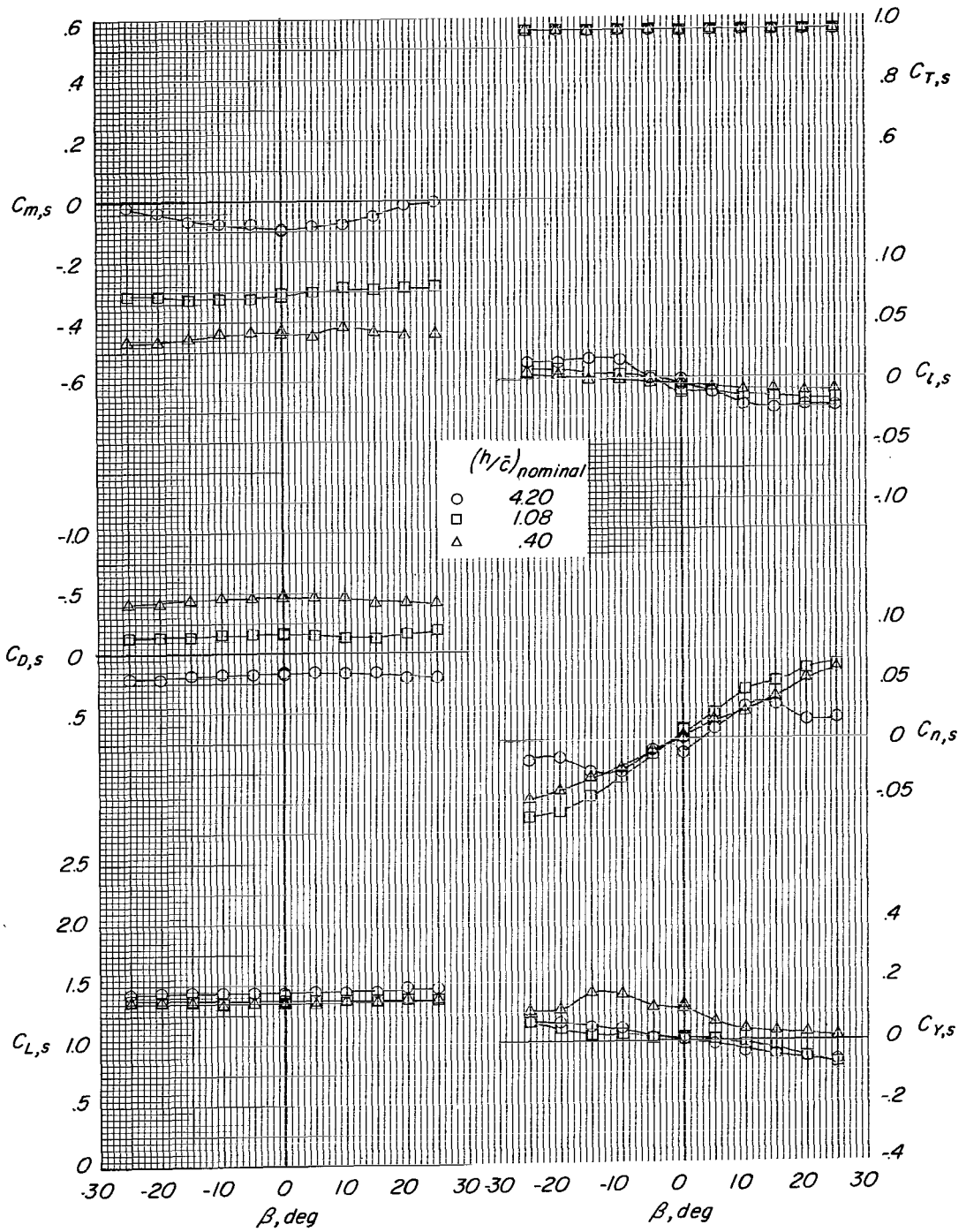

(b) $i_w = 45^o$; $\delta_f = 60^o$.

Figure 17.- Continued.

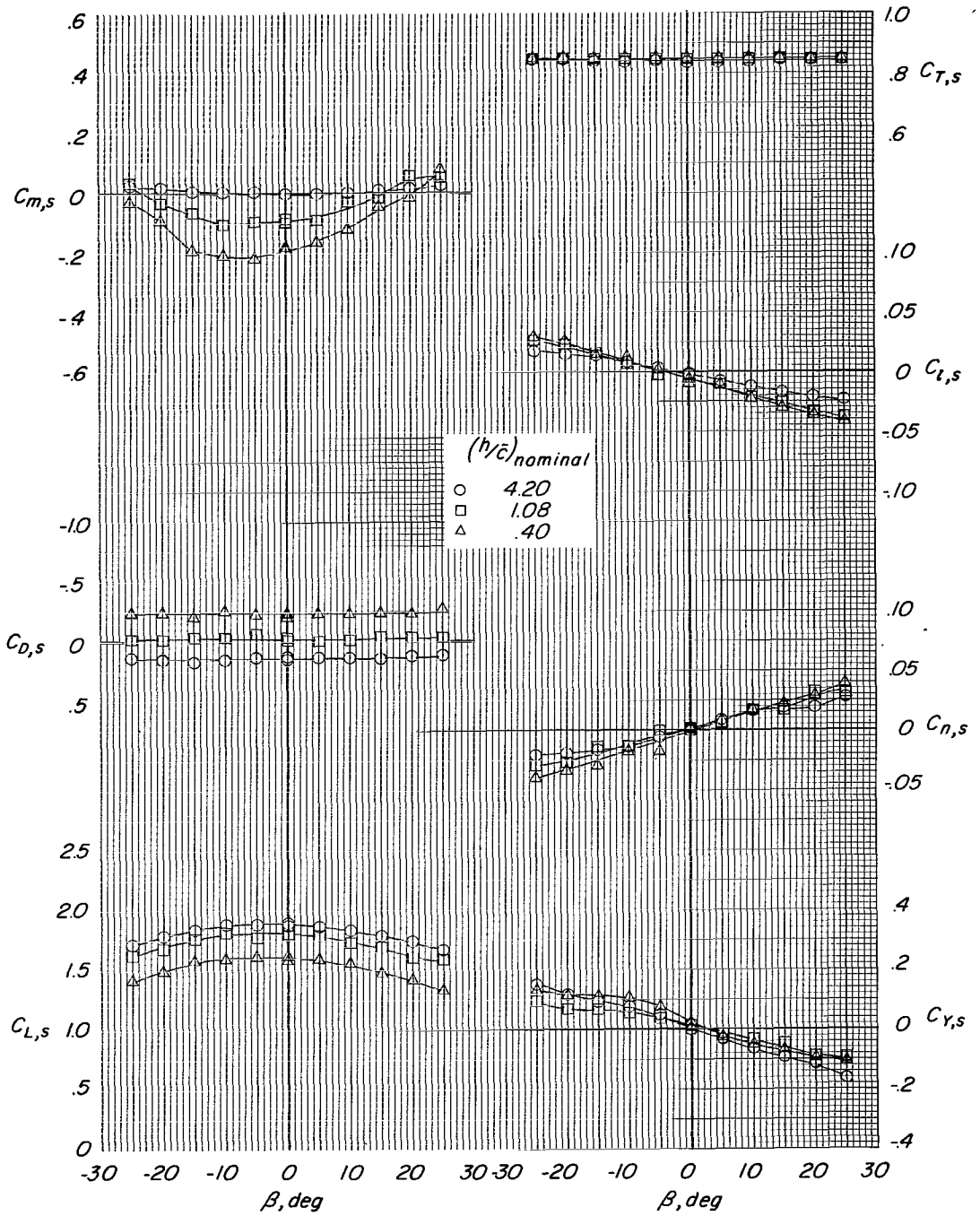

(c) $i_w = 30^0$; $\delta_f = 60^0$.

Figure 17.- Concluded.

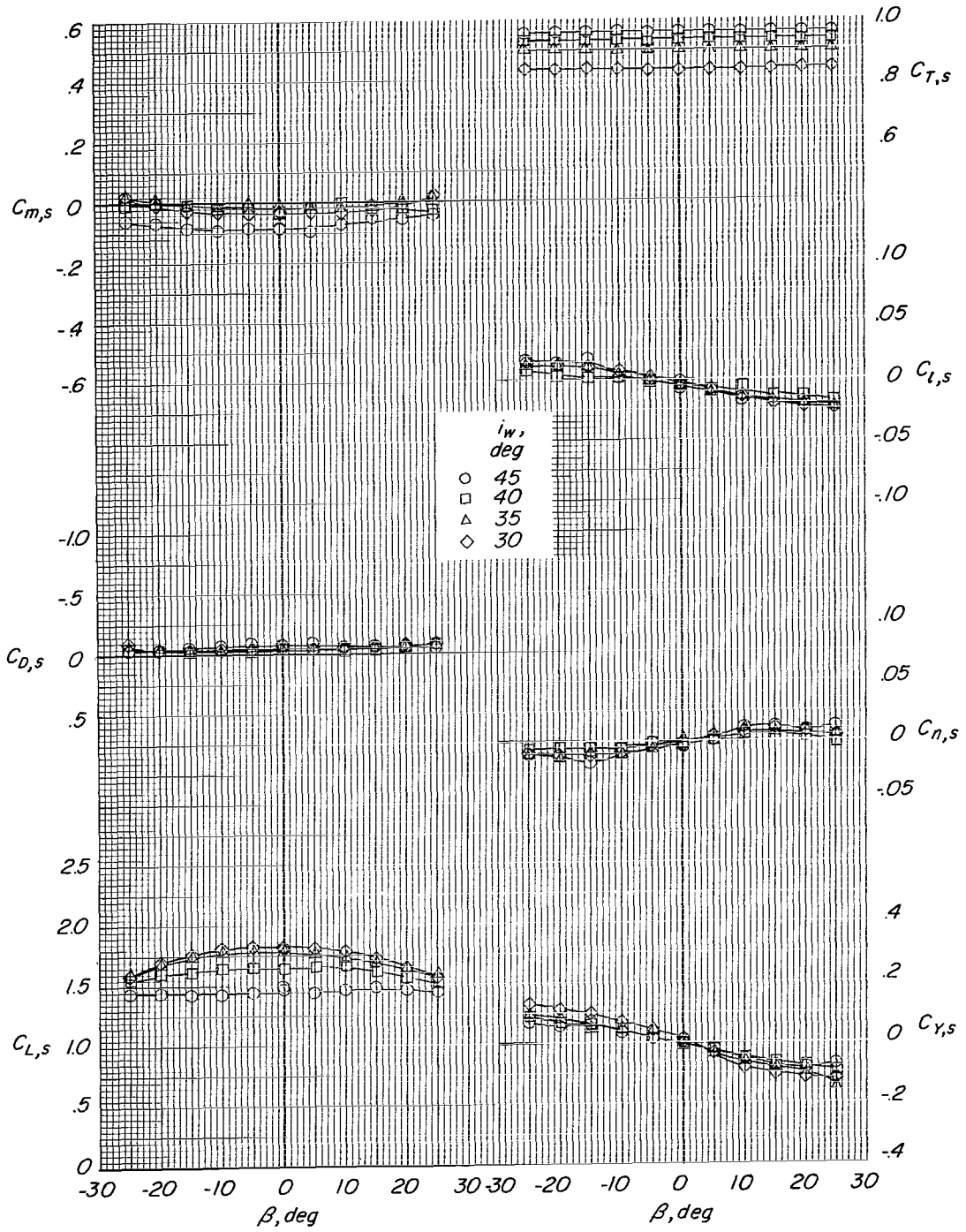

(a) $h/\bar{c}$ = 4.20.

Figure 18.- Lateral aerodynamic characteristics of configurations with various wing-incidence angles and $\delta_f = 60^0$ for several ground-height ratios. $\alpha = 0^0$; belt moving; 7000 rpm; $\delta_a = 0^0$; slat on; $i_t = 20^0$. (q was established at Drag ≈ 0 for $h/\bar{c}$ = 4.20 and $\alpha = 0^0$.)

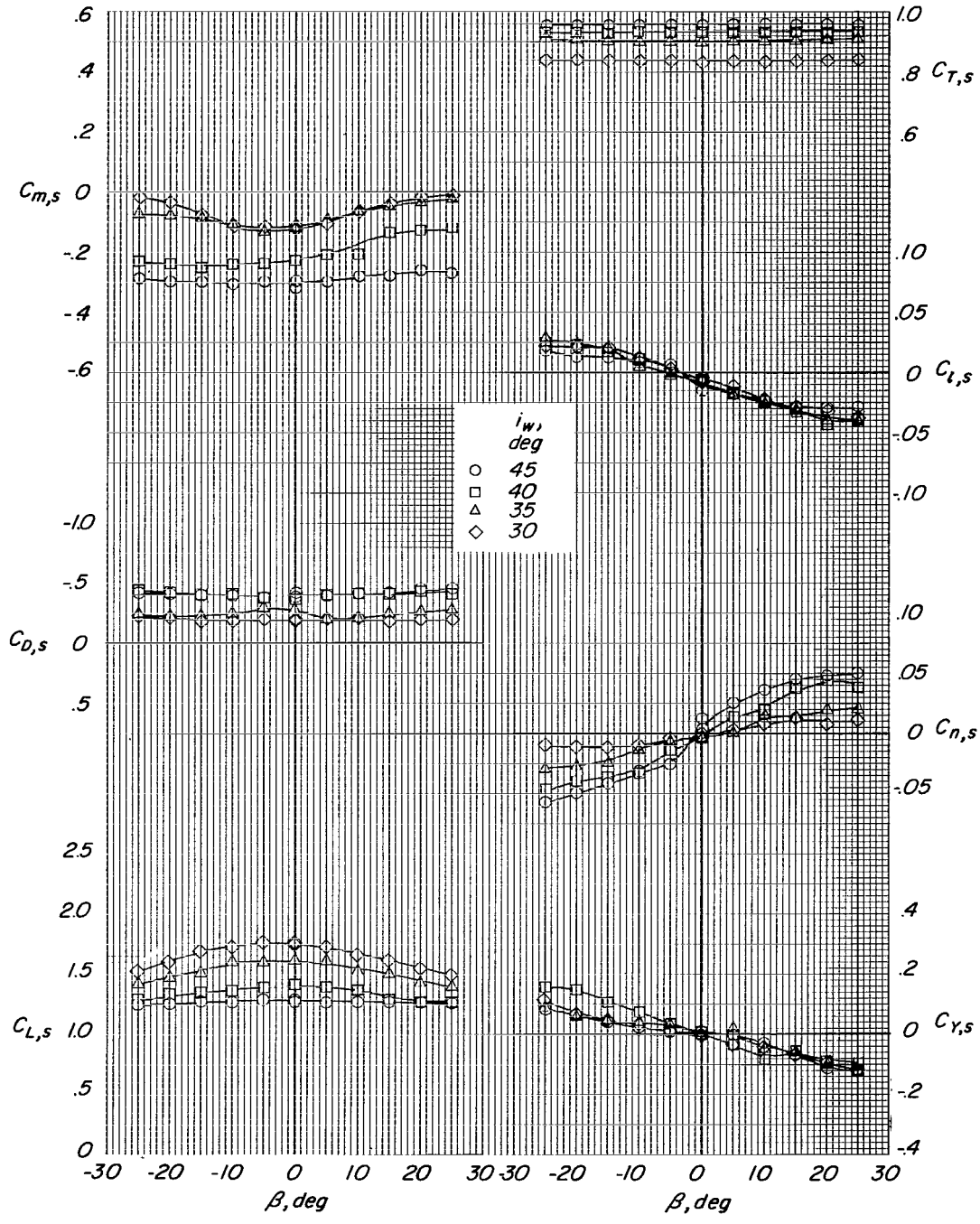

(b) $h/\bar{c} = 1.08$.

Figure 18.- Continued.

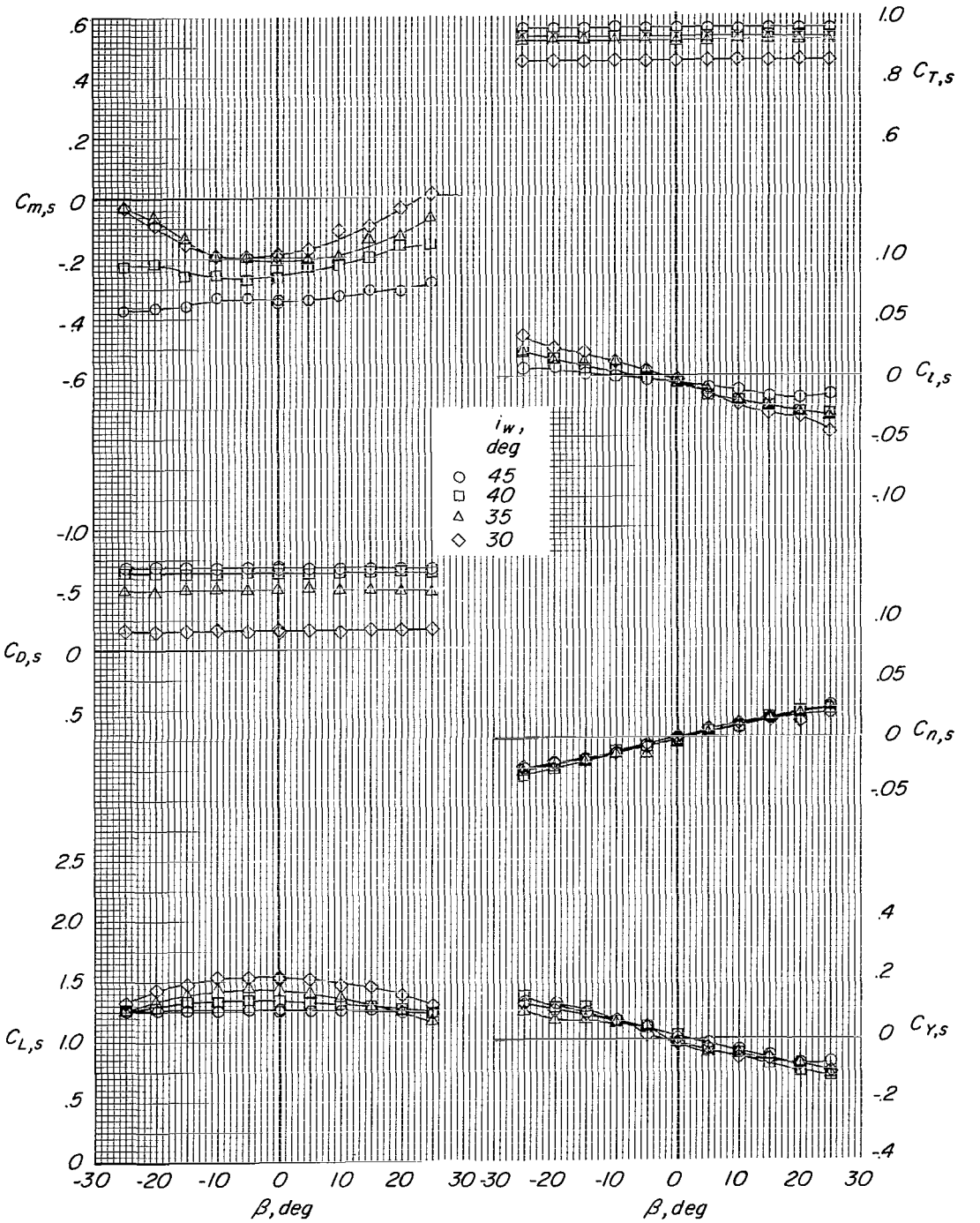

(c) $h/\bar{c} = 0.40$.

Figure 18.- Concluded.

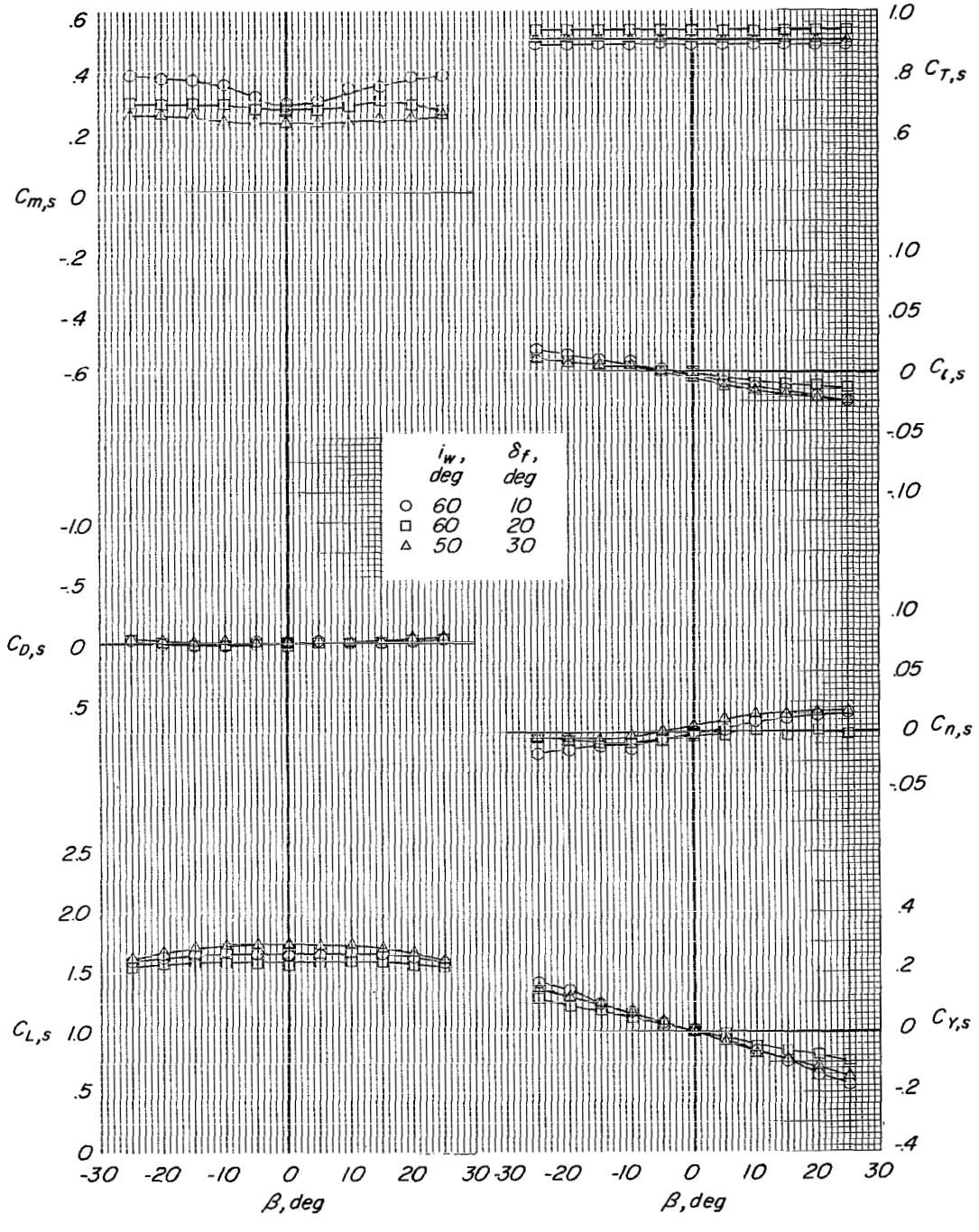

(a) $h/\bar{c}$ = 4.20.

Figure 19.- Lateral aerodynamic characteristics of several wing-tilt—flap-deflection combinations for several ground-height ratios. $\alpha = 0^0$; belt moving; 7000 rpm; $\delta_a = 0^0$; slat on; $i_t = 20^0$. (q was established at Drag ≈ 0 for $h/\bar{c}$ = 4.20 and $\alpha = 0^0$.)

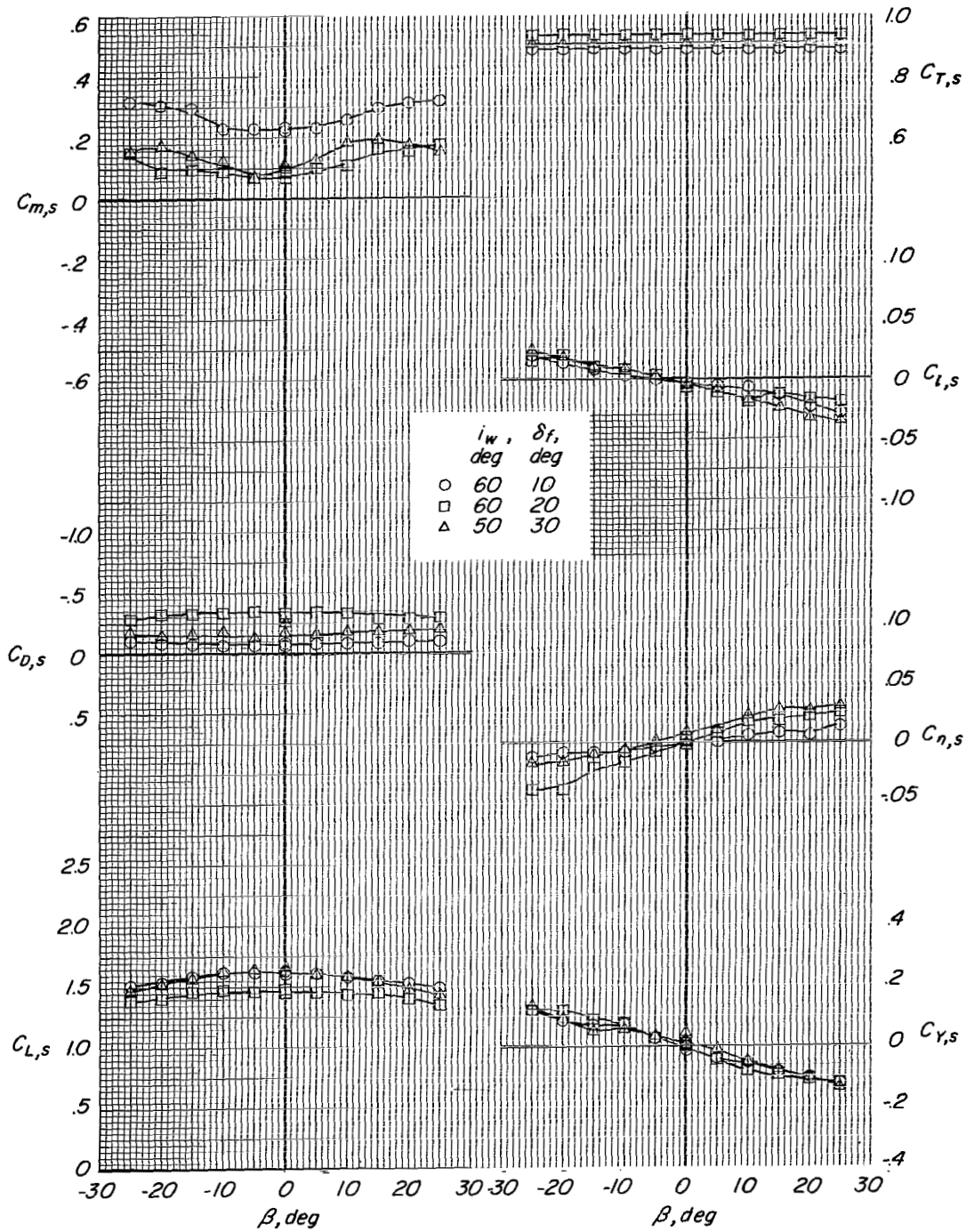

(b) $h/\bar{c} = 1.08$.

Figure 19.- Continued.

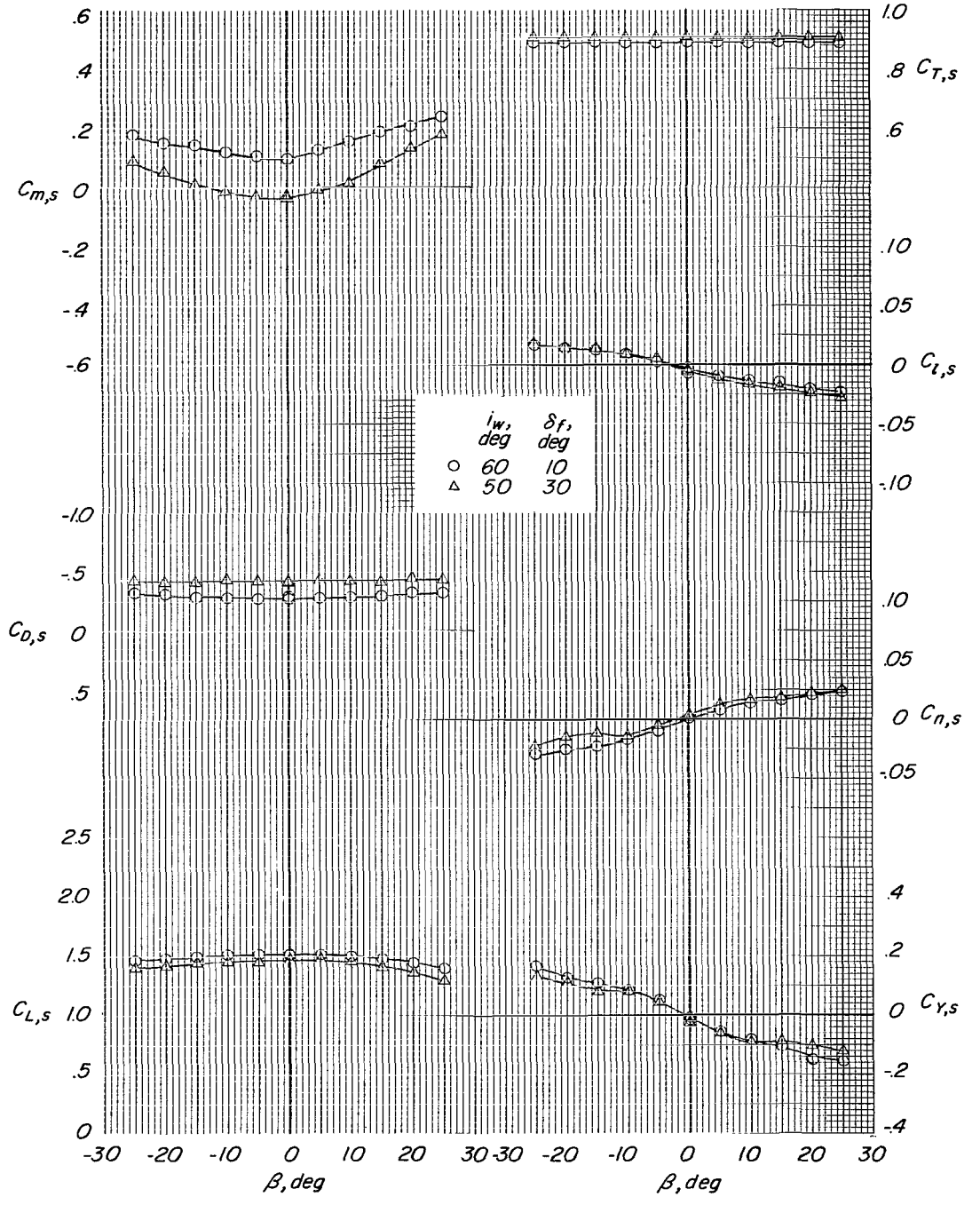

(c) $h/\bar{c} = 0.40$.

Figure 19.- Concluded.

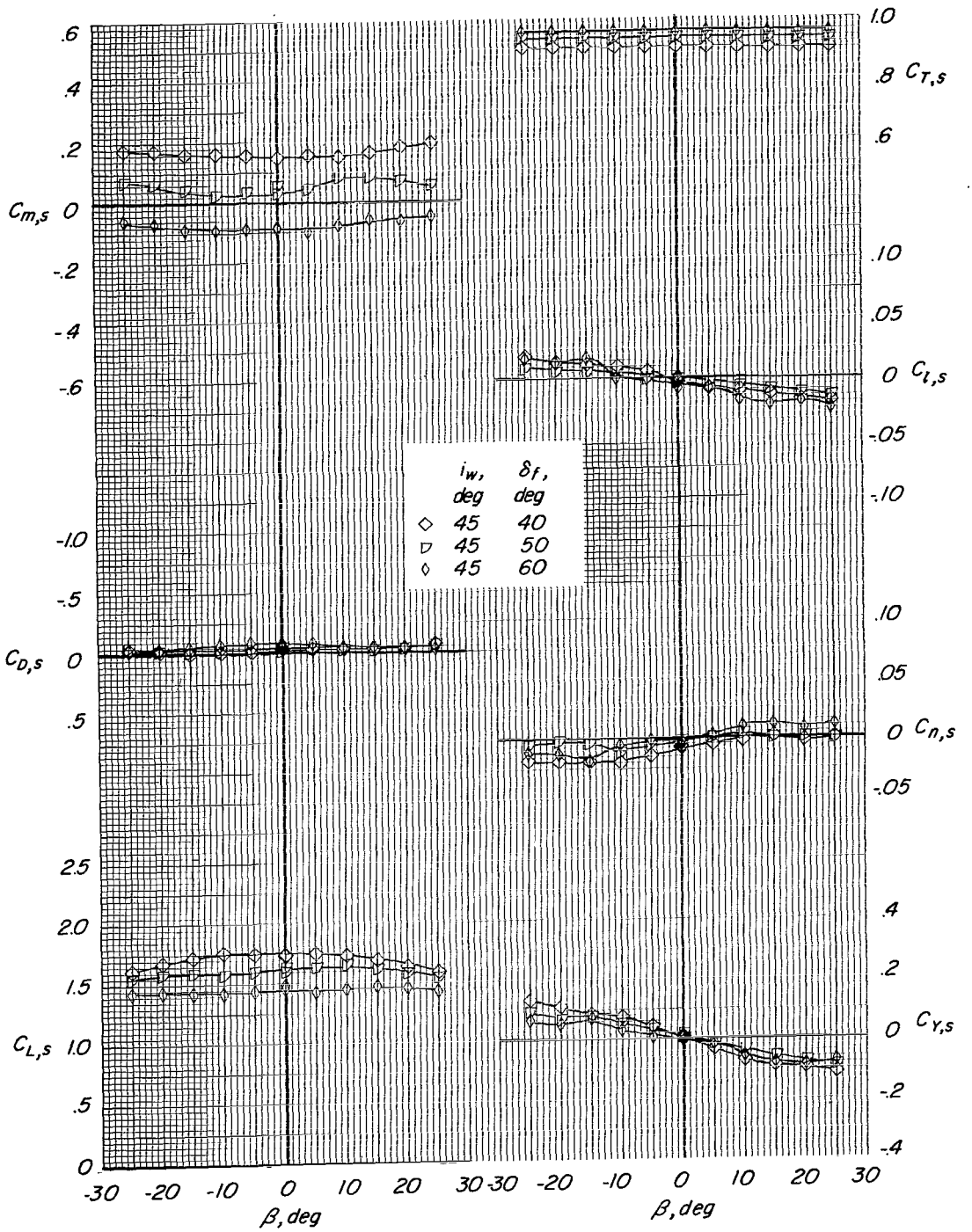

(a) $h/\bar{c} = 4.20$.

Figure 20.- Lateral aerodynamic characteristics of configurations with several flap-deflection angles and $i_w = 45^0$ for several ground-height ratios. $\alpha = 0^0$; belt moving; 7000 rpm; $\delta_a = 0^0$; slat on; $i_t = 20^0$. (q was established at Drag $\approx$ 0 for $h/\bar{c} = 4.20$ and $\alpha = 0^0$.)

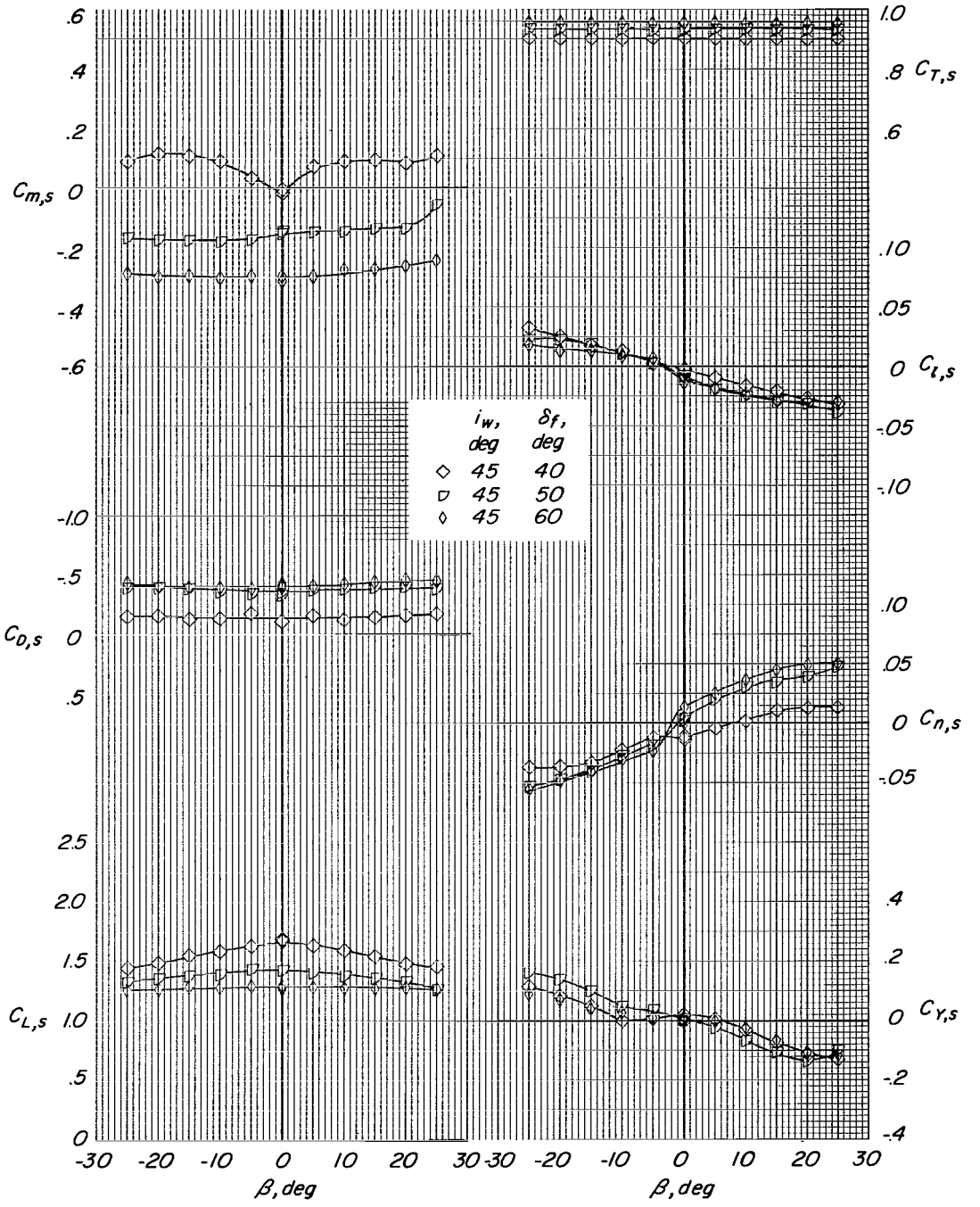

(b) $h/\bar{c} = 1.08$.

Figure 20.- Continued.

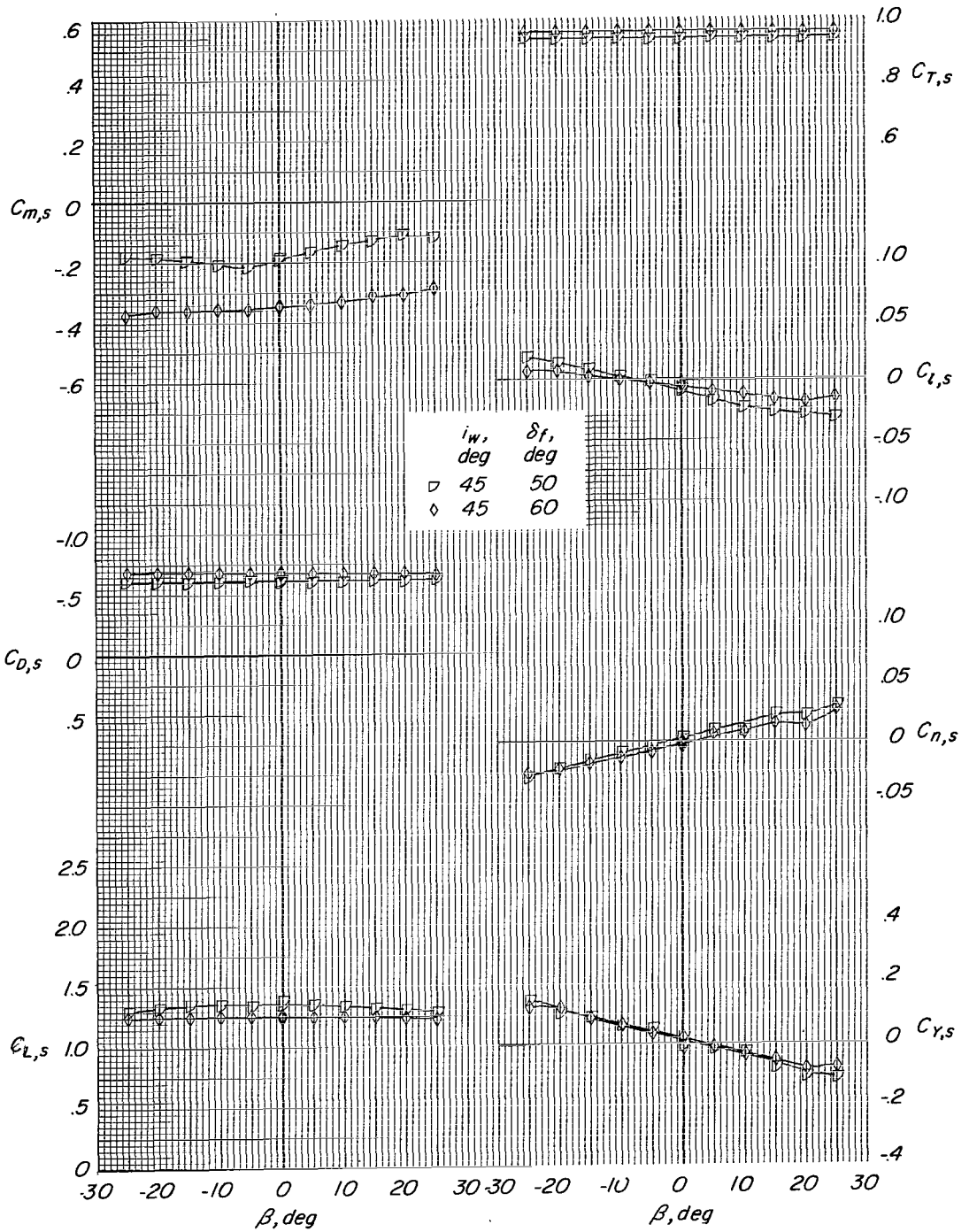

(c) $h/\bar{c} = 0.40$.

Figure 20.- Concluded.

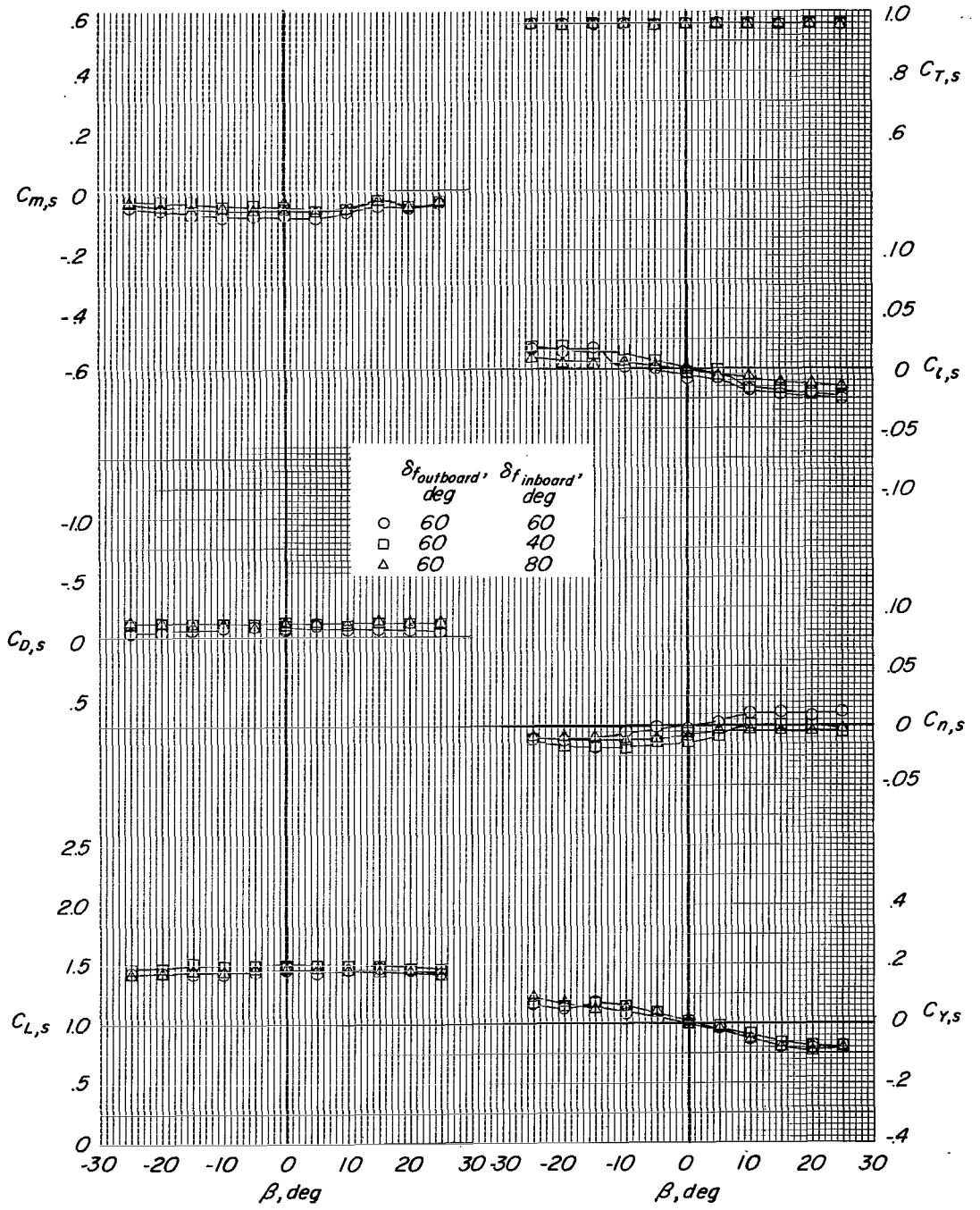

(a) $h/\bar{c} = 4.20$.

Figure 21.- Effect of differential flap deflection on the lateral aerodynamic characteristics with $i_w = 45^0$. $\alpha = 0^0$; belt moving; 7000 rpm; $\delta_a = 0^0$; slat on; $i_t = 20^0$. (q was established at Drag ≈ 0 for $h/\bar{c} = 4.20$ and $\alpha = 0^0$.)

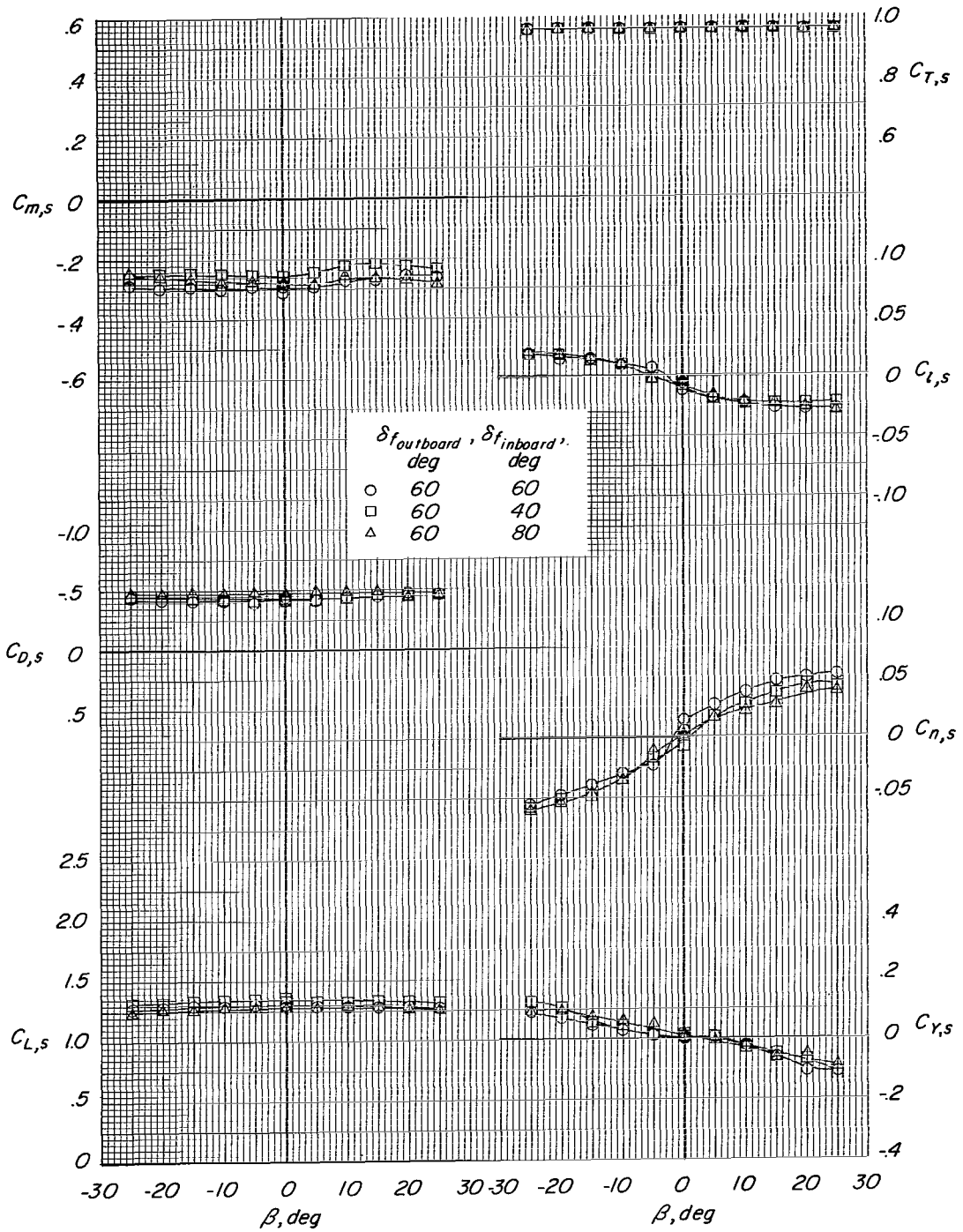

(b) $h/\bar{c} = 1.08$.

Figure 21.- Continued.

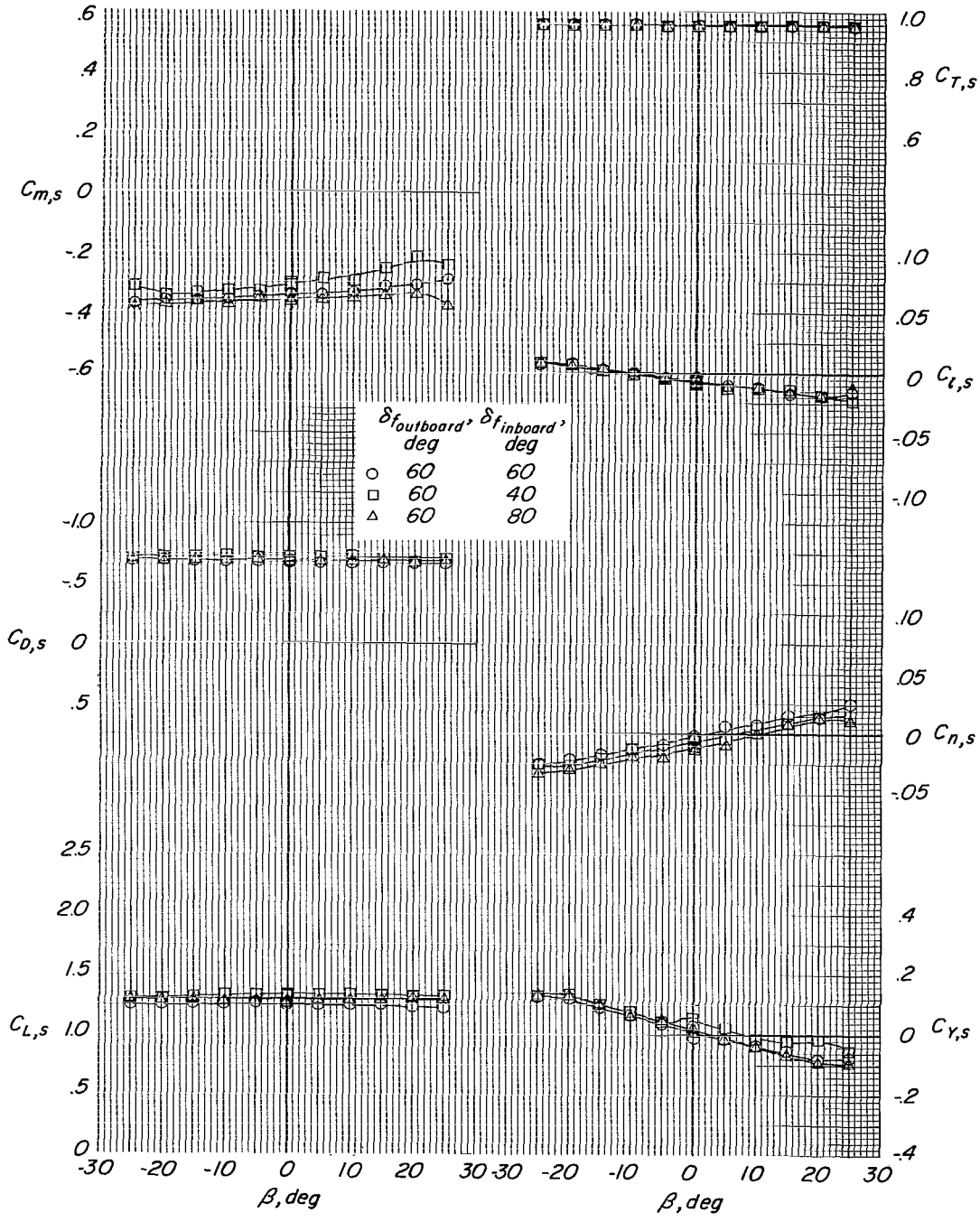

(c) $h/\bar{c} = 0.40$.

Figure 21.- Concluded.

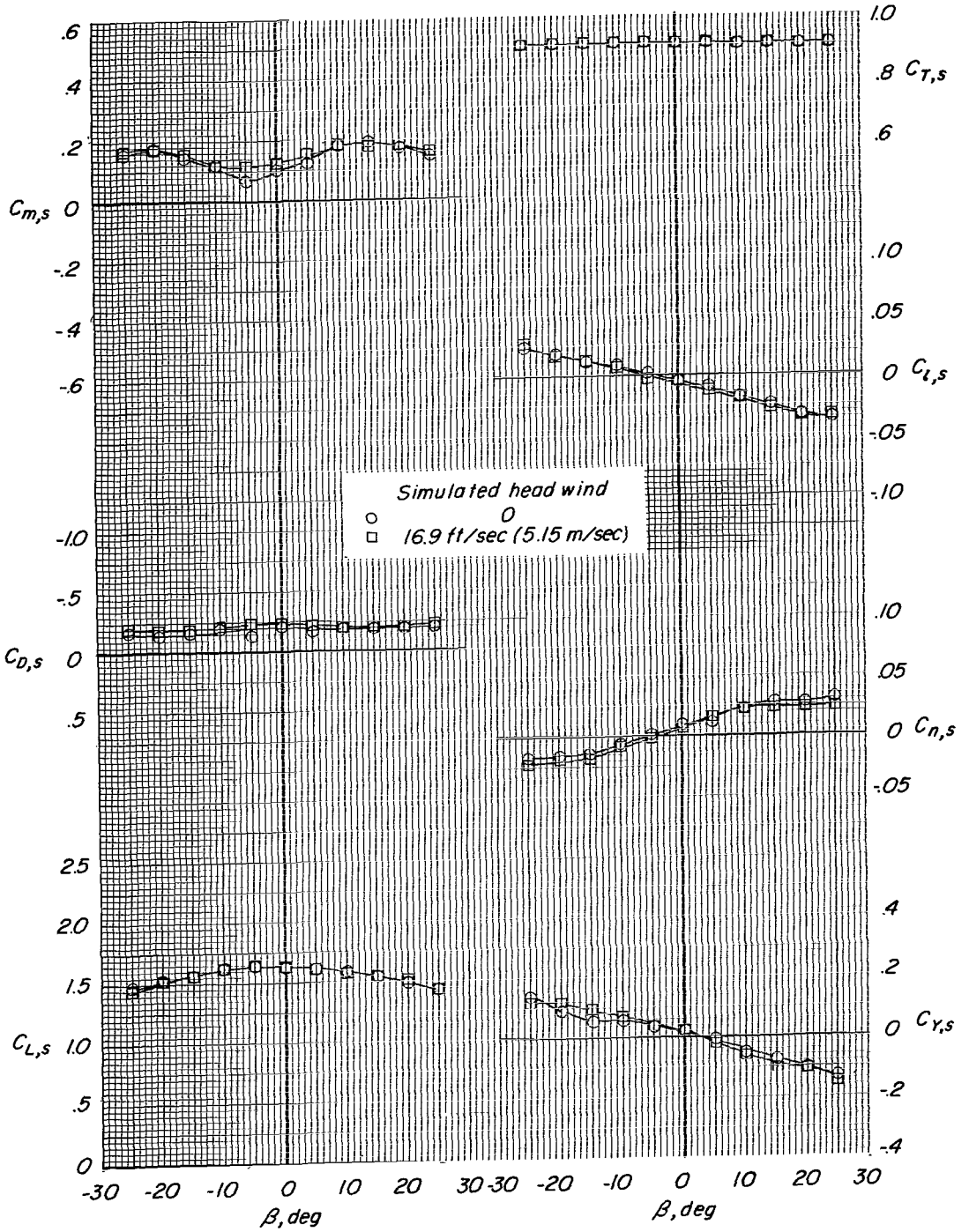

(a) $i_w = 50^0$; $\delta_f = 30^0$.

Figure 22.- Effect of a 16.9-ft/sec (5.15-meter/sec) simulated head wind on the lateral aerodynamic characteristics in sideslip for several wing-incidence—flap-deflection combinations. $\alpha = 0^0$; belt moving; $\delta_a = 0^0$; 7000 rpm; $i_t = 0^0$; $h/\bar{c} = 1.08$. (q was established at Drag $\approx$ 0 for $h/\bar{c} = 4.20$ and $\alpha = 0^0$.)

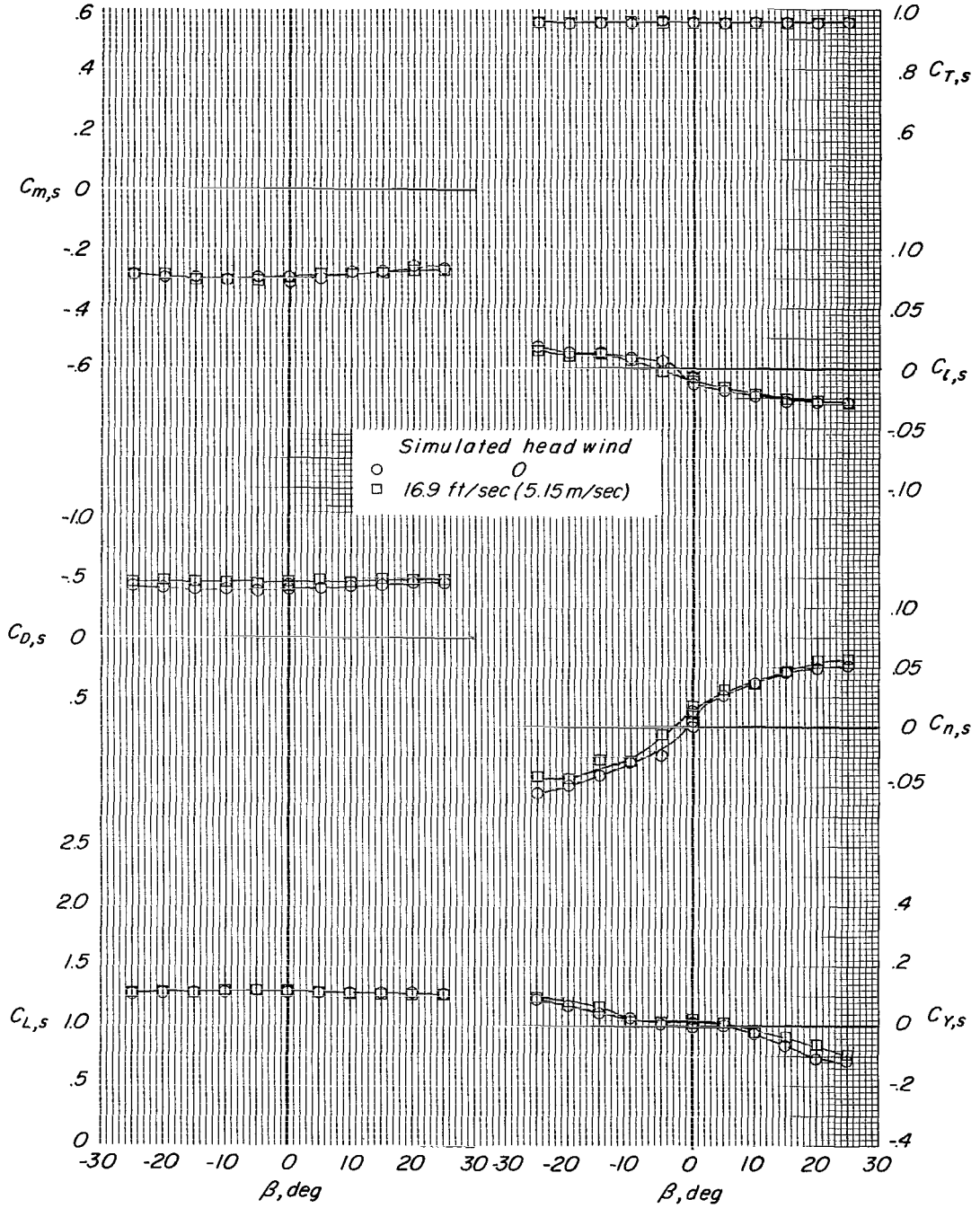

(b) $i_w = 45^0$; $\delta_f = 60^0$.

Figure 22.- Continued.

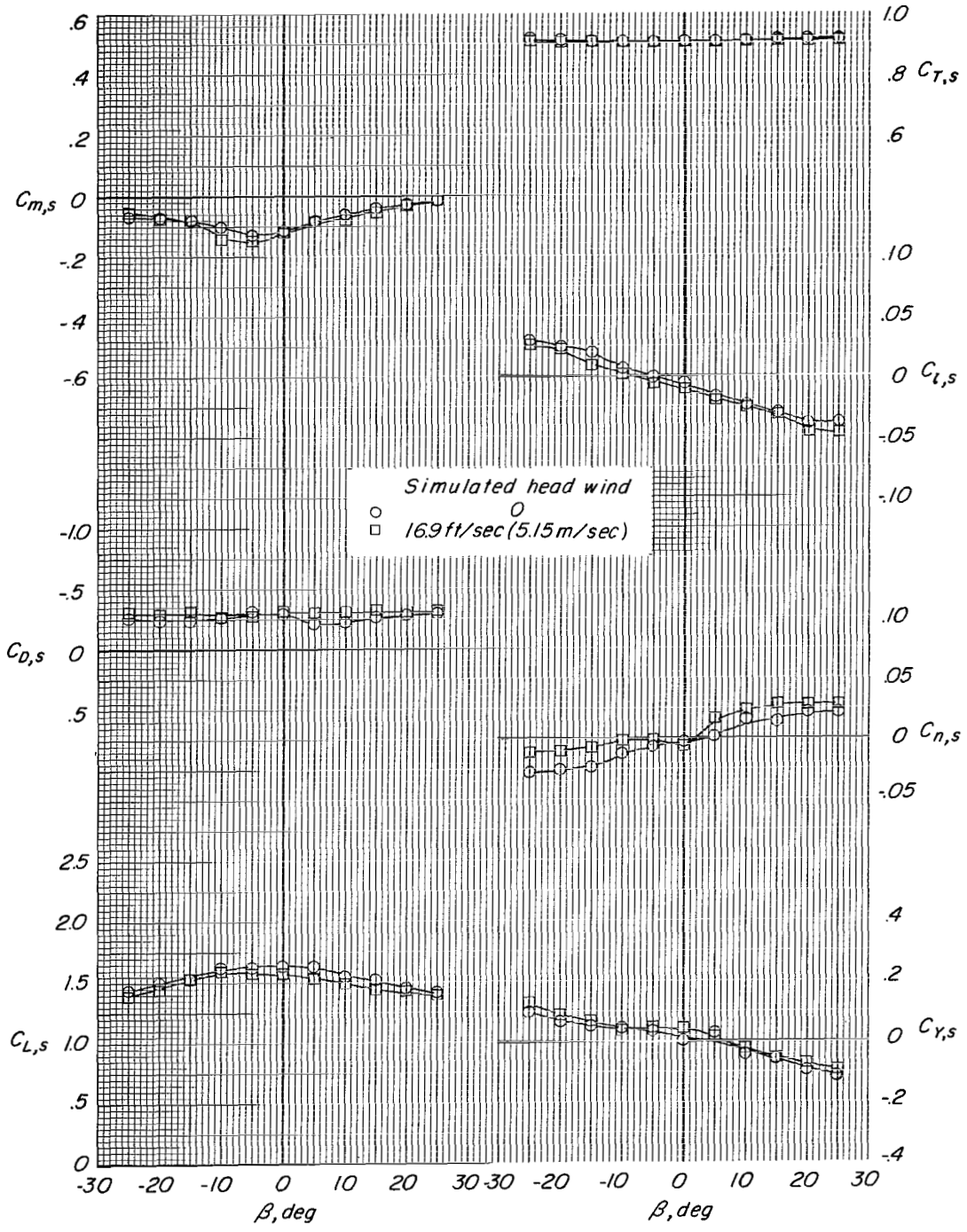

(c) $i_w = 35^0$; $\delta_f = 60^0$.

Figure 22.- Concluded.

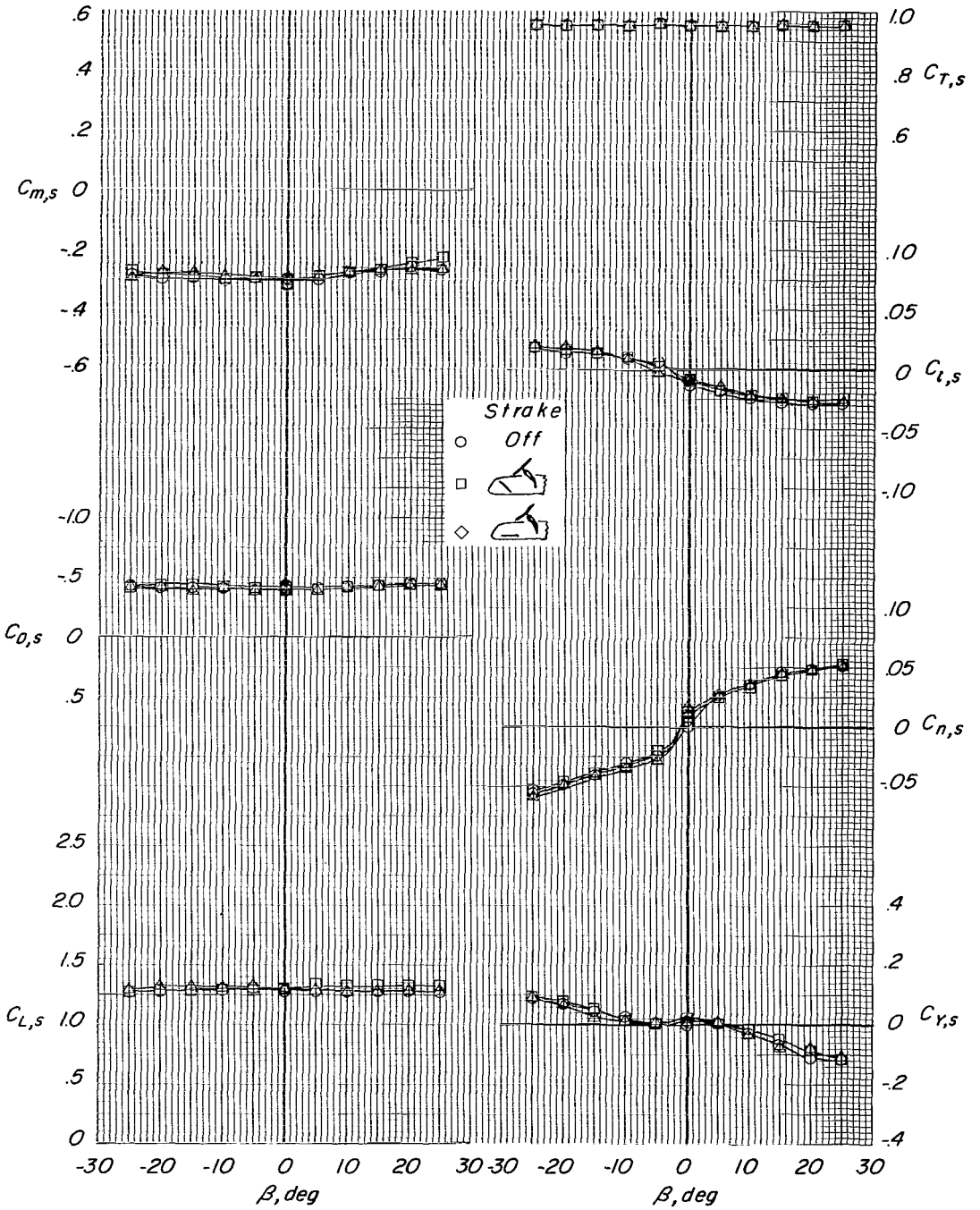

Figure 23.- Effect of fuselage nose strakes on the lateral aerodynamic characteristics in sideslip. $\alpha = 0^0$; $i_w = 45^0$; $\delta_f = 60^0$; $i_t = 20^0$; 7000 rpm; belt moving; slat on; $\delta_a = 0^0$; $h/\bar{c} = 1.08$. (q was established at Drag $\approx$ 0 for $h/\bar{c} = 4.20$ and $\alpha = 0^0$.)

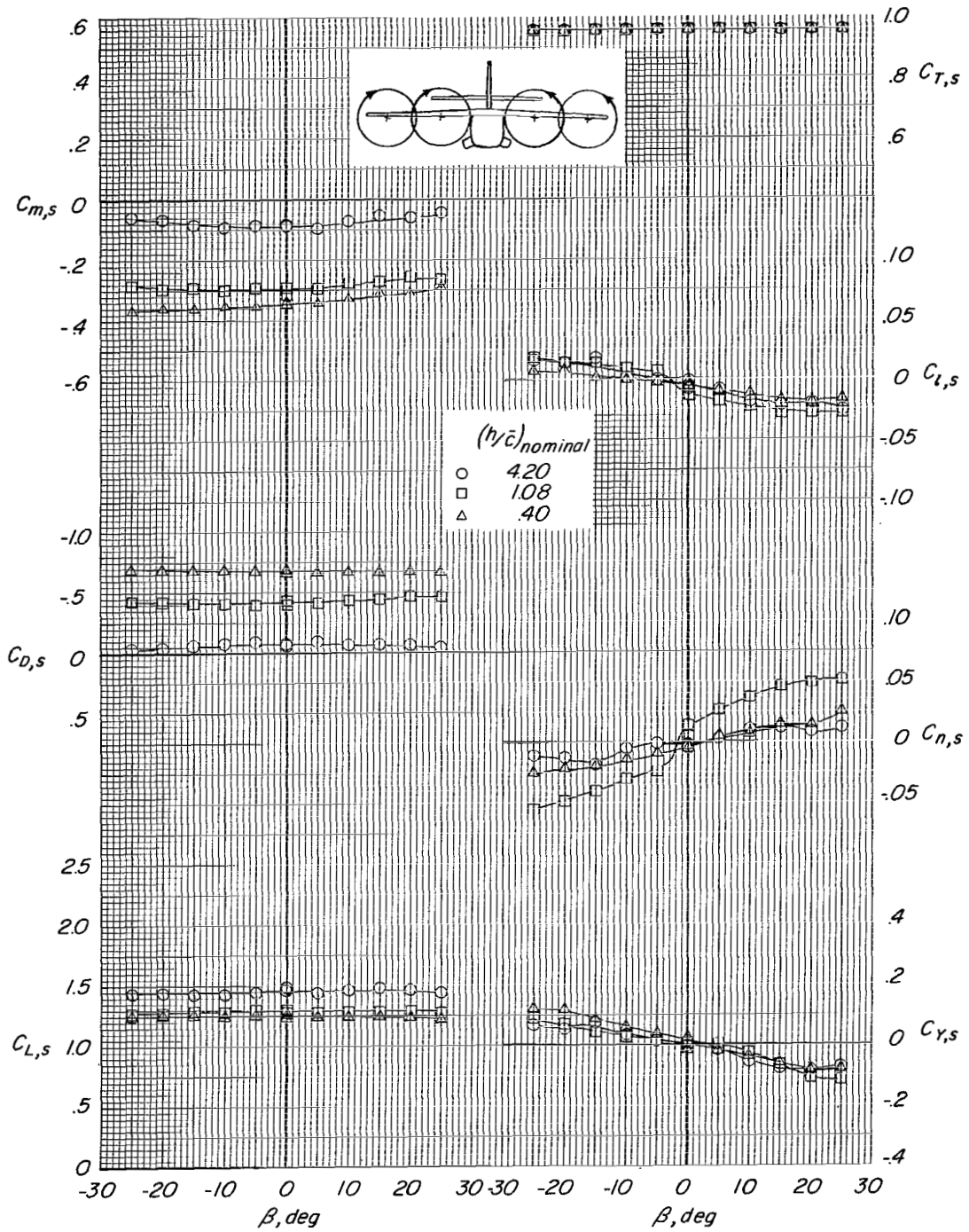

(a) Normal propeller rotation.

Figure 24.- Effect of direction of propeller rotation on the lateral aerodynamic characteristics at several ground-height ratios. $\alpha = 0^0$; $i_w = 45^0$; $\delta_f = 60^0$; $i_t = 20^0$; 7000 rpm; $\delta_a = 0^0$; belt moving; slat on. (q was established at Drag $\approx$ 0 for $h/\bar{c} = 4.20$ and $\alpha = 0^0$.)

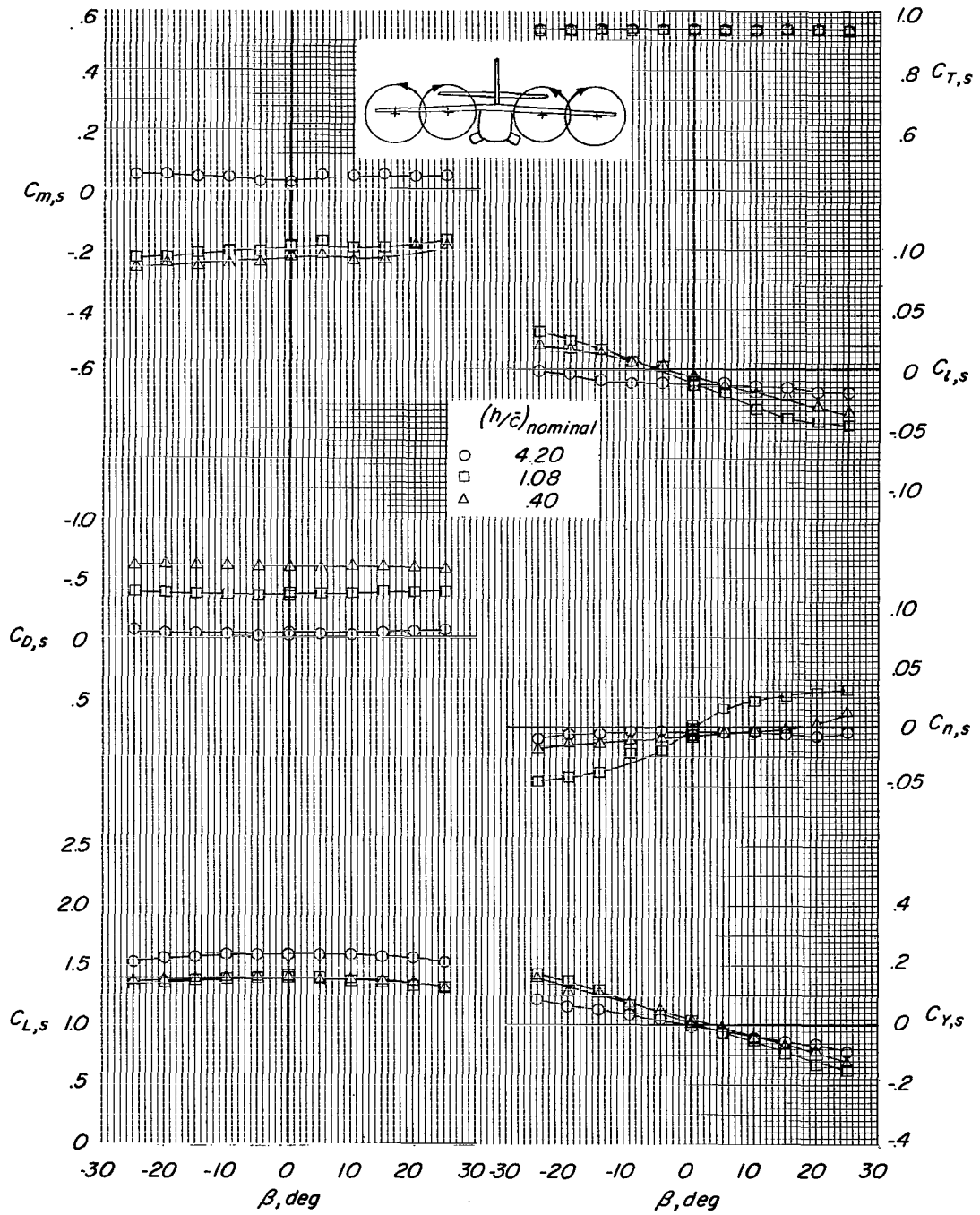

(b) Propeller rotation altered.

Figure 24.- Concluded.

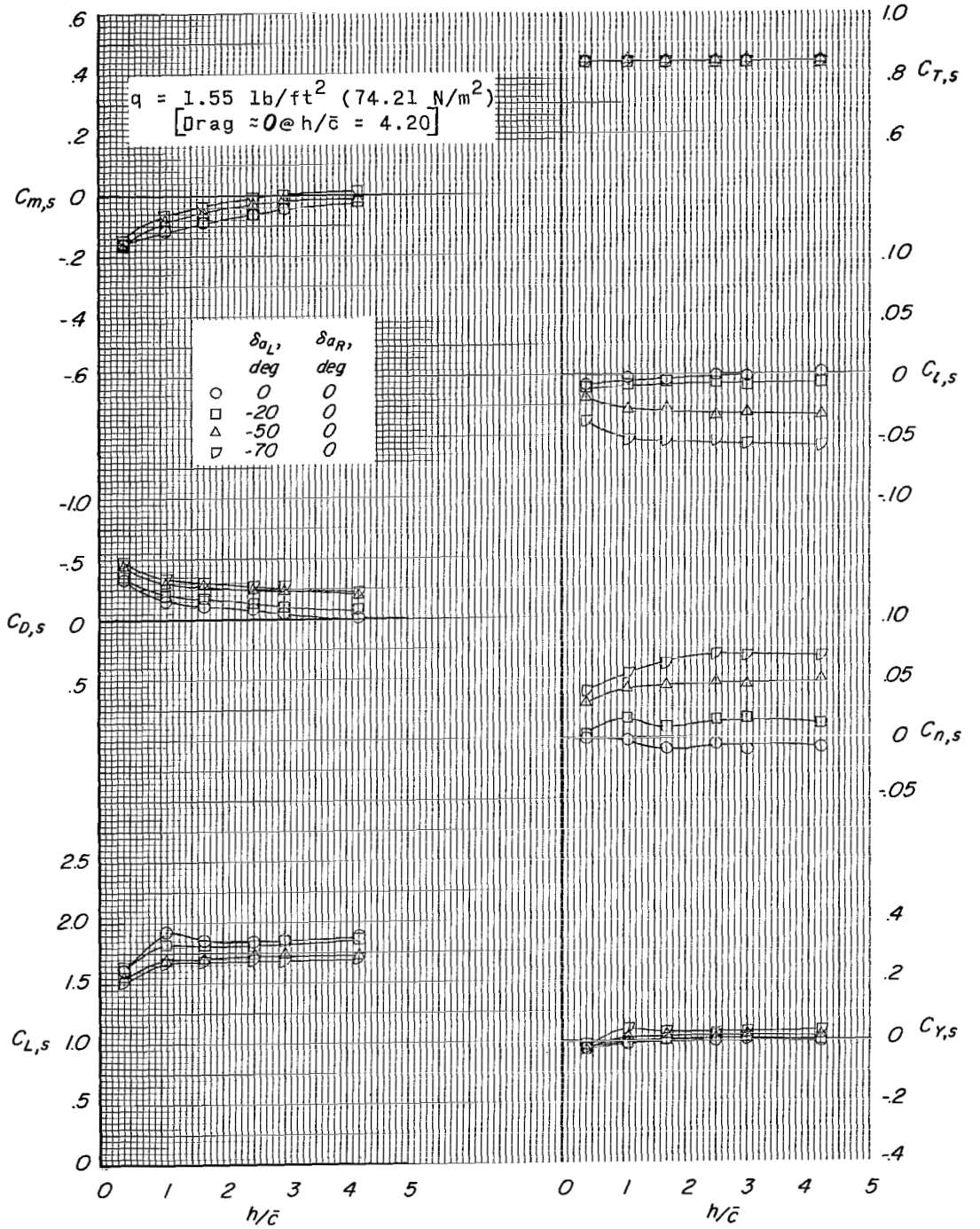

(a) $i_w = 30^0$.

Figure 25.- Effect of aileron deflection over a range of ground-height ratios for two wing-tilt angles under steady level flight and decelerating flight conditions. $\delta_f = 60^0$; $\alpha = 0^0$; $i_t = 20^0$; 7000 rpm; belt moving; slat on; $\beta = 0^0$.

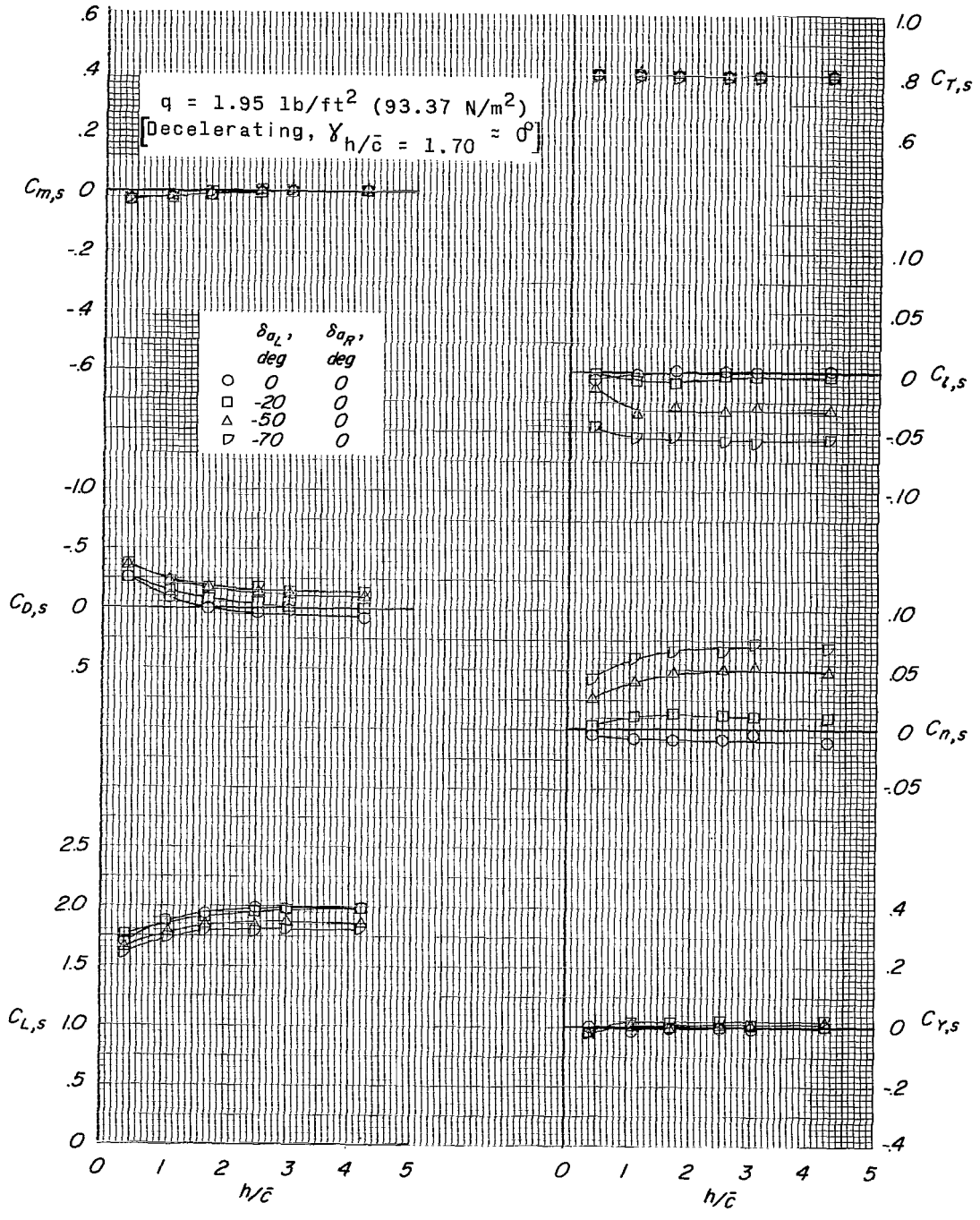

(a) Concluded.

Figure 25.- Continued.

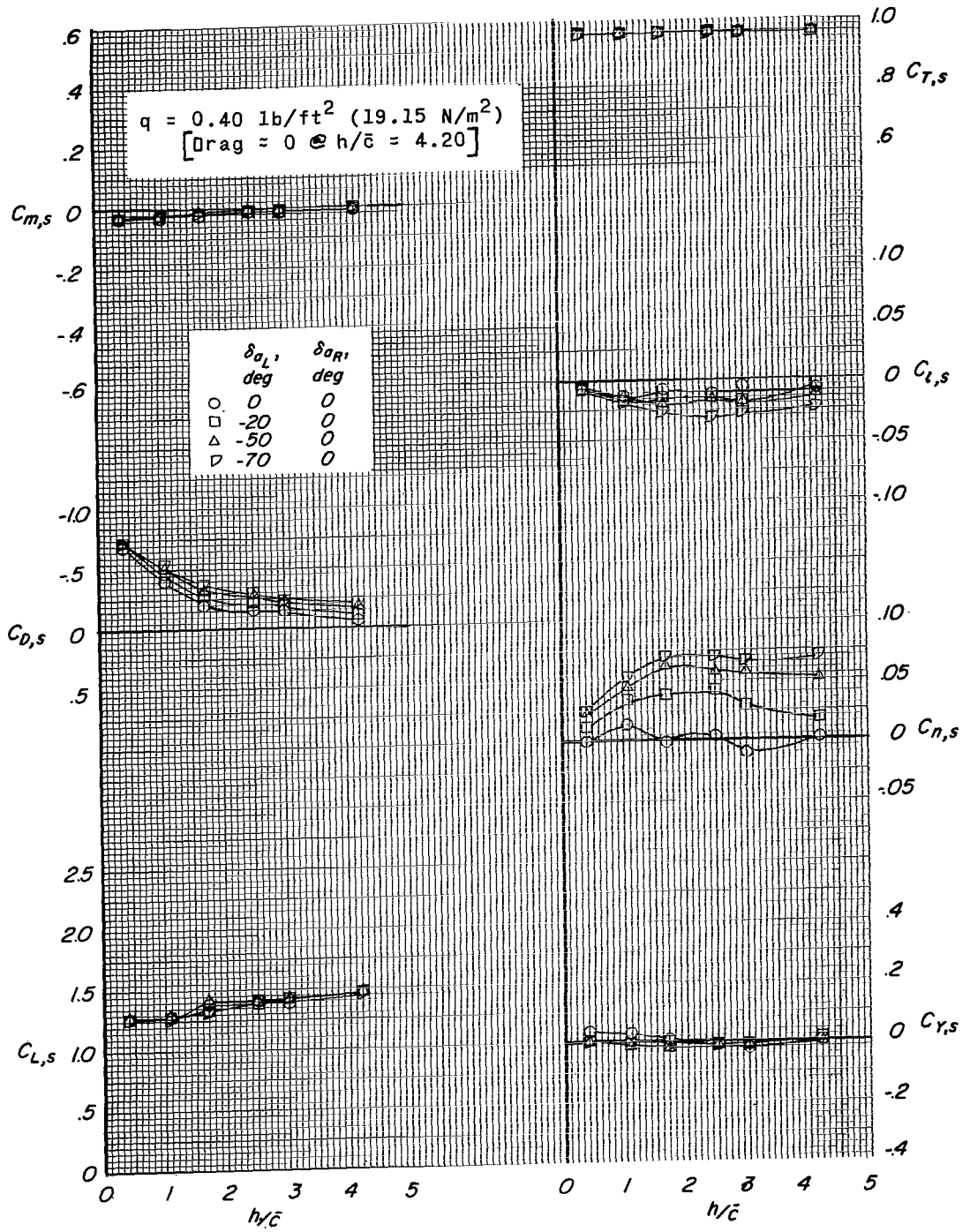

(b) $i_w = 45^0$.

Figure 25.- Continued.

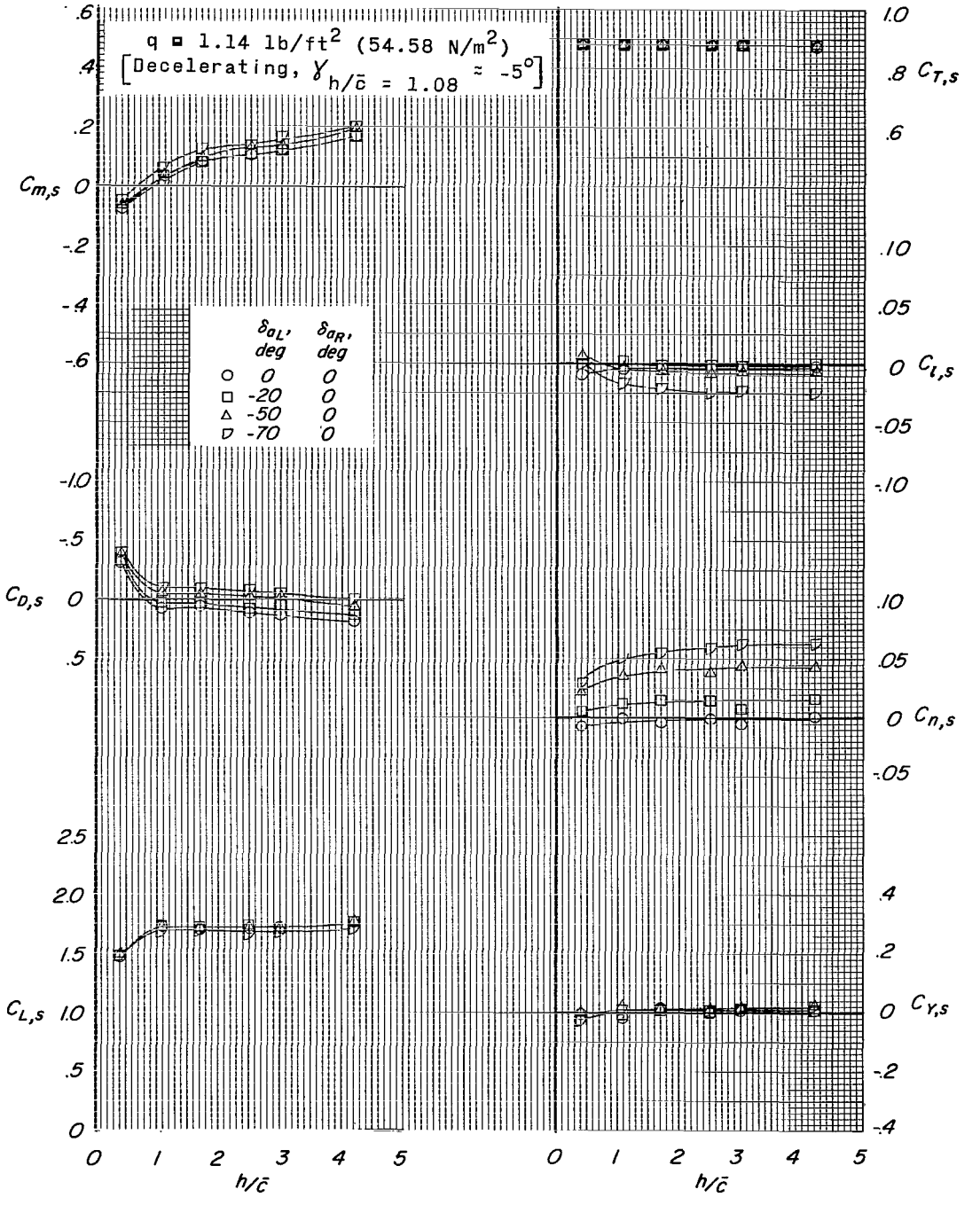

(b) Concluded.

Figure 25.- Concluded.

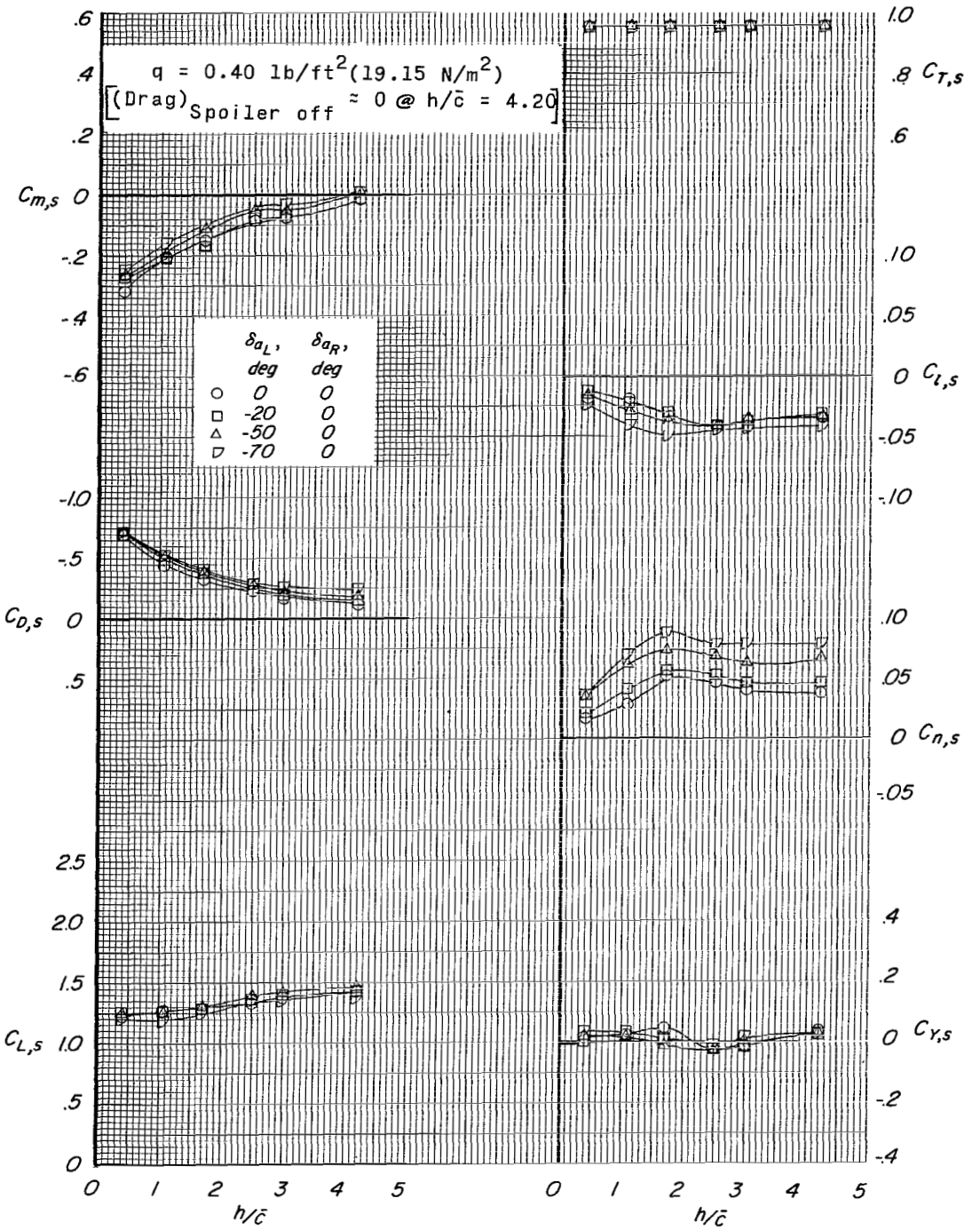

Figure 26.- Effect of aileron-spoiler deflection over a range of ground-height ratios at two flight conditions. $\delta_f = 60^0$; $\alpha = 0^0$; $i_t = 20^0$; 7000 rpm; belt moving; slat on; $\beta = 0^0$; $i_w = 45^0$; 0.10c spoiler deflected.

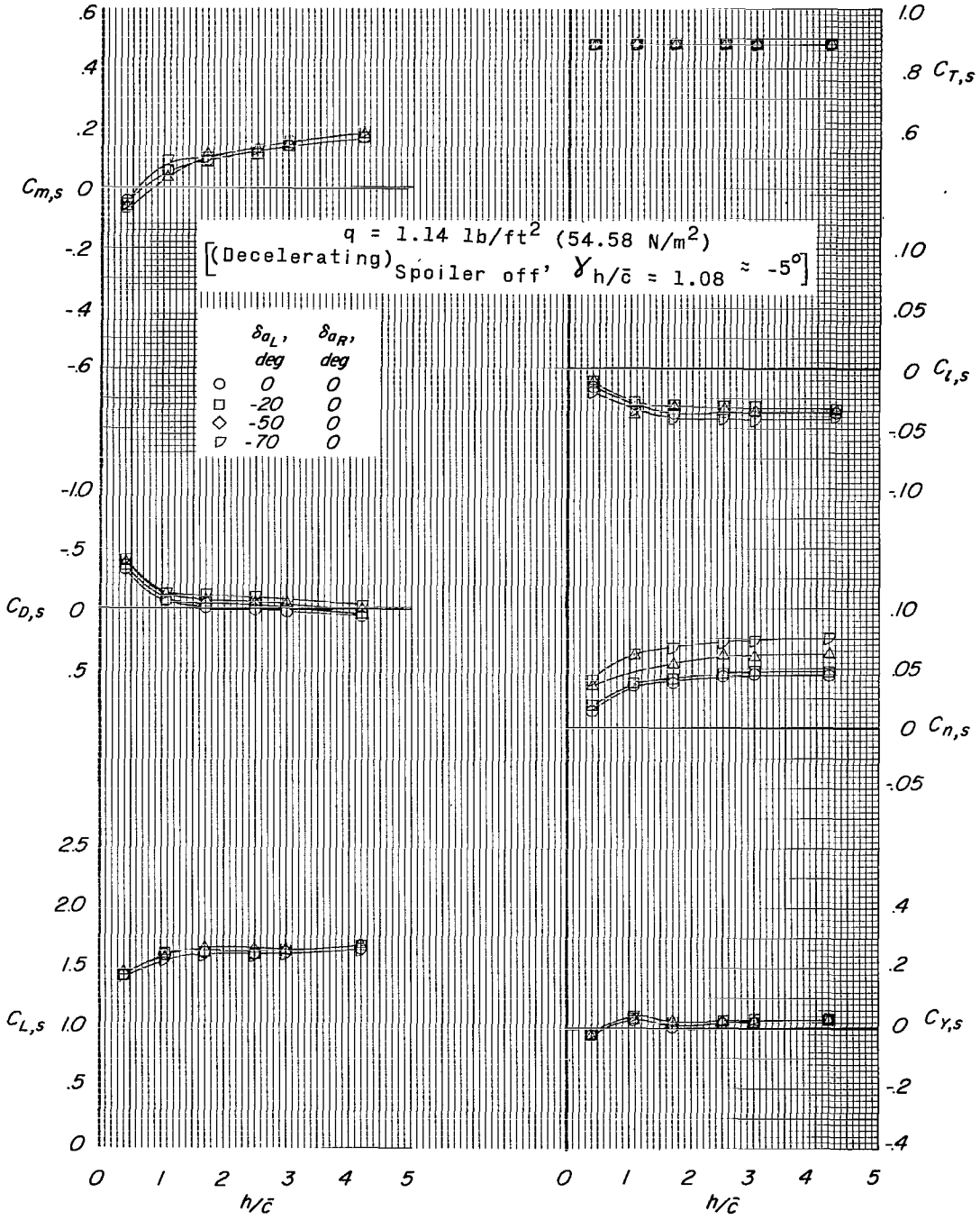

Figure 26.- Concluded.

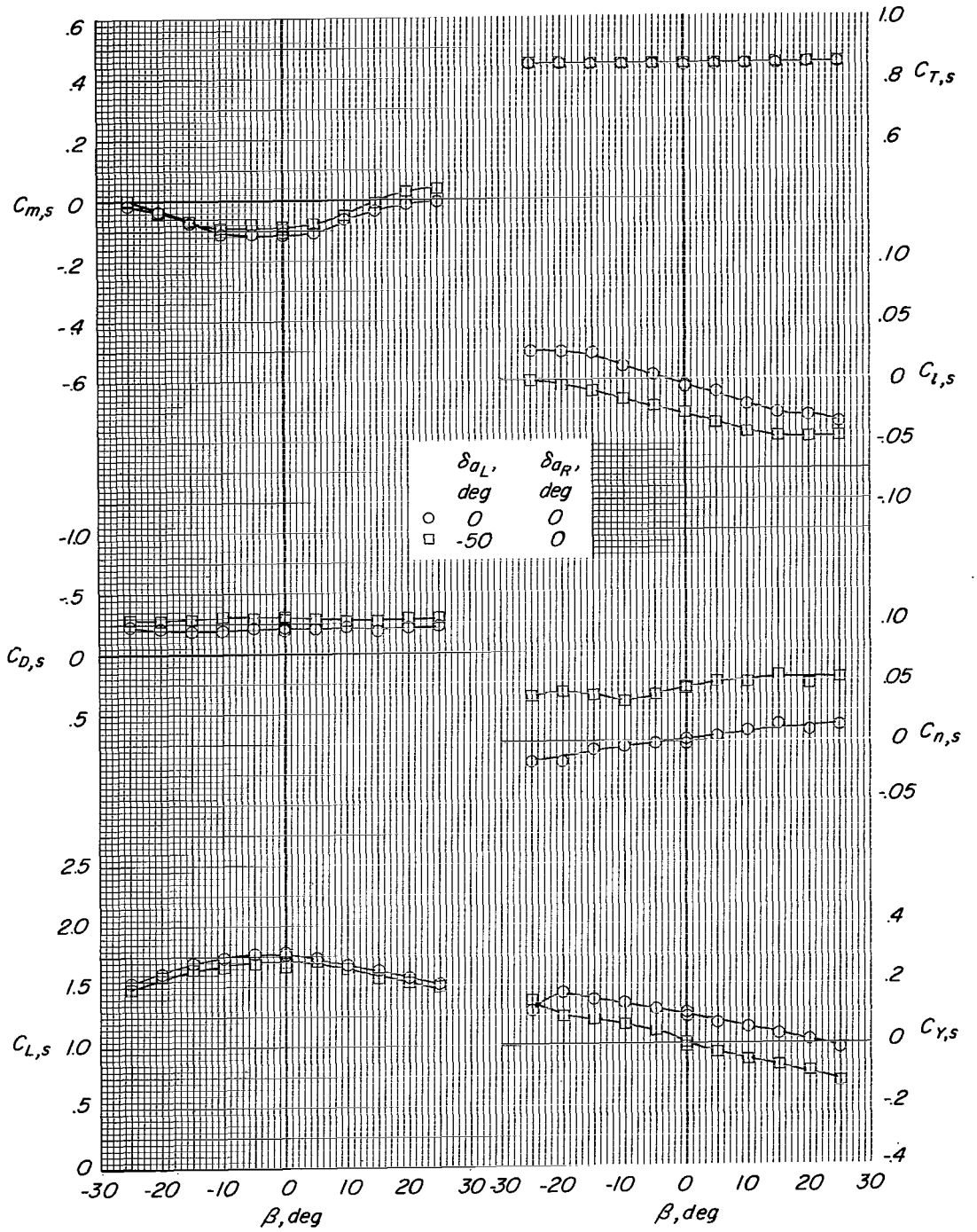

(a) $i_w = 30^0$; $\delta_f = 60^0$.

Figure 27.- Effect of aileron deflection on the lateral aerodynamic characteristics in sideslip for two wing-tilt angles. $\alpha = 0^0$; $h/\bar{c} = 1.08$; belt moving; 7000 rpm; $\delta_a = 0^0$; slat on; $i_t = 20^0$. (q was established at Drag ≈ 0 for $h/\bar{c} = 4.20$ and $\alpha = 0^0$.)

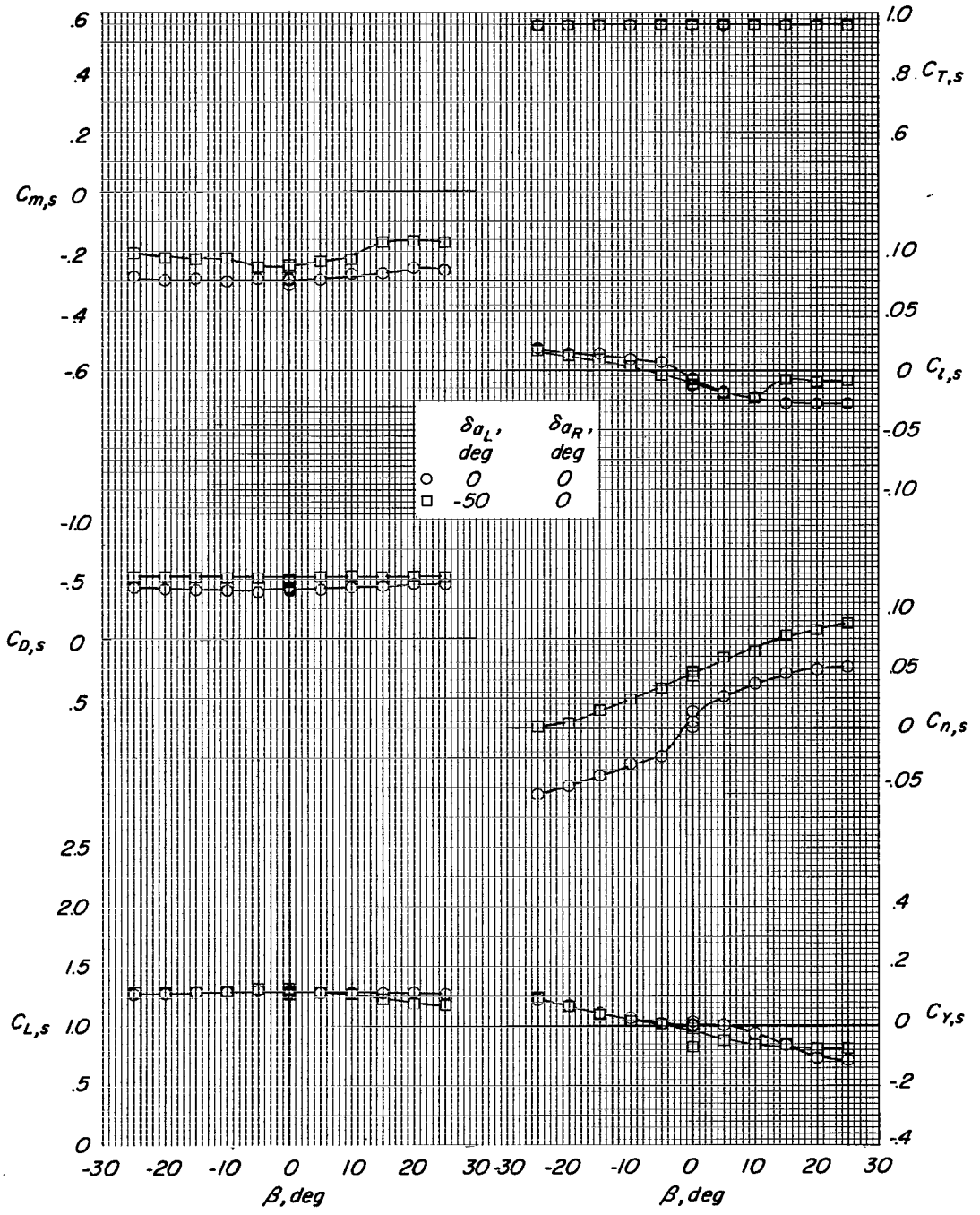

(b) $i_w = 45^0$; $\delta_f = 60^0$.

Figure 27.- Concluded.

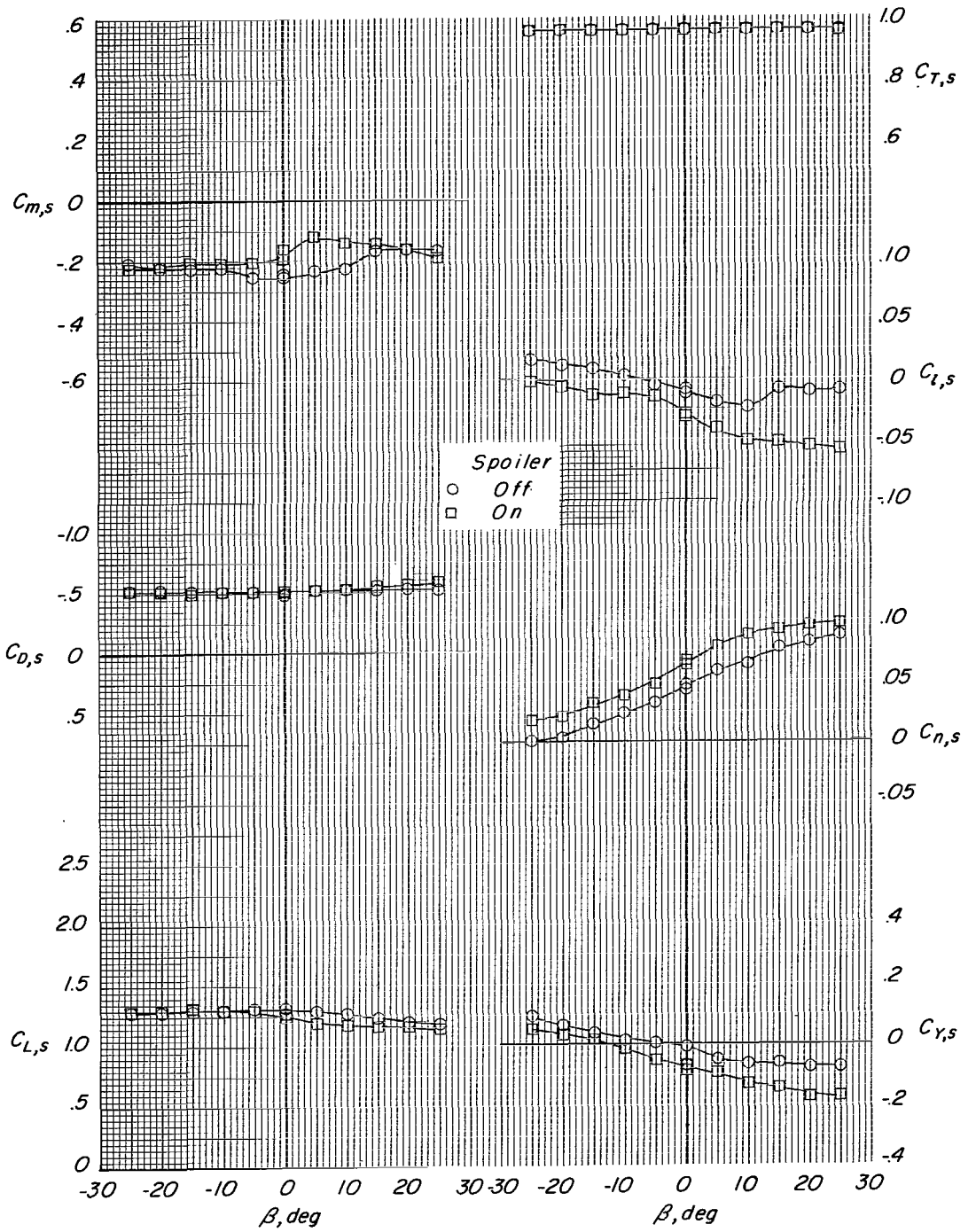

Figure 28.- Effect of spoiler on the lateral aerodynamic characteristics in sideslip. $\alpha = 0^0$; $\delta_{a_L} = -50^0$; $\delta_{a_R} = 0^0$; 7000 rpm; belt moving; slat on; $i_t = 20^0$; $h/\bar{c} = 1.08$. (q was established at Drag $\approx$ 0 for $h/\bar{c} = 4.20$ and $\alpha = 0^0$.)

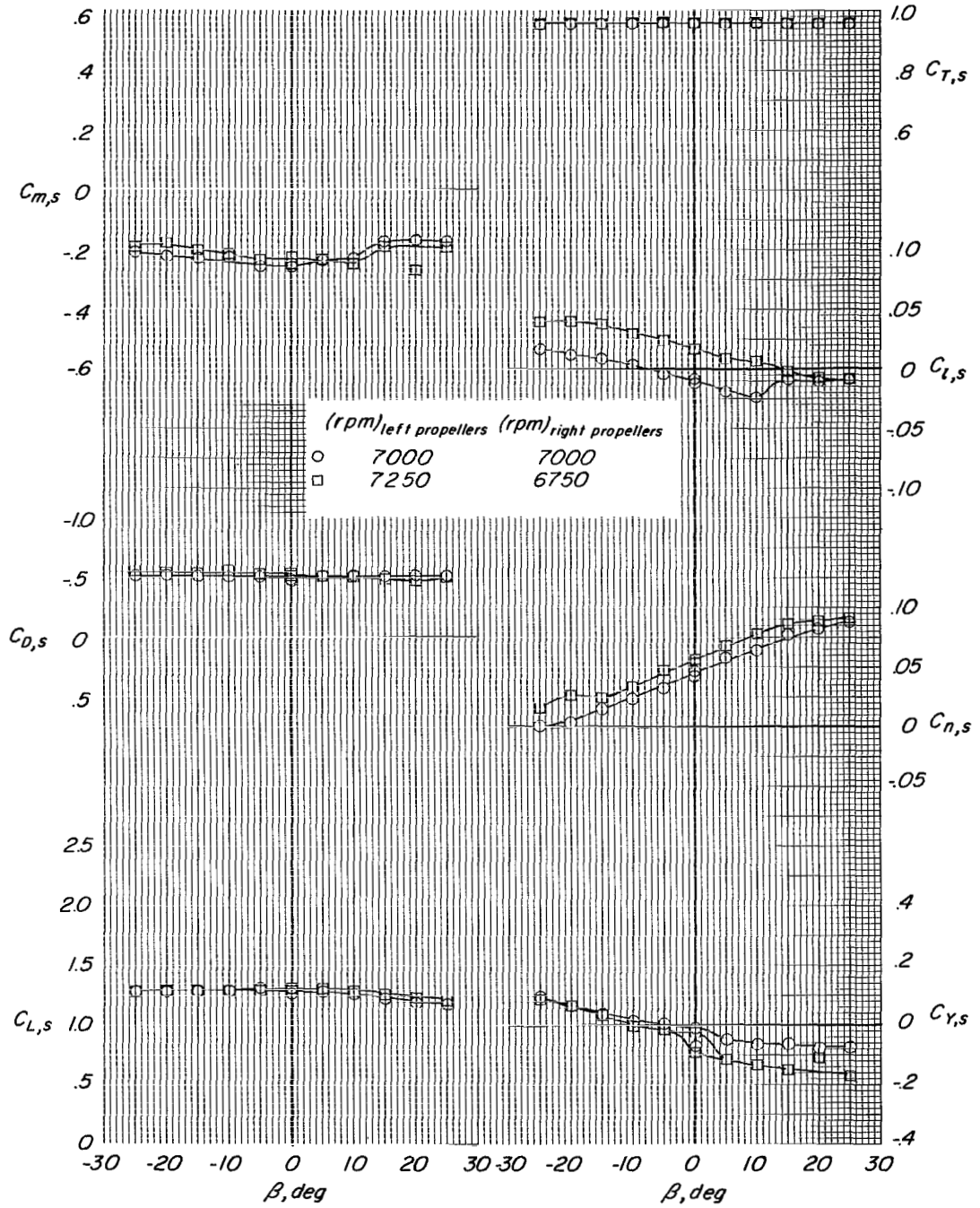

Figure 29.- Effect of asymmetric rpm on the lateral aerodynamic characteristics in sideslip. $\alpha = 0^0$; $\delta_{a_L} = -50^0$; $\delta_{a_R} = 0^0$; 7000 rpm; belt moving; slat on; $i_t = 20^0$; $h/\bar{c} = 1.08$. (q was established at Drag ≈ 0 for $h/\bar{c} = 4.20$ and $\alpha = 0^0$.)

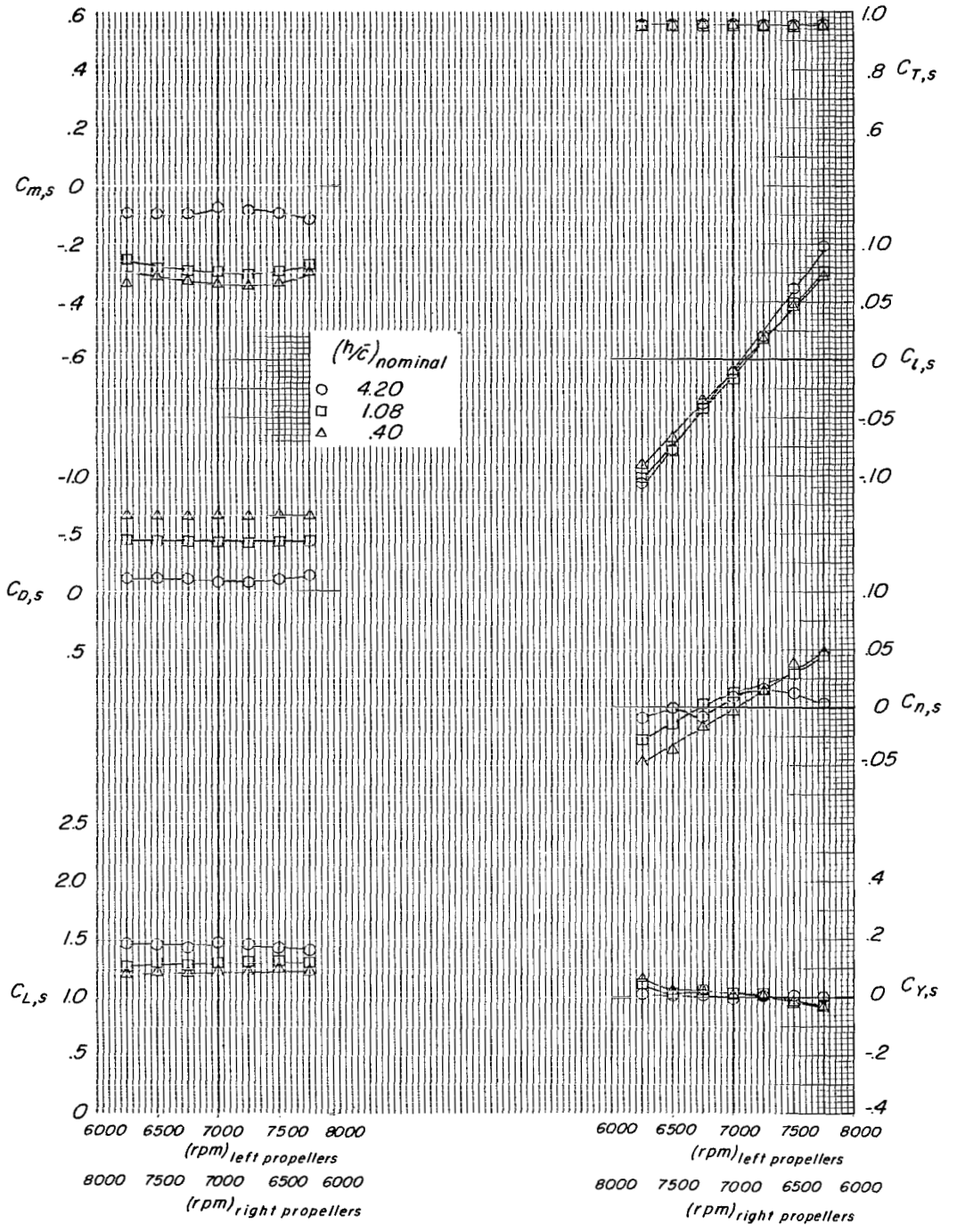

Figure 30.- Effect of ground-height ratio on the aerodynamic characteristics for $i_w = 45^0$ under asymmetric propeller rpm conditions. $\delta_f = 60^0$; $\alpha = 0^0$; $\beta = 0^0$; $\delta_a = 0^0$; $i_t = 0^0$; belt moving; slat on. (q was established at Drag $\approx$ 0 for $h/\bar{c} = 4.20$ and $\alpha = 0^0$.)

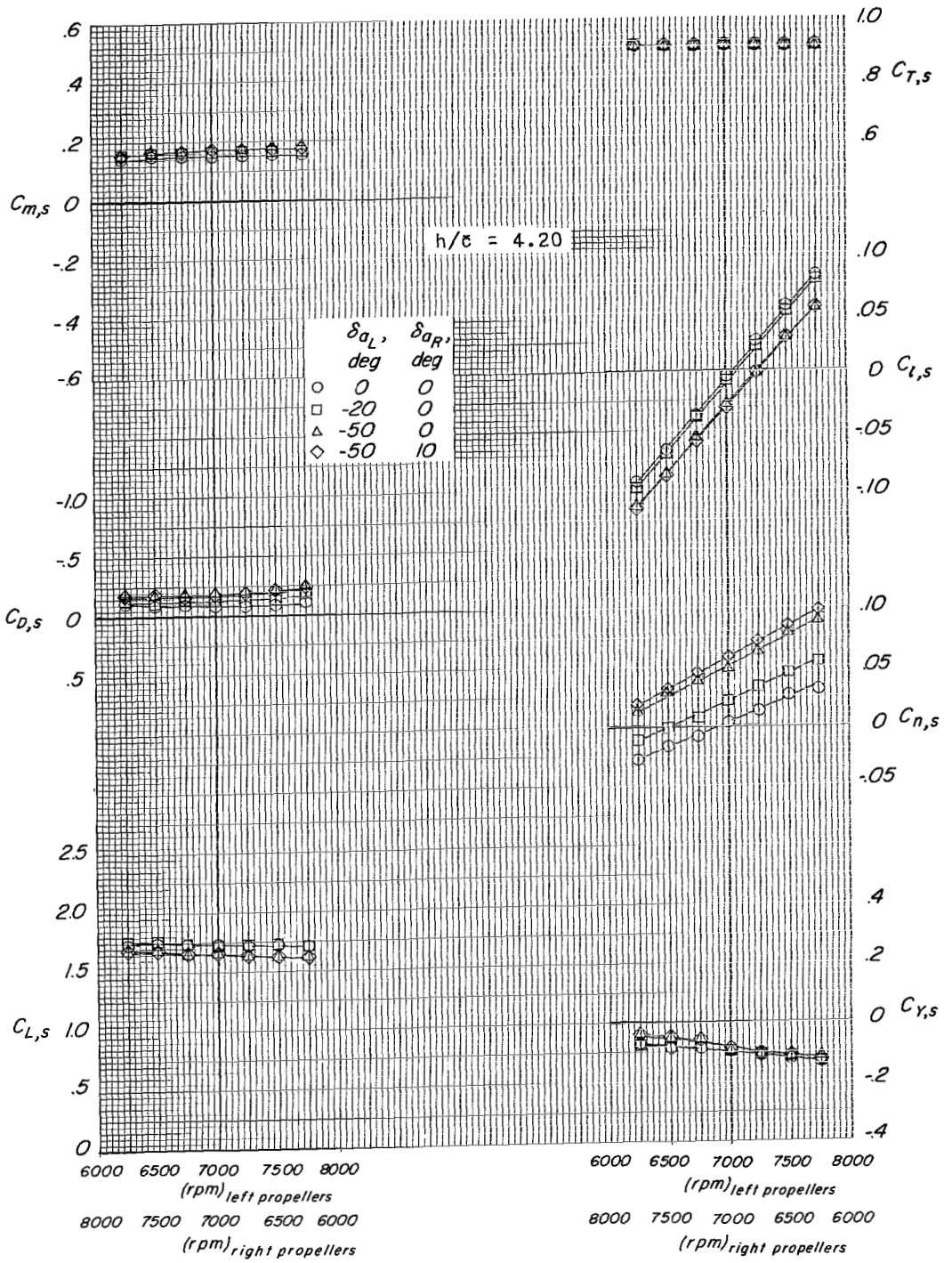

(a) $i_w = 45^0$; $\delta_f = 40^0$.

Figure 31.- Effect of aileron deflection on the aerodynamic characteristics under asymmetric propeller rpm conditions for various wing-tilt--flap-deflection combinations. $\alpha = 0^0$; $\beta = 0^0$; $i_t = 0^0$; belt moving; slat on. (q was established at Drag $\approx$ 0 for $h/\bar{c} = 4.20$ and $\alpha = 0^0$.)

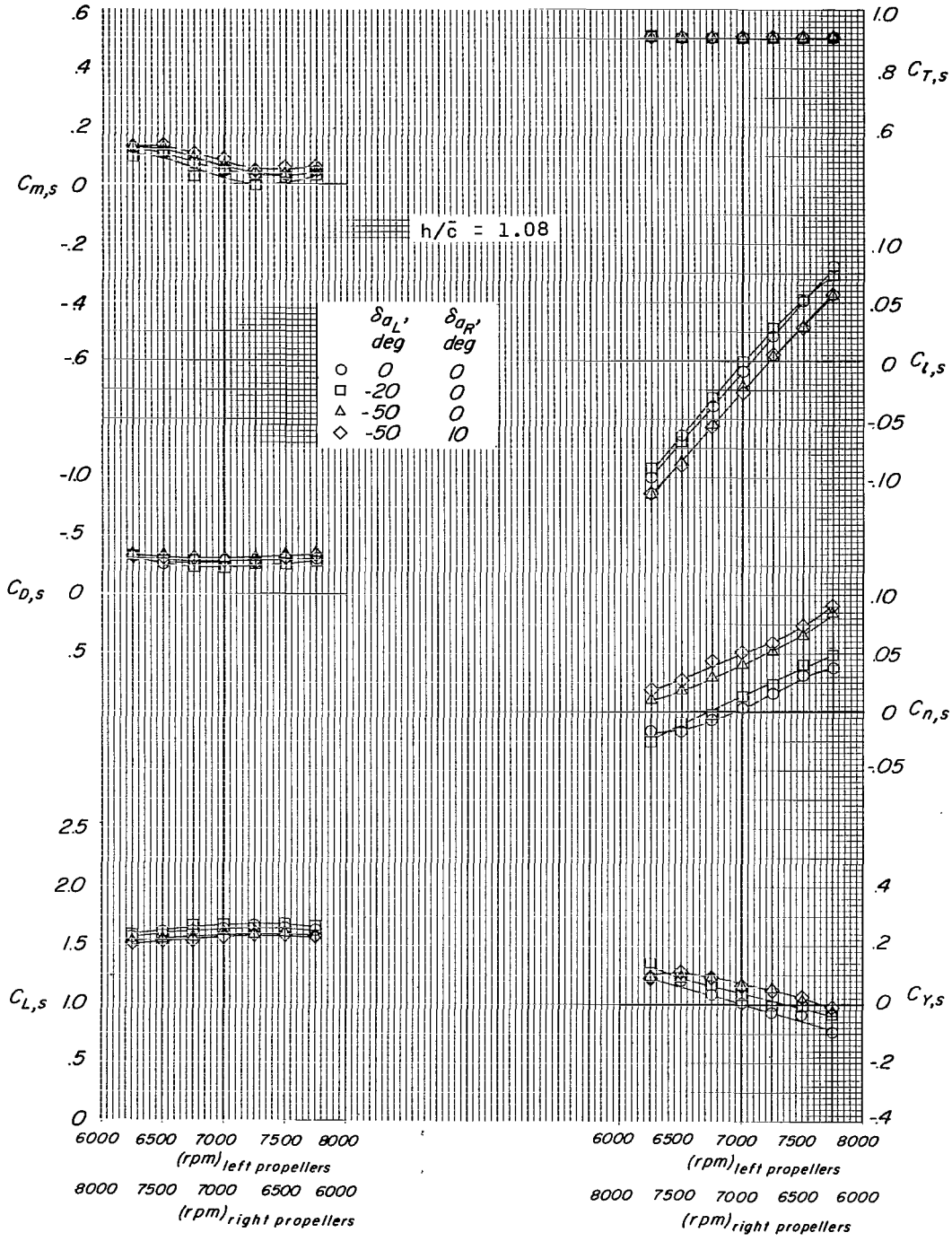

(a) Concluded.

Figure 31.- Continued.

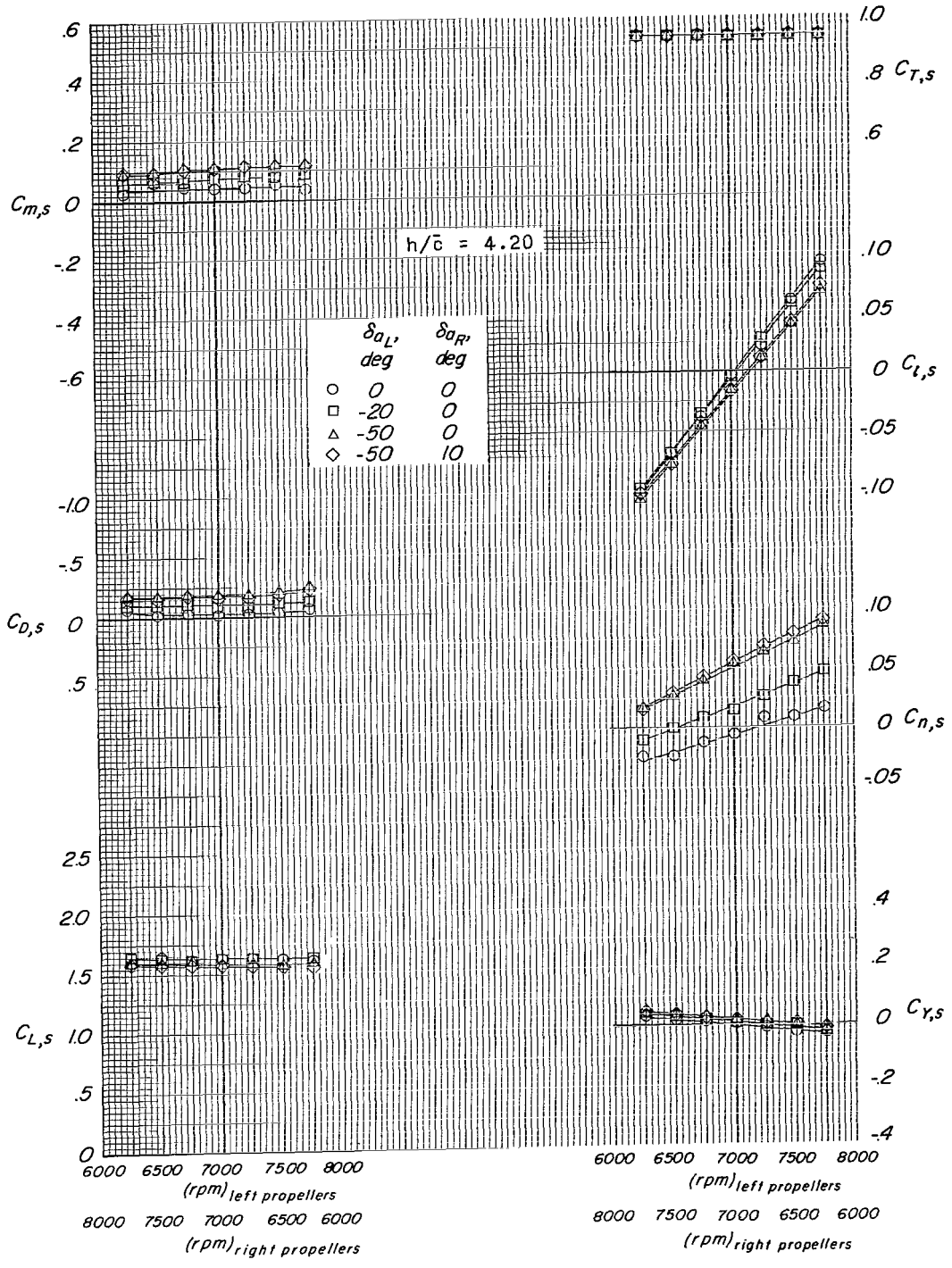

(b) $i_w = 45^0$; $\delta_f = 50^0$.

Figure 31.- Continued.

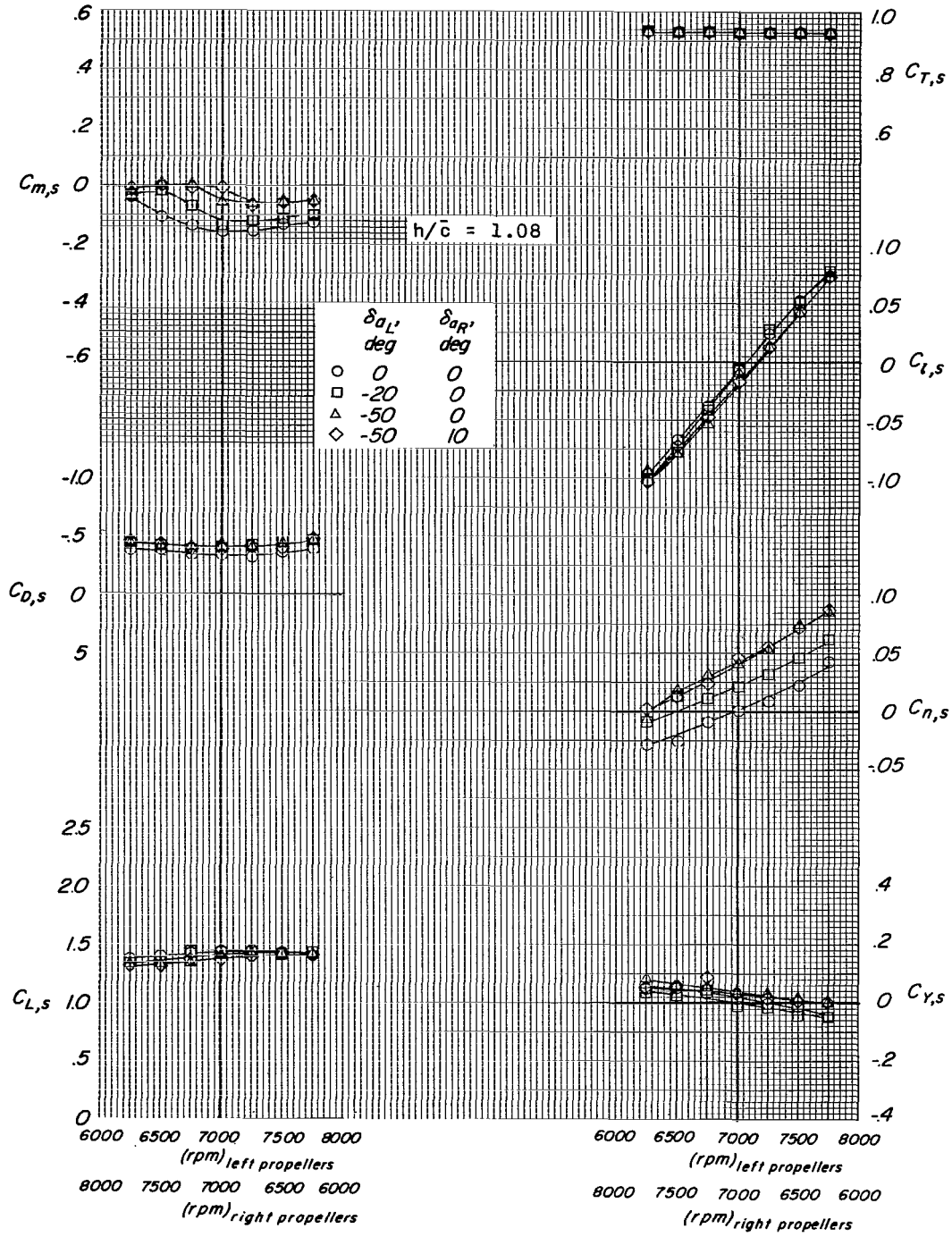

(b) Concluded.

Figure 31.- Continued.

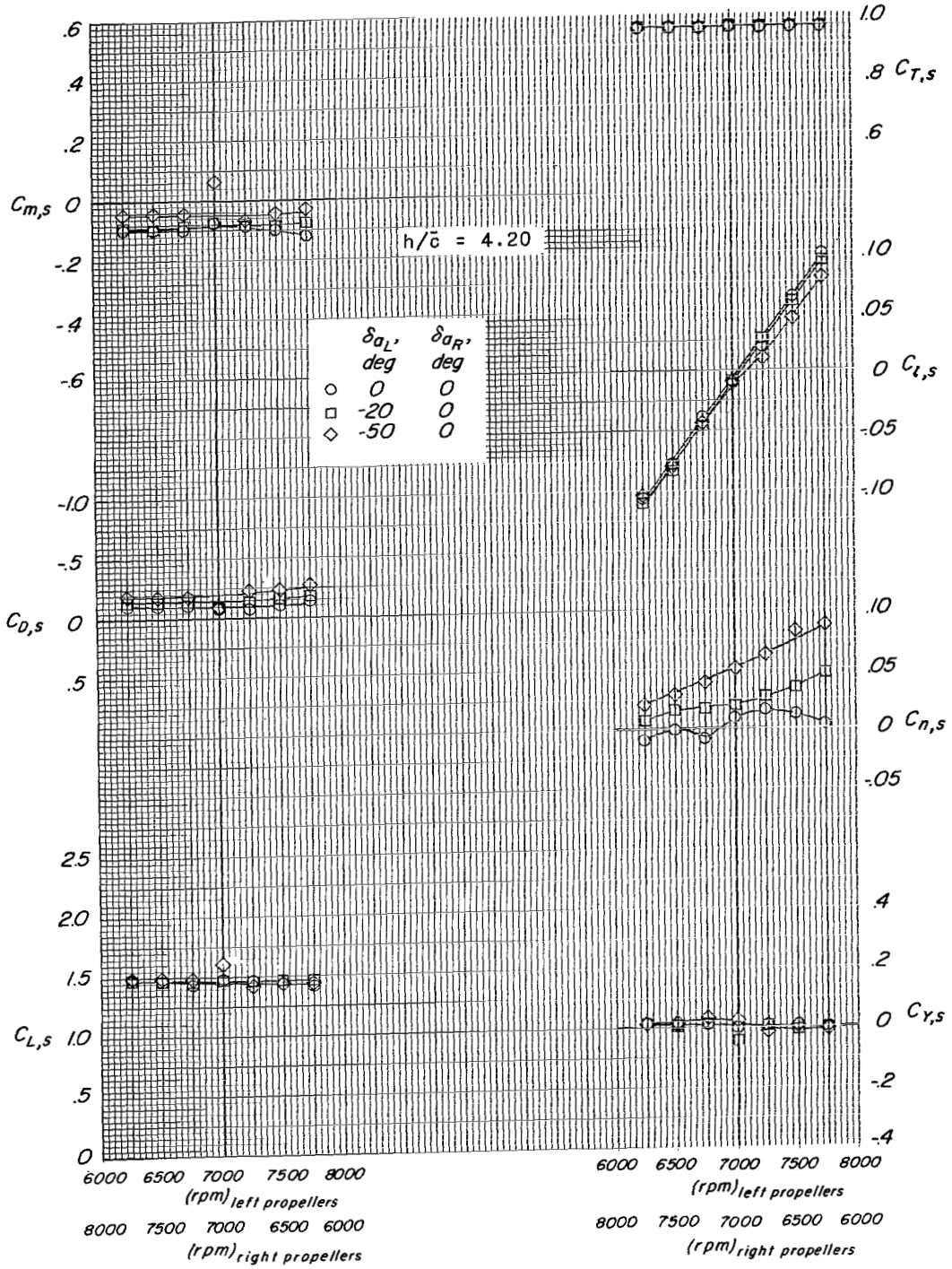

(c) $i_w = 45^0$; $\delta_f = 60^0$.

Figure 31.- Continued.

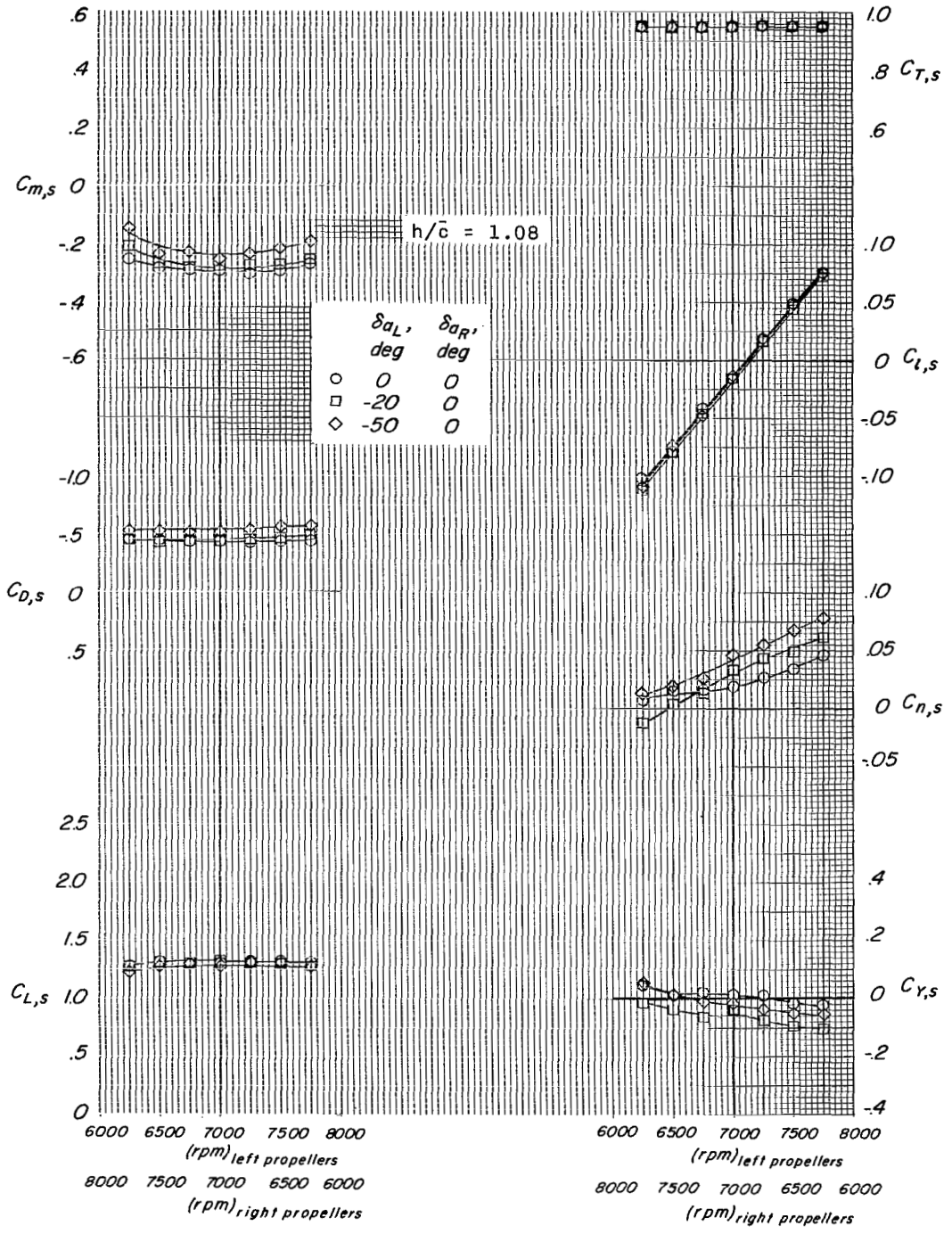

(c) Concluded.

Figure 31.- Continued.

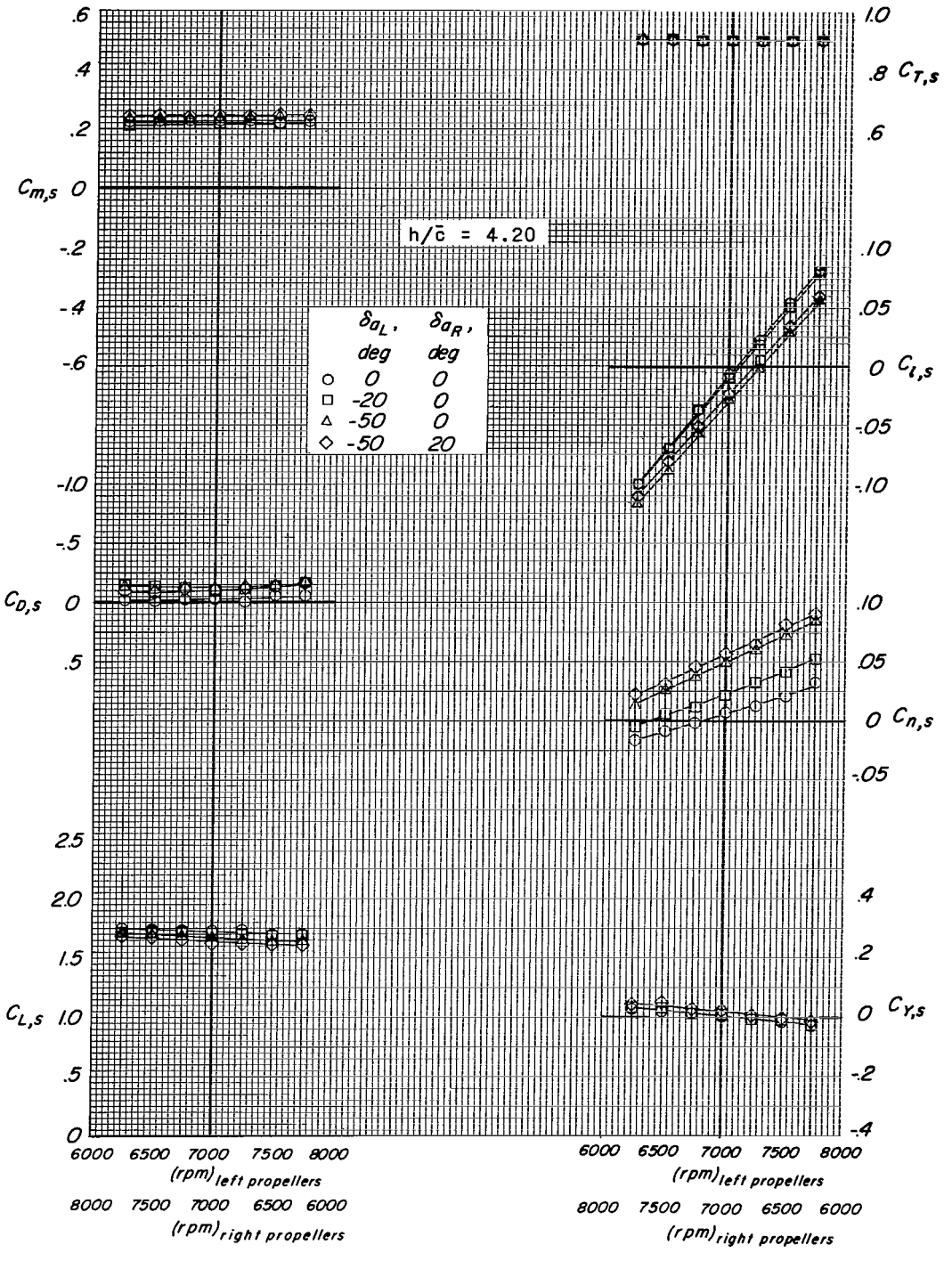

(d) $i_w = 50^0$; $\delta_f = 30^0$.

Figure 31.- Continued.

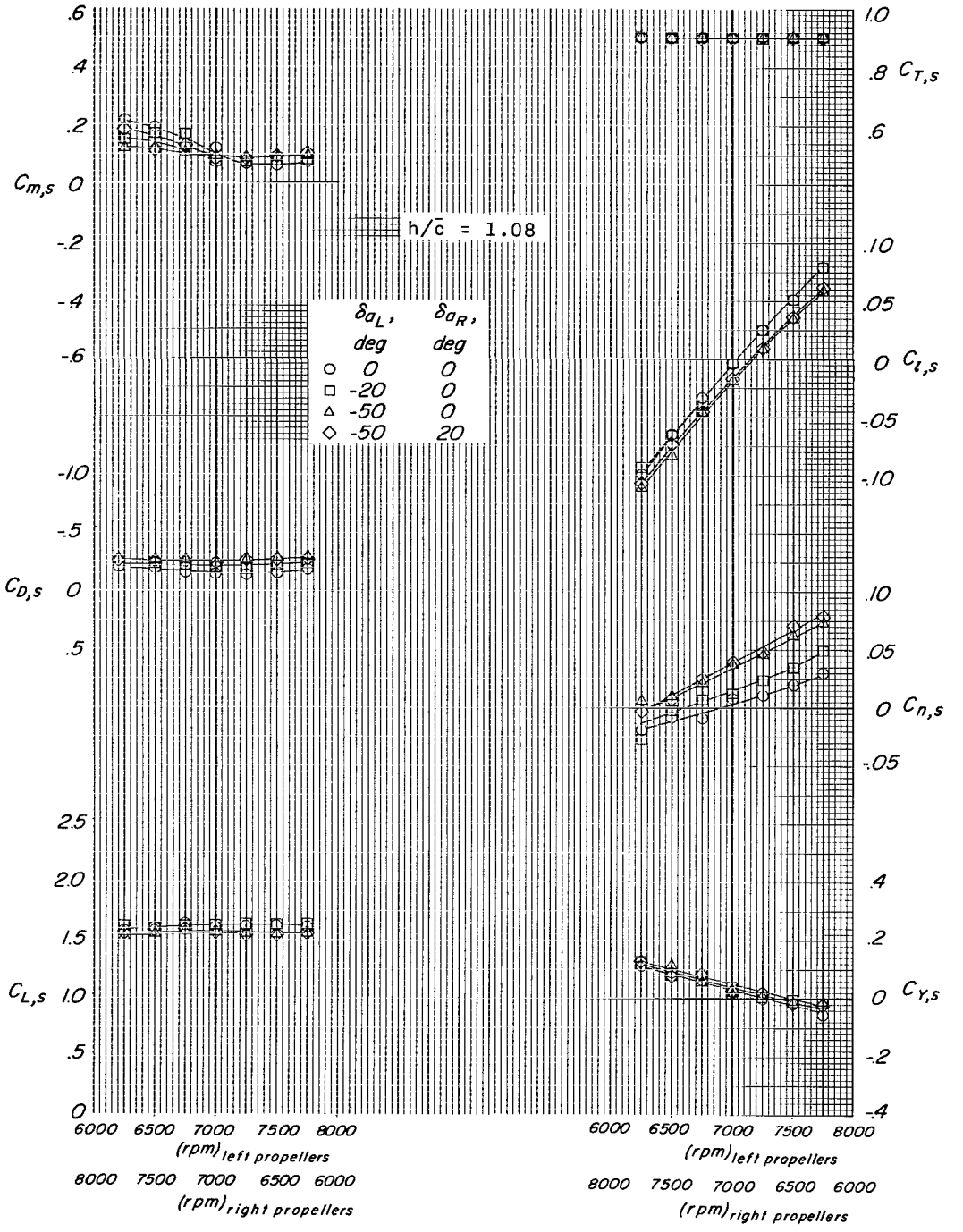

(d) Concluded.

Figure 31.- Continued.

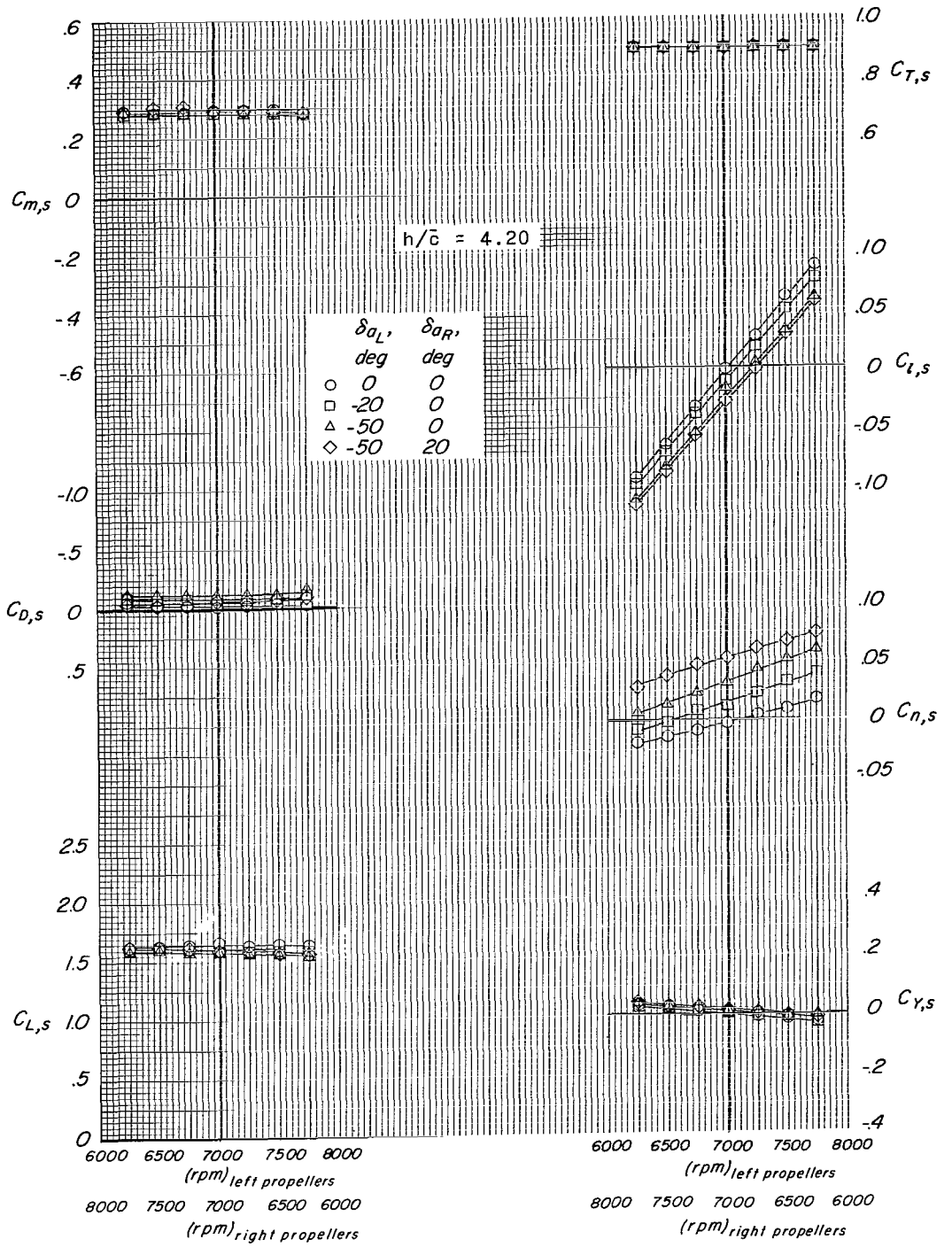

(e) $i_W = 60^0$; $\delta_f = 10^0$.

Figure 31.- Continued.

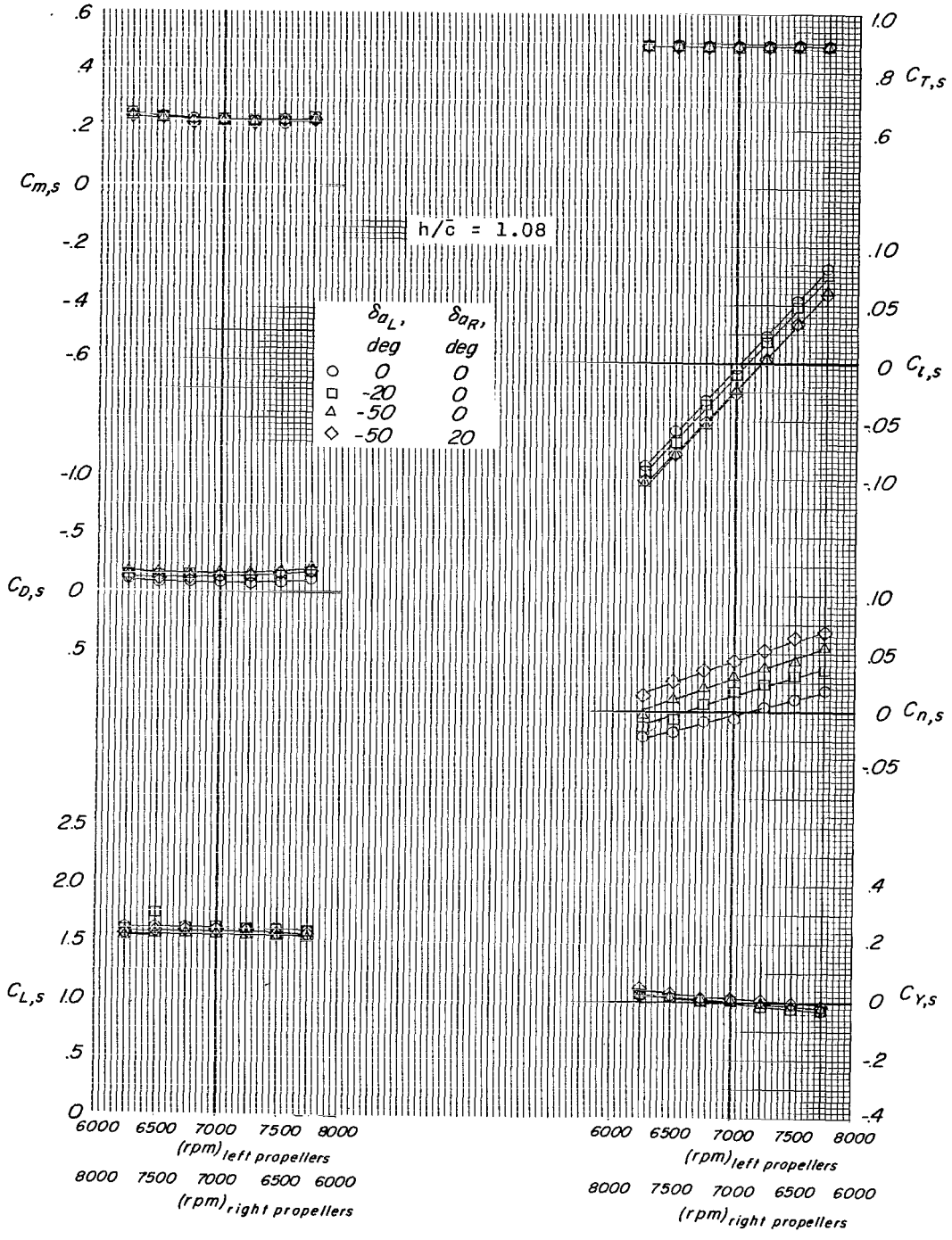

(e) Concluded.

Figure 31.- Concluded.

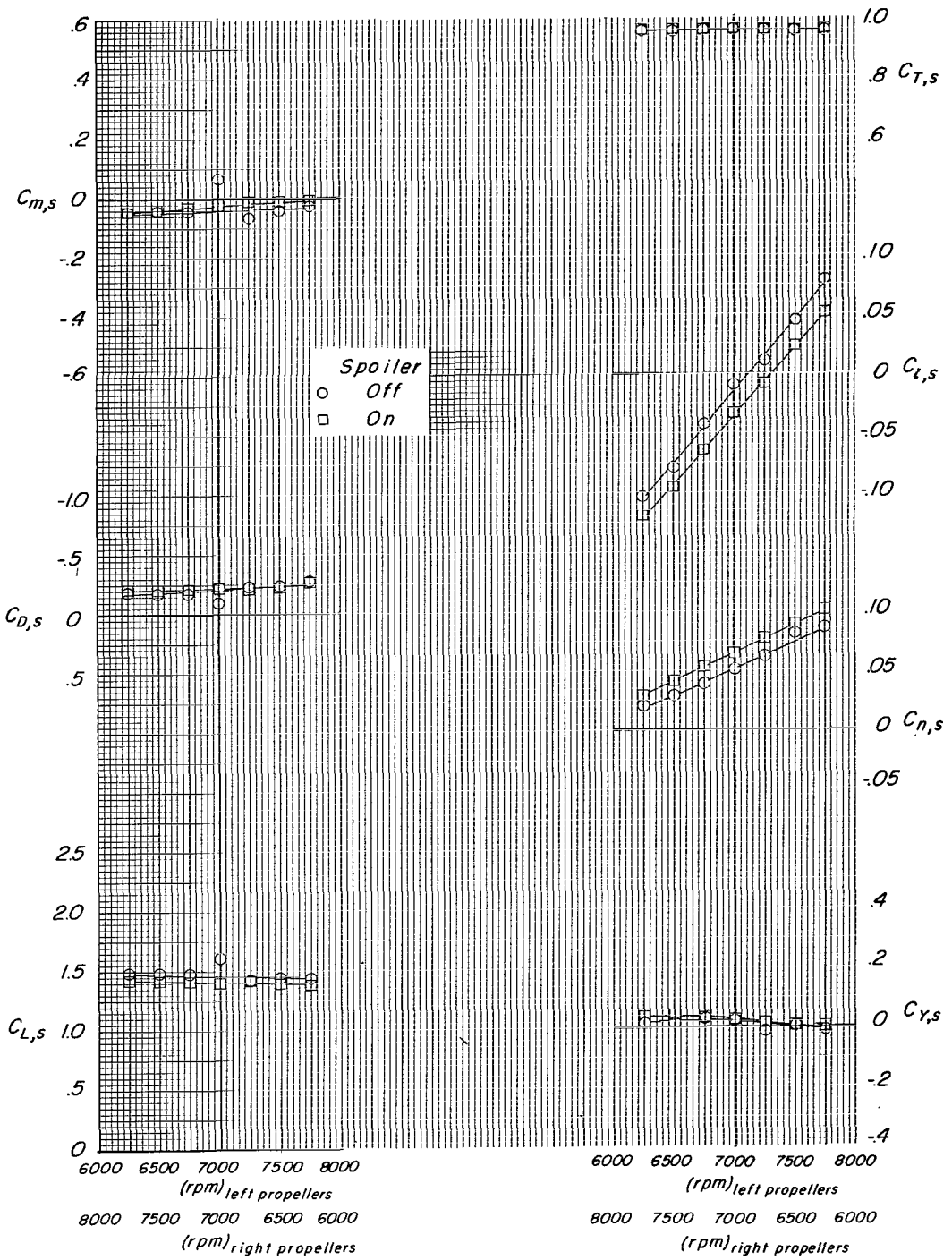

(a) $h/\bar{c} = 4.20$.

Figure 32.- Effect of 0.10c spoiler deflected 45^0 on the upper surface of the left wing under asymmetric propeller rpm conditions. $i_W = 45^0$; $\delta_f = 60^0$; $\delta_{a_L} = -50^0$; $\delta_{a_R} = 0^0$; $i_t = 20^0$; belt moving; slat on. (q was established at Drag $\approx$ 0 for $h/\bar{c} = 4.20$ and $\alpha = 0^0$ with spoiler off.)

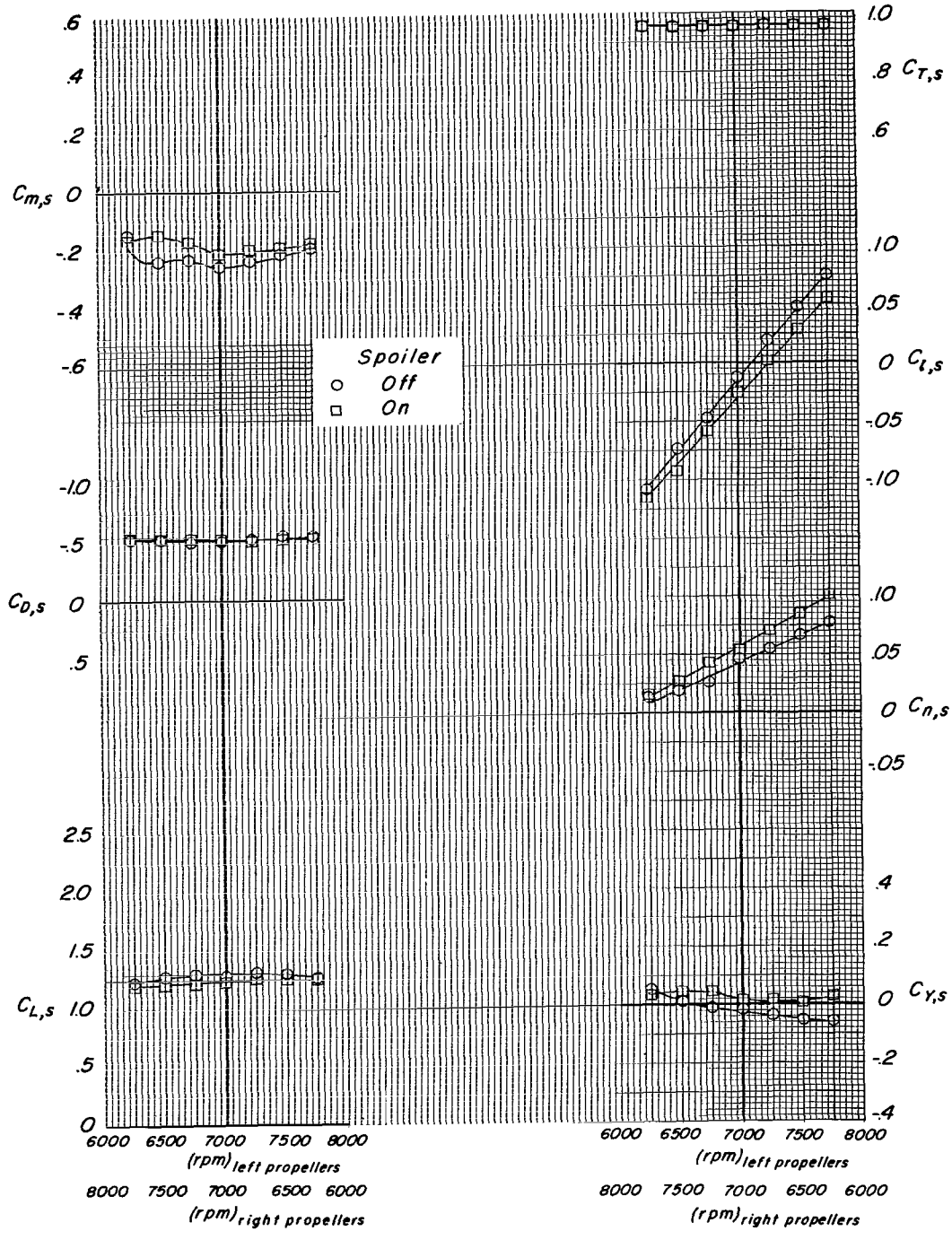

(b) $h/\bar{c} = 1.08$.

Figure 32.- Concluded.

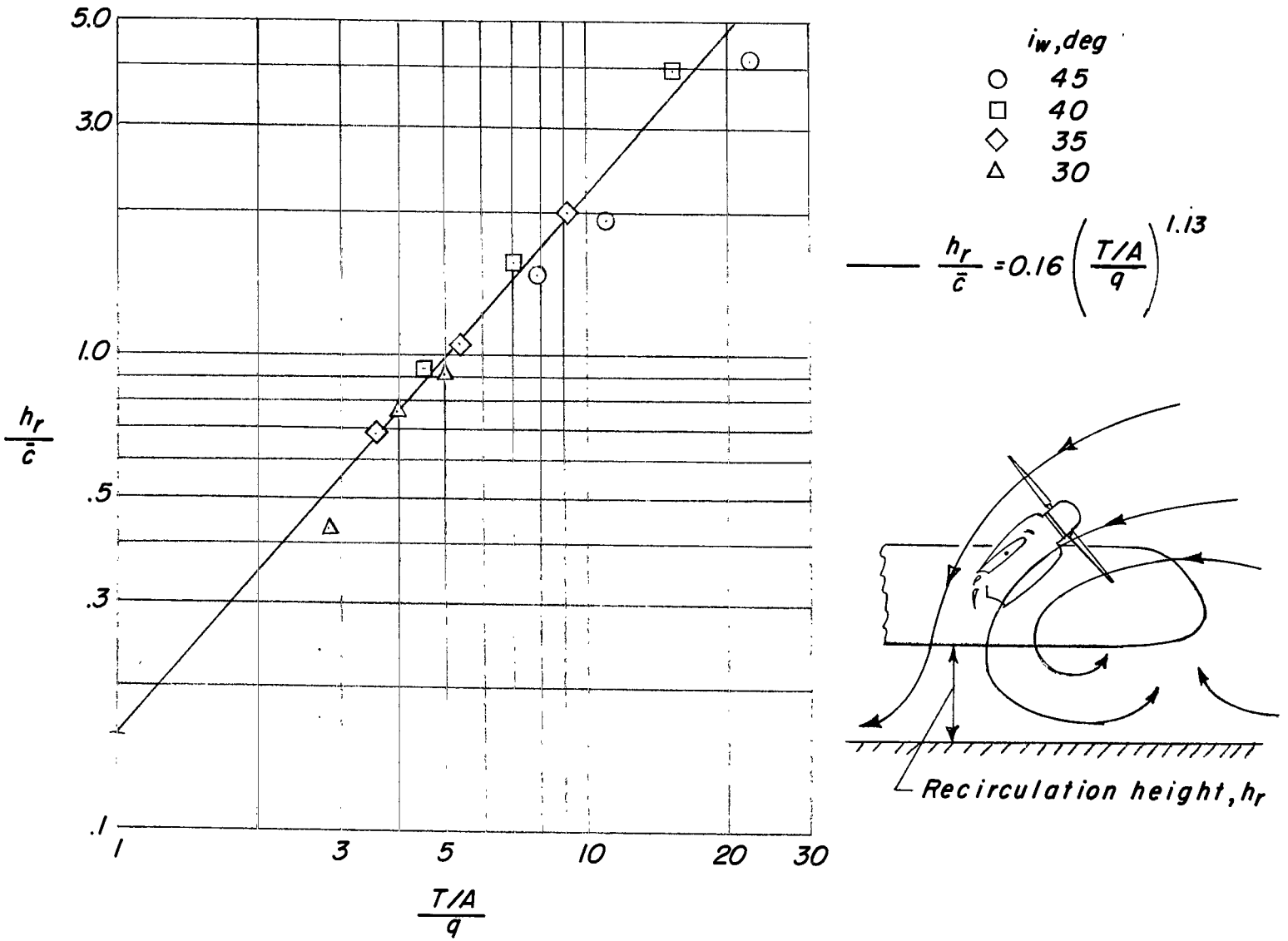

Figure 33.- Variation of flow recirculation height-chord ratio with ratio of disk loading to free-stream dynamic pressure. $\delta_f = 0^0$; $\alpha = 0^0$.

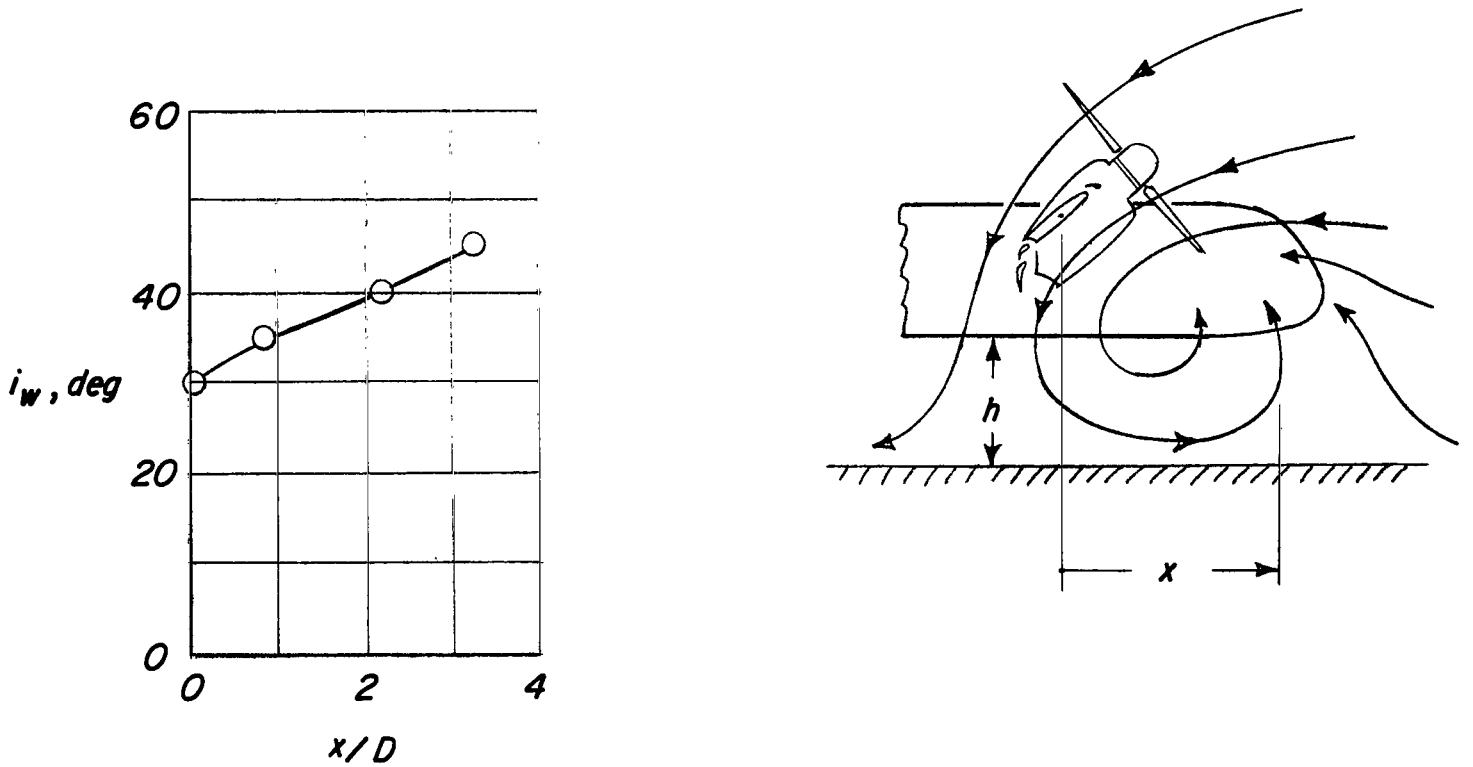

Figure 34.- Forward extent of disturbed flow as a function of wing-tilt angle at a critical ground height $h/\bar{c} = 1.08$. $\delta_f = 60^0$; $\alpha = 0^0$.

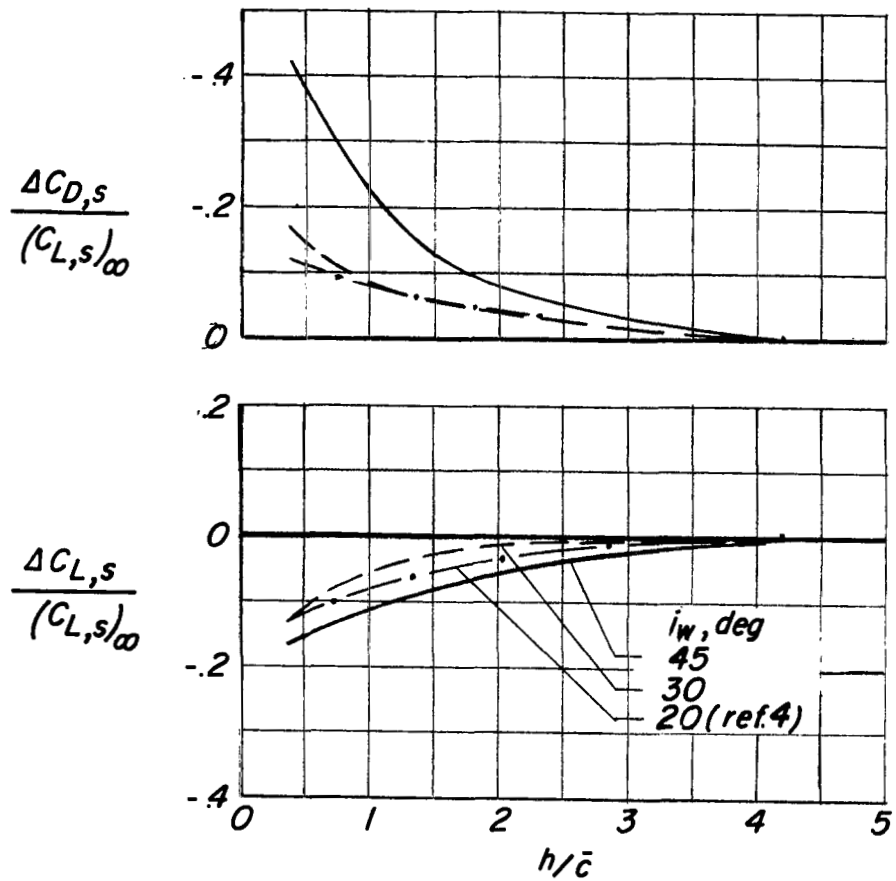

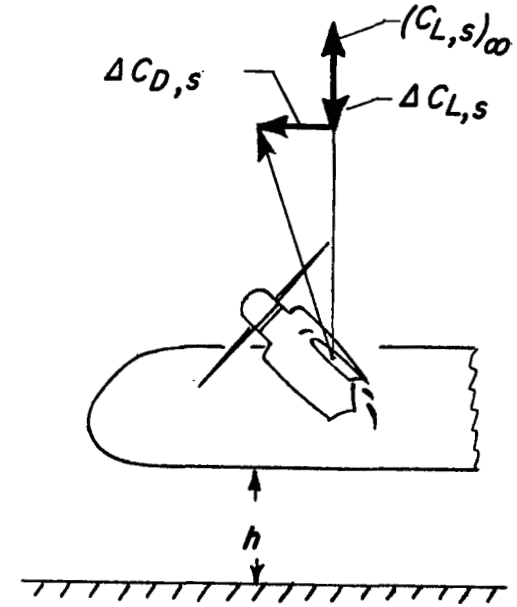

Figure 35.- Effect of ground proximity on lift and drag coefficients at several wing-tilt angles. $\delta_f = 60^0$; $i_t = 20^0$; $\alpha = 0^0$.

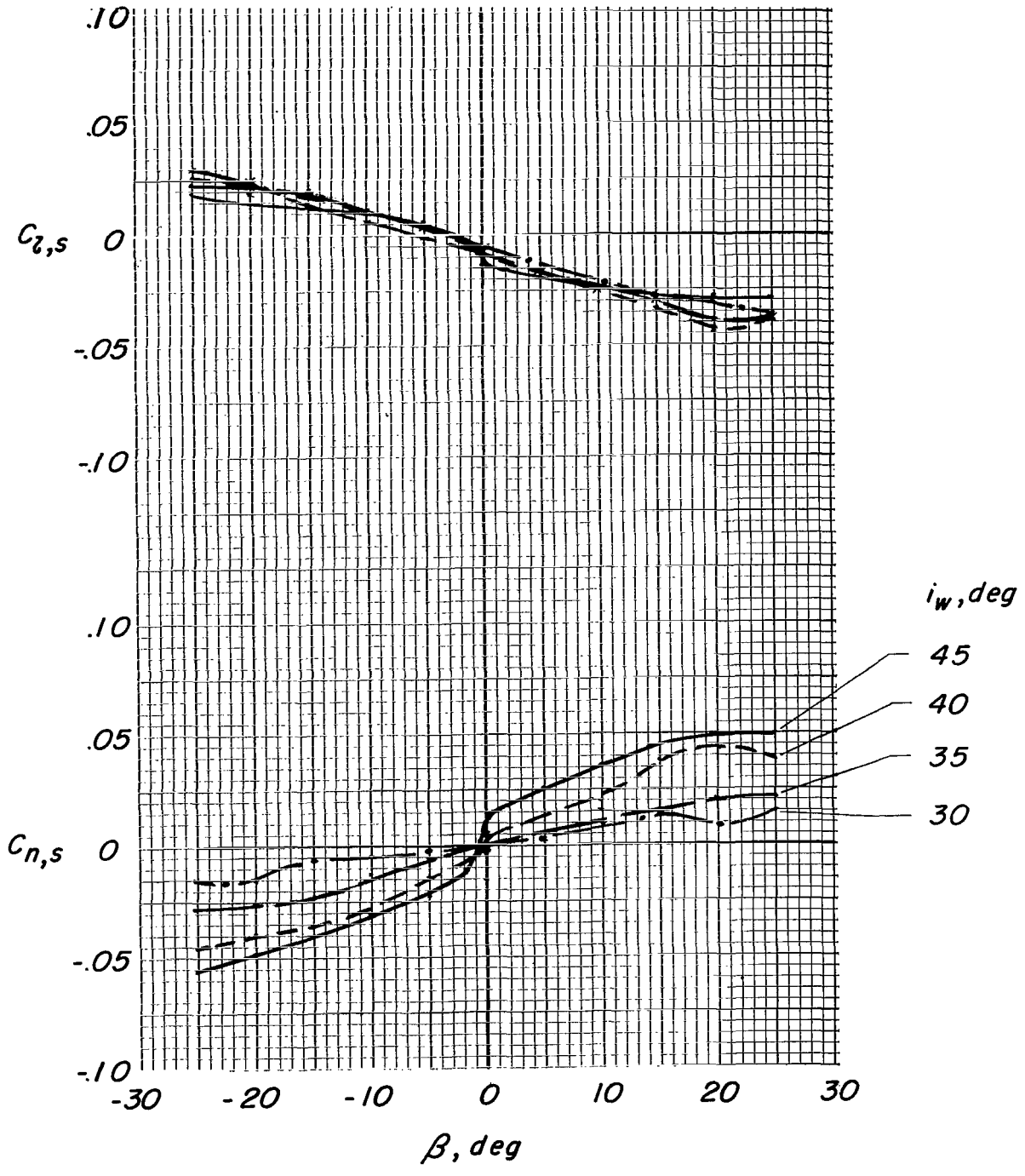

Figure 36.- Variation of yawing-moment and rolling-moment coefficients with sideslip angle for several wing-tilt angles. $\delta_f = 0^o$; $i_t = 20^o$; $h/\bar{c} = 1.08$; $\alpha = 0^o$.

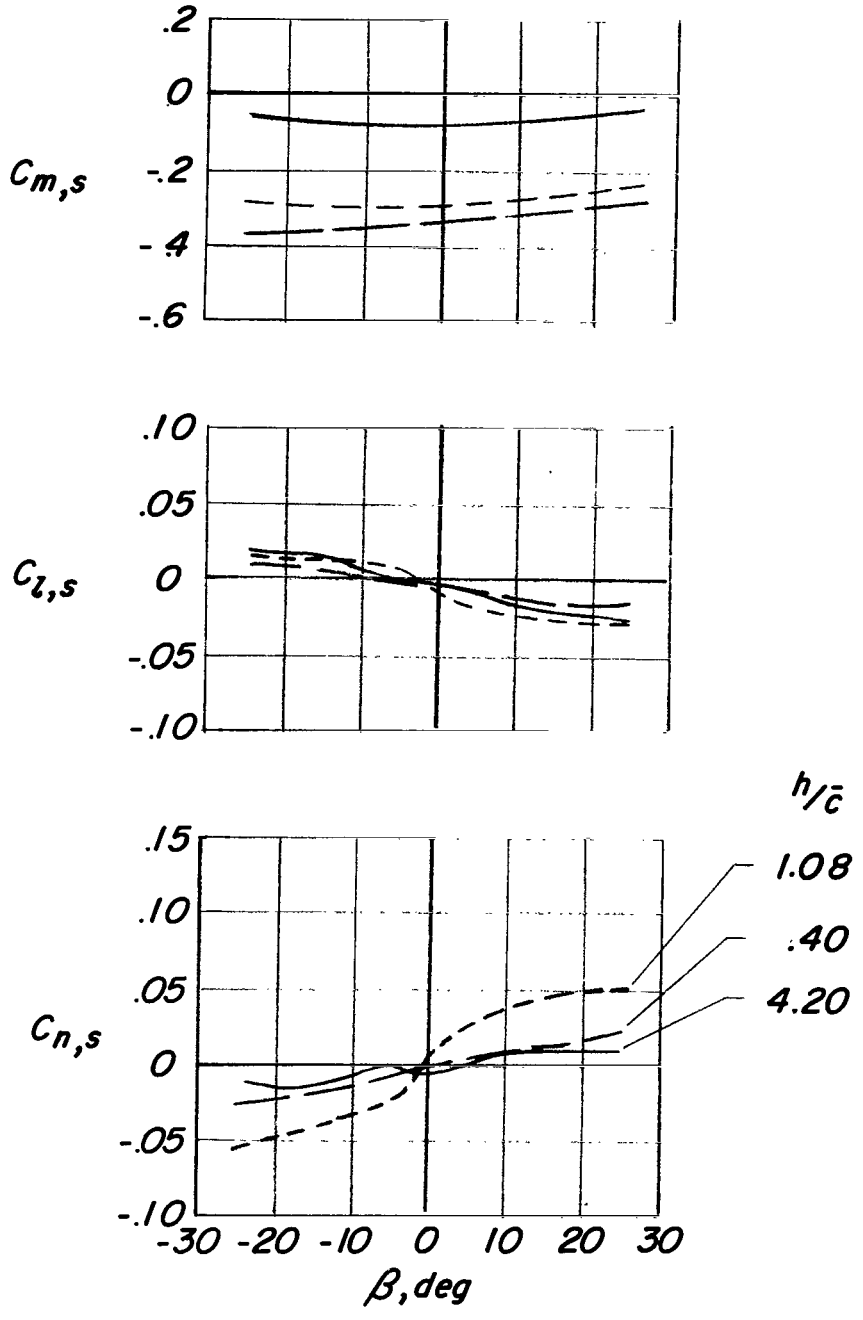

Figure 37.- Effect of ground-height ratio on the yawing-moment, rolling-moment, and pitching-moment coefficients in sideslip. $i_w = 45^0$; $\delta_f = 60^0$; $i_t = 20^0$; $\alpha = 0^0$.

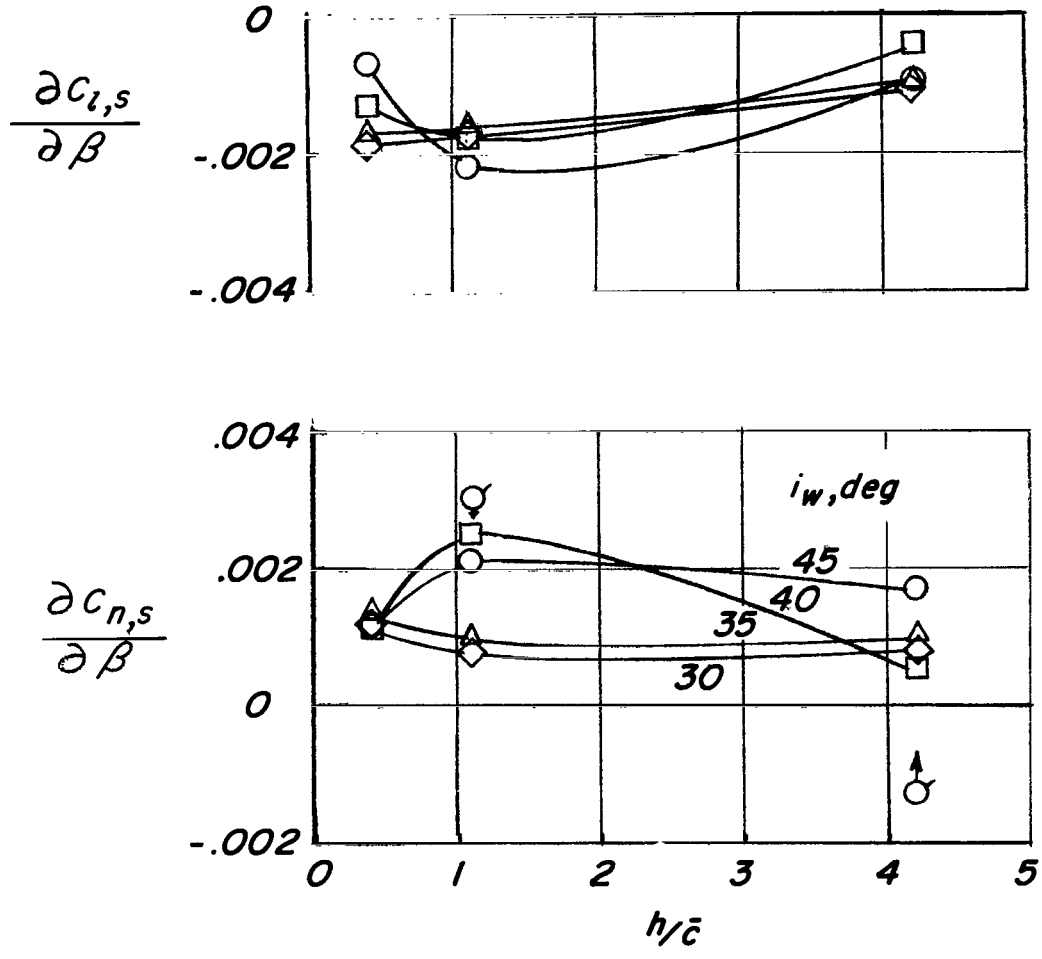

Figure 38.- Variation of lateral stability parameters with ground-height ratio for several wing-tilt angles. $\delta_f = 60^o$; $i_t = 20^o$; $\alpha = 0^o$.

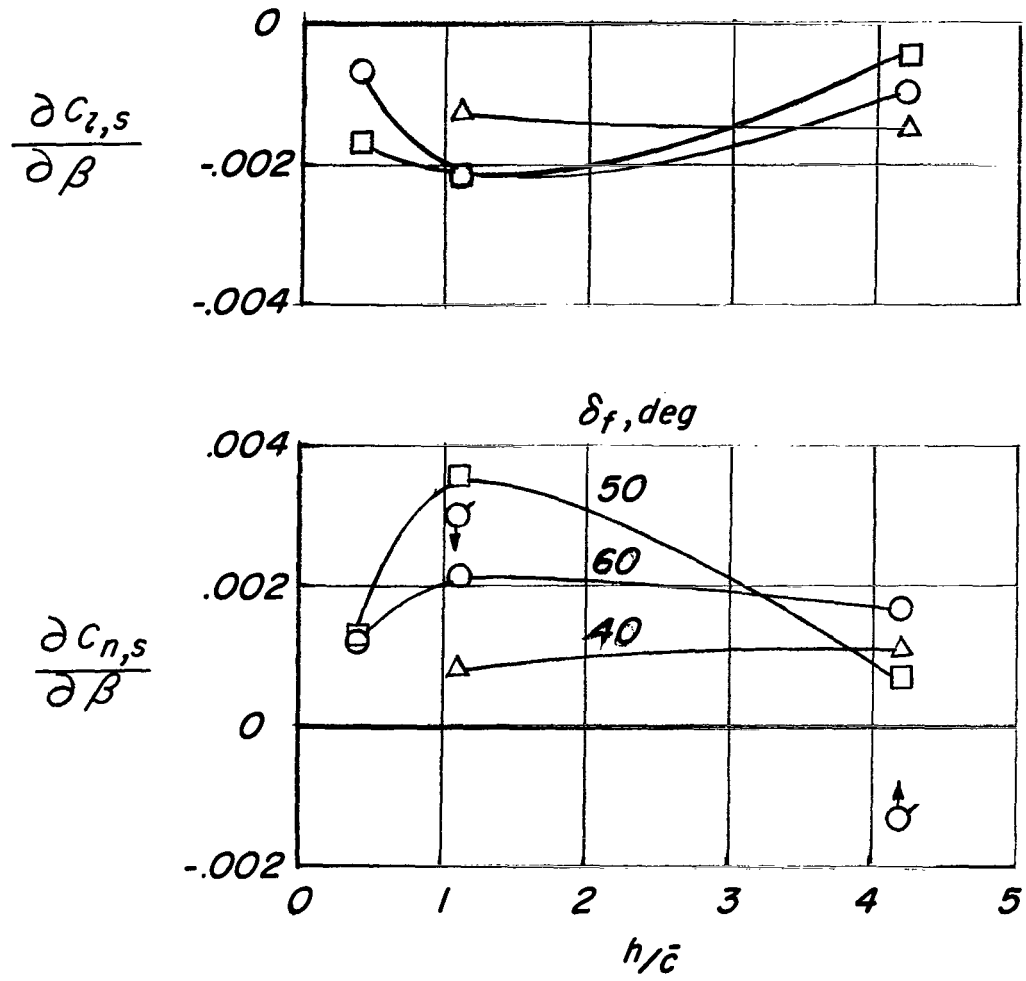

Figure 39.- Variation of lateral stability parameters with ground-height ratio for several flap-deflection angles. $i_w = 45^0$; $i_t = 20^0$; $\alpha = 0^0$.

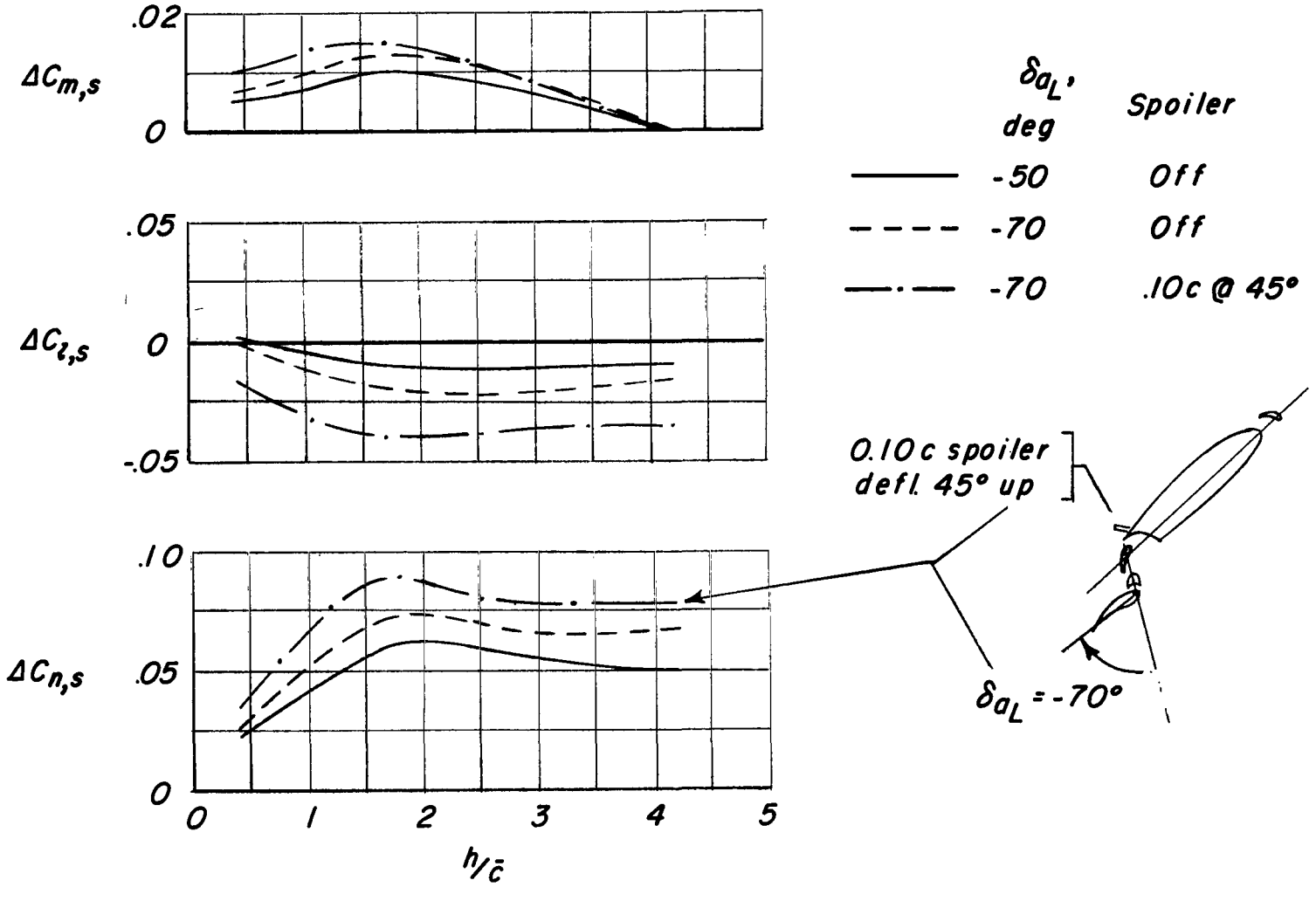

Figure 40.- Yawing-moment, rolling-moment, and pitching-moment control available from aileron and aileron-spoiler deflection over a range of ground heights. $i_w = 45^0$; $\delta_f = 60^0$; $i_t = 20^0$; $\alpha = 0^0$; $C_{T,S} = 0.96$.

"The aeronautical and space activities of the United States shall be conducted so as to contribute . . . to the expansion of human knowledge of phenomena in the atmosphere and space. The Administration shall provide for the widest practicable and appropriate dissemination of information concerning its activities and the results thereof."

—NATIONAL AERONAUTICS AND SPACE ACT OF 1958

NASA SCIENTIFIC AND TECHNICAL PUBLICATIONS

TECHNICAL REPORTS: Scientific and technical information considered important, complete, and a lasting contribution to existing knowledge.

TECHNICAL NOTES: Information less broad in scope but nevertheless of importance as a contribution to existing knowledge.

TECHNICAL MEMORANDUMS: Information receiving limited distribution because of preliminary data, security classification, or other reasons.

CONTRACTOR REPORTS: Scientific and technical information generated under a NASA contract or grant and considered an important contribution to existing knowledge.

TECHNICAL TRANSLATIONS: Information published in a foreign language considered to merit NASA distribution in English.

SPECIAL PUBLICATIONS: Information derived from or of value to NASA activities. Publications include conference proceedings, monographs, data compilations, handbooks, sourcebooks, and special bibliographies.

TECHNOLOGY UTILIZATION PUBLICATIONS: Information on technology used by NASA that may be of particular interest in commercial and other non-aerospace applications. Publications include Tech Briefs, Technology Utilization Reports and Notes, and Technology Surveys.

Details on the availability of these publications may be obtained from:

SCIENTIFIC AND TECHNICAL INFORMATION DIVISION

NATIONAL AERONAUTICS AND SPACE ADMINISTRATION

Washington, D.C. 20546